Akhilesh arora

Thesis Sandeep kumar

Research paper

Document Details

Submission ID
trn:oid:::27535:147962295

Submission Date
Aug 11, 2026, 4:04 PM GMT+5:30

Download Date
Aug 11, 2026, 4:11 PM GMT+5:30

File Name
Thesis Sandeep kumar.pdf

File Size
2.9 MB

112 Pages

27,557 Words

154,229 Characters

4% Overall Similarity

The combined total of all matches, including overlapping sources, for each database.

Filtered from the Report

- Bibliography
- Quoted Text
- Cited Text
- Small Matches (less than 14 words)

Exclusions

- 4 Excluded Sources
- 5 Excluded Matches

Match Groups

45 Not Cited or Quoted 4%
Matches with neither in-text citation nor quotation marks

0 Missing Quotations 0%
Matches that are still very similar to source material

0 Missing Citation 0%
Matches that have quotation marks, but no in-text citation

0 Cited and Quoted 0%
Matches with in-text citation present, but no quotation marks

Top Sources

1% Internet sources
3% Publications
1% Submitted works (Student Papers)

Integrity Flags

0 Integrity Flags for Review

Our system's algorithms look deeply at a document for any inconsistencies that would set it apart from a normal submission. If we notice something strange, we flag it for you to review.

A Flag is not necessarily an indicator of a problem. However, we'd recommend you focus your attention there for further review.

Match Groups

- **45** Not Cited or Quoted 4%
  Matches with neither in-text citation nor quotation marks
- **0** Missing Quotations 0%
  Matches that are still very similar to source material
- **0** Missing Citation 0%
  Matches that have quotation marks, but no in-text citation
- **0** Cited and Quoted 0%
  Matches with in-text citation present, but no quotation marks

Top Sources

1% Internet sources
3% Publications
1% Submitted works (Student Papers)

Top Sources

The sources with the highest number of matches within the submission. Overlapping sources will not be displayed.

1	Internet	
www.researchgate.net		1%
2	Publication	
Rashin Khera, Akhilesh Arora, B.B. Arora. "Performance Analysis and Multi-Object...		<1%
3	Student papers	
Georgia Military College (Canvas PF) on 2026-02-16		<1%
4	Publication	
Zhiqi Wang, Yabin Zhao, Xiaoxia Xia, Sifeng Zhang, Yao Xiao, Xiaoyue Zhang, Weis...		<1%
5	Internet	
hal.science		<1%
6	Publication	
Progress in Sustainable Energy Technologies Generating Renewable Energy, 2014.		<1%
7	Publication	
Dincer, Ibrahim, and Marc A. Rosen. "Exergy and Multiobjective Optimization", EX...		<1%
8	Publication	
Liu, Mingxi, Yang Shi, and Fang Fang. "Combined cooling, heating and power syst...		<1%
9	Student papers	
University of Greenwich on 2025-09-01		<1%
10	Student papers	
Teaching and Learning with Technology on 2026-03-31		<1%

11 Publication
Shane D. Garland, Jeff Noall, Todd M. Bandhauer. "Experimentally validated mode... <1%

12 Publication
Ananth S. Iyengar, Pritam Bhat, Pavan Kumar Reddy, N Abhilash. "Experimental I... <1%

13 Student papers
Middlesbrough College on 2026-05-22 <1%

14 Student papers
University of South Australia on 2025-06-15 <1%

15 Student papers
RMIT University on 2023-10-15 <1%

16 Publication
Susanta Kumar Das, Madhusweta Das. "Fundamentals and Operations in Food Pr... <1%

17 Student papers
Trinity College Dublin on 2026-04-01 <1%

18 Student papers
University of Witwatersrand on 2025-09-02 <1%

19 Internet
dspace.iiuc.ac.bd:8080 <1%

20 Publication
A. Baghernejad, E. Aslanzadeh. "Application of multiobjective optimization in ther... <1%

21 Publication
K. Madhesh, D.R. Devesh, T. Vivin, M. Praveen Raj, Patrick E. Phelan, V. Vignesh Ku... <1%

22 Student papers
King Saud University on 2016-04-29 <1%

23 Publication
Oguzhan Pektezel, Mehmet Das, Halil Ibrahim Acar. "Experimental Analysis of Dif... <1%

24 Student papers
University Tun Hussein Onn Malaysia on 2018-05-29 <1%

25 Publication

Zhiqi Wang, Feiyi Zhu, Yabin Zhao, Xiaoxia Xia, Qianghui Yi, Hongpeng Li. "Off-des... <1%

26 Internet

pubs.sciepub.com <1%

27 Internet

www.jnamt.org <1%

28 Internet

www.mdpi.com <1%

ANALYSIS OF HEAT OPERATED CHP SYSTEMS

Sandeep Kumar

ABSTRACT

The increasing global energy demand and environmental concerns have accelerated the search for sustainable and energy-efficient technologies. Waste heat recovery from low- and medium-grade sources has emerged as an effective approach to improve energy efficiency and reduce fossil fuel dependence. This study presents a thermodynamic investigation of integrated Organic Rankine Cycle-Vapor Compression Refrigeration (ORC-VCR) systems for simultaneous power generation and cooling using waste heat. The system aims to efficiently convert unused thermal energy into useful power and refrigeration.

The first part of this study presents a numerical thermodynamic analysis of a low-temperature CHP system validated with published experimental data. The system uses a turbine–compressor assembly mounted on a common shaft, enabling direct mechanical coupling between the power and refrigeration cycles. A low-grade thermal energy source with a capacity of 60 kW at 348 K is working as the driving source for the ORC. Wide-ranging energy and exergy examine are conducted to assess the system performance across a variety of working circumstances. Under the design condition, the system achieves an organic Rankine cycle's efficiency of 5.15%, a cooling capacity of 10.85 kW, and a coefficient of performance (COP) of 4.105. The results further disclose a decline in exergy efficiency with rising source temperature, highlighting the importance of attaining suitable thermal matching in waste-heat recovery applications.

The R1233zd(E)-R1233zd(E) refrigerant pair displays the most favorable combination of thermophysical and environmental qualities. To further improve system performance, a GA-based multi-objective optimization strategy is employed, with the two main target functions being exergetic efficiency and refrigerating effect. The optimization findings show that system performance is significantly impacted by ambient temperature. The system's COP and cooling capacity increase as the outside temperature decreases.

The research's additional section examines a multi-source cooling, heating, and power (CHP) system that combines solar thermal energy with diesel engine exhaust heat. The ORC's primary thermal input comes from high-temperature exhaust gasses between

690 and 810 K, while solar thermal energy between 433 and 473 K serves as a supplementary energy source. Better energy recovery and increased operational continuity under changeable conditions are made possible by the hybridization of various thermal sources. To assess how sensitive the system's performance is to changes in the temperatures of the condenser, evaporator, and turbine-inlet, extensive energy and exergy analyzes are used.

The findings confirm that the chosen refrigerant pairings and operational settings have a significant impact on the thermodynamic performance of the CHP system. Benzene-R601 has about 18% higher exergetic efficiency than the Cyclohexane-R1234yf refrigerant combo and has the highest COP of 1.18 of the suggested couples. Under variable heat-source circumstances, the addition of solar thermal energy increases system efficiency and improves operational reliability. According to multi-objective optimization, a high-pressure turbine temperature of 548.33 K and a low-pressure turbine temperature of 439.19 K yield the highest cooling capacity of 33.72 TR. While maintaining a reasonable degree of thermodynamic efficiency, these improved conditions greatly improve cooling performance. Furthermore, at lower ambient temperatures, the system performs better.

The combined results of the two ORC-VCR systems under investigation showed promise as a practical strategy for sustainable refrigeration and waste heat usage. The system's efficiency, adaptability, and operation compliance across a range of temperatures are enhanced by parameters like the thermal source, working fluids, and optimization approaches. The systems are effective for converting medium- and low-grade waste heat into valuable energy uses in the automotive industry, power-producing industries, and industrial settings.

CHAPTER 1

INTRODUCTION

1.1 Overview

The energy demand in the world is rising day by day, and unavoidability to reduce greenhouse gas exhaust have encouraged researchers to discover sustainable technologies that enhance utilization and energy efficiency although minimizing environmental effects [1]. Amid the available techniques, the integrated Organic Rankine Cycle (ORC) with the Vapor Compression Refrigeration (VCR) cycle has garnered noteworthy attention. This combined ORC-VCR system gives an efficient approach for transforming low-and medium-grade thermal energy into a valuable cooling effect. The ORC-VCR/VCC system is famous for utilizing industrial waste heat, heat from the exhaust of vehicles, and renewable energy sources, thereby enhancing energy efficiency and promoting environmental sustainability [2].

The ORC is a thermodynamic cycle that is utilized to produce mechanical energy through operating working fluids with a low boiling point in the ORC to convert low-grade heat energy. When this ORC system is attached with a VCR system to produce a cooling effect by transferring mechanical power of the turbine to the compressor of the refrigerating cycle, it eliminates the requirement for external electrical energy. This arrangement is especially beneficial in a state where waste heat is present but remains unused. The amounts of thermal heat produced from production processes, Industrial furnaces, and internal combustion engines that can be captured and utilized. In addition, renewable heat sources such as geothermal energy, solar energy, and biomass burning can be employed as heat inputs. All these such as geothermal energy, solar energy, and biomass burning energy are in the category of low and medium range heat source. The compliance of ORC-VCR systems allows them to operate in different situations and cooling requirements, making them suitable for many applications [3].

Integrating waste heat utilization with Solar energy, geothermal energy, and biomass burning energy and other types of renewable energy within a centralized

thermodynamics framework significantly improve energy conservation efficiency and mitigates harmful environmental impacts. All above energy are remained as unutilized form of energy. Cutting-edge sustainable cooling modalities facilitate the substitution of conventional thermal regulation with low-carbon alternatives, thereby mitigating primary energy consumption. As a result, CHP system is achieved serious purchase in automotive, green energy, and industrial applications. The rising demand for efficient thermal-energy consumption has inspired substantial advancements in CHP system over the last 20 years, positioning these systems as a promising approach for sustainable energy conversion and waste-heat recovery. Such systems are highly beneficial for CHP arrangements due to their capacity to repurpose low-and medium-grade thermal exhaust into useful cooling [4]. A characteristic ORC-VCR system consists various components such as a generator or boiler, turbine and compressor knowingly influence on overall system performance, as they directly affect power generation and cooling capacity [5]. In this research focus on implementation of integrated ORC and VCR systems and evaluating the function of each component in this hybrid system. The ORC-VCR system contains a boiler, turbine, condenser, pump, evaporator, and compressor, which collectively facilitate the conversion of thermal energy into cooling effect. This chapter provides a overview of the system configuration, describes the operation of individual components, and justifies the selection of these components based on their performances metrics and efficiency attributes.

1.2 Components of CHP System

The cooling, Heating and Power (CHP) system contain of numerous significant parts that work together to produced cooling from low-grade heat [6]. Some major elements in CHP system include the boiler, turbine, condenser, pump, evaporator, and compressor. Above listed components are performing a specific role in the process and contributes to the overall efficiency of the system. The selection of these components is depended upon type of heat sources, which include the diesel engine exhaust gas and waste heat from industries are influenced by factors such as efficiency, reliability, and compatibility. This section explains how each component works and their implication in improving the performance of the system.

The utilization of low- and medium temperature heat sources in combined ORC-VCR system for refrigeration purpose is a very effect method. This can be achieved through running of ORC and VCR cycles using different type of working fluids. The ORC will utilize a fluid depending on the temperature of the heat source, while the VCR uses appropriate refrigerant for the cooling process.

In the case where heat sources at low temperatures, i.e., temperatures within the range of 60 0C - 100 0C, available, the ORC operates a working fluid with a low boiling point to improve heat recovery and energy conversion. The mechanical has generated in the form of the expansion of the working fluid in expander via thermal energy absorbed. In the presence of medium-temperature heat sources i.e. temperature in the range of 100 0C - 200 0C, high boiling point working fluids can be used to maximize efficiency and improve turbine performance. To produced mechanical power through mechanical belt drive subsequently, transmitted directly to the compressor of VCR system with the help of shaft or belt-driven system. The mechanical energy generated from ORC turbine is then transferred to compressor of the VCR system [7].

The VCR system operates with a dedicated refrigerant designed specifically operate under refrigeration mode. Since the compressor is mechanically motorized by turbine function in ORC cycle, it eliminates the need for an independent electricity supply required for refrigeration, enhancing energy efficiency and lower operational expenditures. The heat removed to atmosphere through condenser in the VCR also utilized for supplementary heating. The diagram in Fig. 1.1 illustrates the CHP system

which is combination of both ORC and VCR cycle.

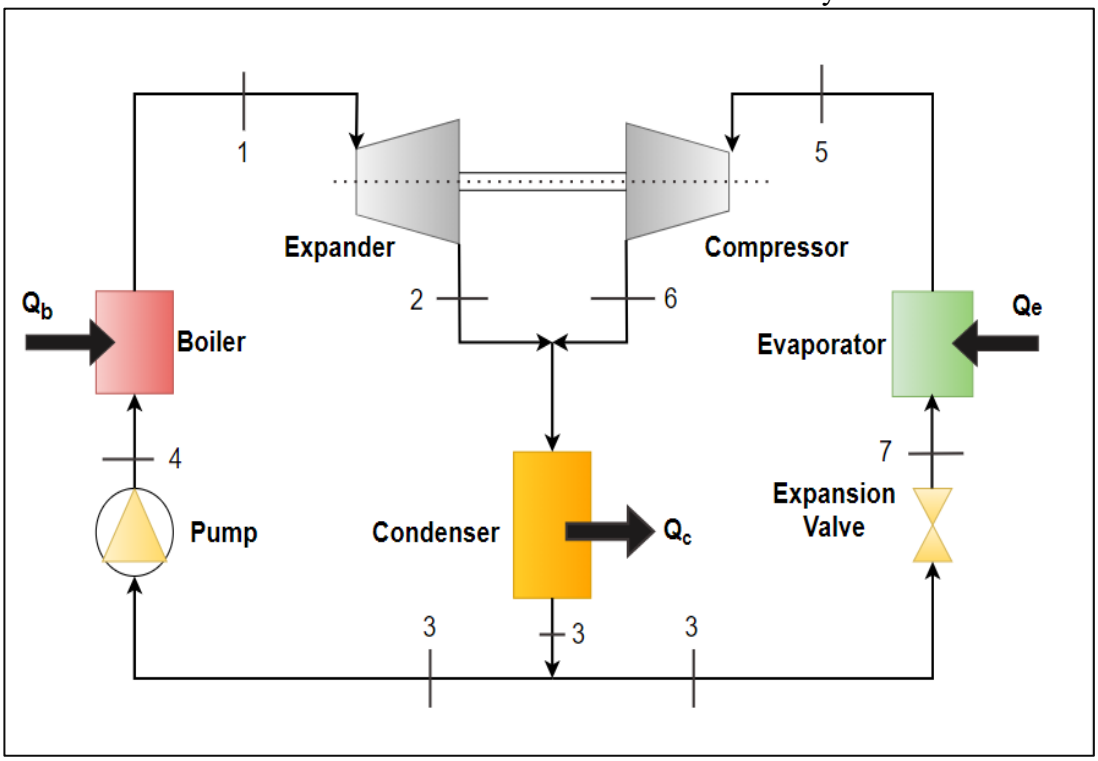

Fig. 1.1 Schematic diagram of CHP system

This mechanically coupled with the help of metal shaft an ORC-VCR system design is predominantly beneficial for solar thermal plants, industrial processes, cooling effect, and waste heat recovery, where low- or medium-grade heat is plentifully available but often less exploited. The separation of working fluids ensures operational safety, prevents cross-contamination, and allows independent optimization of both cycles for their respective temperature ranges and working conditions.

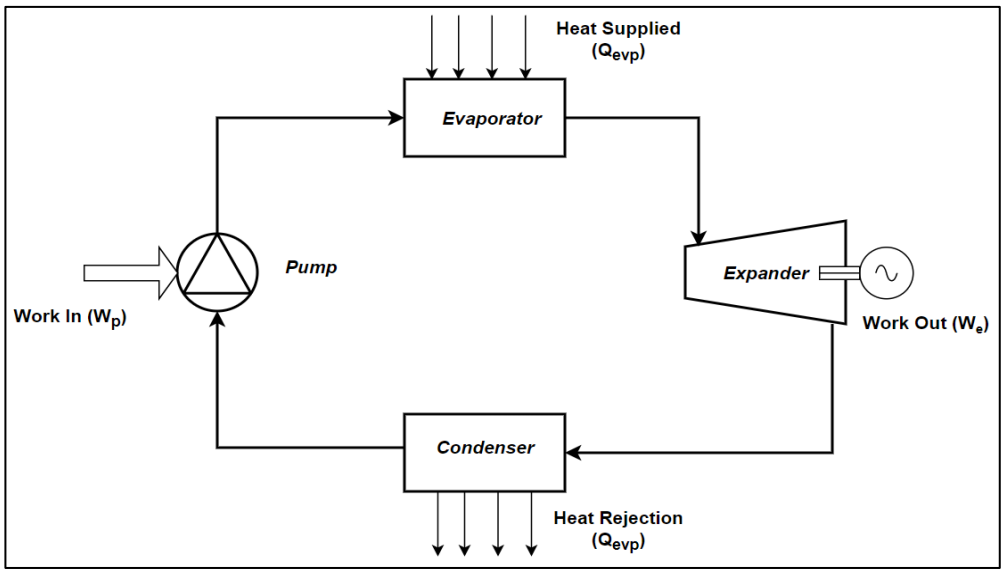

Fig. 1.2 Schematic diagram of ORC

The ORC is a thermodynamic process used to convert low - to medium- temperature heat into mechanical work and electricity. Unlike the conventional Rankine cycle that uses water/steam, the ORC employs organic working fluids with lower boiling points and higher vapor pressures, such as R245fa or toluene. This makes it well-suited for recovering energy from low-grade heat sources like industrial waste heat, geothermal energy, biomass combustion, or solar thermal system. The Fig. 1.2 represents the schematic diagram of ORC. The cycle consists of four main components: (1) Evaporator; (2) Expander (Turbine); (3) Condenser; and (4) Pump.

1.2.1 Boiler

The boiler in the ORC system is responsible for absorbing thermal energy from the waste heat source. In the context of diesel engine exhaust, industrial waste heat, or renewable heat sources, the boiler transfers heat to working fluid until it vaporizes. The selection of the working fluid is critical and depends on the heat source temperature and environmental considerations [8]. The Low boiling point and high thermal stability working fluid is usually selected.

A. Function

- The heat absorbs from thermal sources is of low-grade.
- The organic working fluid converted from liquid to vapor phase.
- Boiler is the primary energy input unit for the ORC cycle.

B. Efficiency Consideration:

Plate-type and shell-and-tube heat exchangers are commonly used as ORC boilers because of their high heat transfer effectiveness. The heat exchangers are the best gears to transfer heat through direct and in-direct contact at their best efficiency. Their larger heat transfer area and improved thermal contact enable effective heat recovery, quicker heat transfer, and better overall performance than traditional fire-tube or coil-type heat exchangers.

1.2.2 Turbine

The working fluid in form of vapours enters the (turbine) and undergoes expansion, resulting in a reduction in temperature and pressure while producing power-driven [8]. The power generated by the turbine is then conveyed to the VCR compressor through a belt-and-pulley machine or direct shaft connection.

A. Function:

- Convert thermal energy of the vapor into mechanical energy.
- Drives the compressor of the VCR system.
- Enables direct mechanical coupling, reducing the need for electrical energy.

B. Efficiency Consideration:

Radial inflow turbines are extensively employed in ORC systems because they perform efficiently under low mass flow rate and low enthalpy drop circumstances. For small-scale tenders, they often provide higher isentropic efficiency and require less fixing space than axial turbines.

1.2.3 Condenser (ORC)

After expansion in the turbine, the refrigerant exits as a low-pressure vapor and go in the condenser. In the condenser, heat is removed from the vapor, causing it to change into a liquid state. The rejected heat is usually transferred to the surrounding environment or to a cooling medium [9].

A. Function:

- Removes residual heat from the working fluid.
- Converts vapor back into liquid for recirculation.
- Completes the ORC loop by repairing the fluid for the pump.

B. Efficiency Consideration:

Air-cooled and water-cooled plate heat exchangers are widely used because of their compact structure and effective heat transfer characteristics. In recent years, microchannel condensers have gained attention as they offer improved thermal performance while requiring a smaller refrigerant charge.

1.2.4 Pump (ORC)

The condensed working fluid leaving the condenser is circulated back to the boiler by a pump. During this process, the pump increases the fluid pressure, allowing it to absorb heat effectively in the boiler and continue the cycle [10].

A. Functions:

- Circulates the organics working fluid throughout the ORC loop.
- Increases fluid pressure for effective vaporization.
- Consumes a small amount of mechanical energy compared to turbine output.

B. Efficiency Consideration:

Magnetically coupled hermetic pumps are used to prevent leakage and ensure long-term reliability. These pumps are optimized for high volumetric efficiency and are selected based on working fluid compatibility and required flow rate.

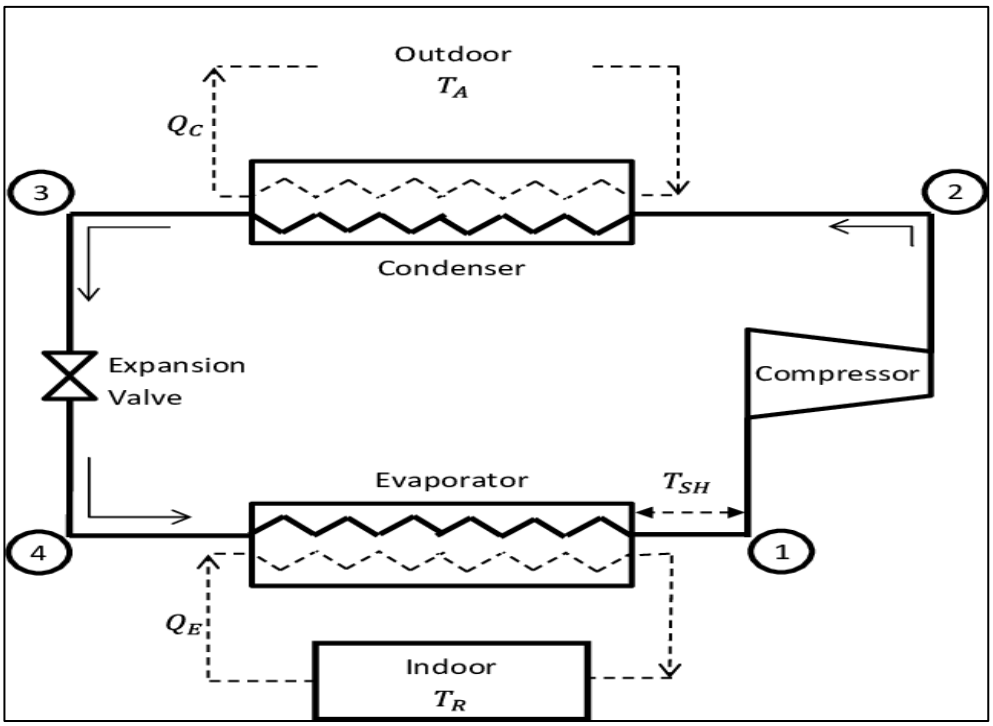

Fig. 1.3 Schematic diagram of VCR cycle

The Vapor compression Cycle (VCR) is the most widely used refrigeration and air-conditioning process, operating on the principle of phase change of refrigerant. It consists of four main components: Compressor, Condenser, expansion device, and evaporator. In this cycle, the compressor raises the pressure and temperature of the refrigerant vapor, which then releases heat to the surroundings in the condenser and condenses into liquid form. The liquid refrigerant passes through an expansion device, reducing its pressure and temperature, before entering the evaporator. Here, it absorbs heat from the cooled space, evaporators into vapor, and returns to the compressor to repeat the process. The fig. 1.3 show the schematic diagram of VCR cycle.

1.2.5 Compressor (VCR)

The compressor is a key component of the VCR system. It compresses the refrigerant vapor, increasing its pressure and temperature before it enters the condenser. The compressor is driven by turbine output power [11] in the integrated CHP system.

A. Function:

- Compresses low-Pressure refrigerant vapor from evaporator.
- Enables consideration at higher temperature in the condenser.

- Powered by mechanical energy from ORC turbine.

B. Efficiency Consideration:

Scroll compressors are typically used because they operate with low noise and vibration while provided that good isentropic efficiency. In applications requiring higher refrigerating effect, screw compressors are regularly preferred due to their reliable operation and skill to perform effectively under varying load conditions.

1.2.6 Condenser (VCR)

In the VCR cycle, the high-pressure working fluid releases heat to the surrounding medium as it passes through the condenser. As a consequence, the working fluid undergoes a phase change from vapor to liquid.

A. Function:

- Rejects heat from the system to the ambient.
- Facilitates phase changes of refrigerant from vapor to liquid.

B. Efficiency Consideration:

Enhanced-surface condensers and brazed plate heat exchangers are regularly selected to recover heat rejection performance. Features such as hydrophilic surface coatings and multi-pass flow arrangements help increase heat transfer effectiveness and overall system efficiency.

1.2.7 Evaporator

17

At the exit of the condenser the working fluid as a liquid, the refrigerant flows through the expansion valve, where its pressure is reduced before incoming the evaporator. In the evaporator, it absorbs heat from the space or load being chilled, evaporates into a vapor, and then proceeds to the next stage of the refrigeration cycle [12].

A. Function:

- Absorbs heat from the desired cooling space.
- Enables refrigeration effect by vaporizing the refrigerant.
- Provides low-pressure vapor to the compressor.

B. Efficiency Consideration:

Finned-tube evaporators and microchannel heat exchangers are commonly employed to increase the heat transfer area and improve heat absorption. The use of electronic expansion valves and proper superheat regulation helps maintain efficient operation and enhances overall evaporator performance.

1.3 Advantages of CHP system

An efficient method for increasing energy efficiency and encouraging sustainable cooling is the combination of the Organic Rankine Cycle (ORC) with the Vapor Compression Refrigeration (VCR) technology. This setup lessens reliance on traditional power sources by converting low-grade waste heat or renewable thermal energy into usable cooling. Lower energy consumption and running expenses can be achieved by using the mechanical power produced by the ORC turbine to run the VCR cycle's compressor. By using energy that would otherwise be squandered, the system not only improves the economy but also reduces greenhouse gas emissions. The ORC-VCR system is appropriate for a variety of industrial, commercial, and distributed energy applications due to its capacity to deliver electricity and cooling at the same time. Additionally, the system may be adjusted to varied heat source temperatures and operating conditions thanks to the availability of numerous organic working fluids. Utilizing locally accessible waste heat resources promotes the growth of compact and decentralized energy systems while also enhancing energy security [13].

Plant efficiency may be greatly increased and total operating costs can be decreased by using CHP systems. Using a zeotropic combination of hexane and R245fa, a comparison between a traditional ORC-VCR system and a modified configuration with a flash tank and other parts showed significant performance gains. Along with improvements in the coefficient of performance (COP), exergetic efficiency (about 29%), and total cost function (about 41%), the upgraded system demonstrated an increase in cooling capacity of about 23% [14].

Additional research has demonstrated that the use of zeotropic working-fluid mixes like pentane and hexane can enhance the performance of ORC-VCR systems. The recuperative dual-pressure arrangement generated the maximum power output of 2038 kW and achieved more than 16% greater efficiency than the basic ORC system, according to a study of simple, dual-pressure, and recuperative ORC arrangements.

Zeotropic mixes were used to increase thermodynamic performance and reduce energy destruction. With a stated net present value of almost 4.53 million dollars over a 20-year period, economic study also showed that recuperative setups offer good financial returns, making them a viable choice for real-world deployment [15].

Advanced optimization and decision-making approaches have also been used to assess the benefits of ORC-VCR systems. To find operating settings that balance thermodynamic performance, economic concerns, and environmental effect, techniques like the Evaluation of Distance from Average Solution (EDAS) in conjunction with entropy weighting have been used. The dependability of system optimization has been claimed to be enhanced by the combination of EDAS with gray relational analysis; a cross-comparison of the approaches revealed high agreement, with discrepancies of less than 10%. The total attractiveness score improved by about 30% as a result of the adjusted operating conditions, demonstrating the system's increased sustainability and efficiency [16].

Researchers and system designers have given CHP systems a great deal of attention because of these benefits. Adoption of CHP technology is still primarily driven by advances in energy efficiency, but economic considerations must also be carefully considered. To guaranty that the chosen CHP design is both technically and financially feasible, evaluations of capital expenditure, operational expenses, and long-term performance are crucial.

1.4 2E Analyses

The Fig. 1.4 represents the 2E analysis includes the energy and exergy methods of assessment of any thermal system [17]. The performance evaluation of an energy conversion system is based on energy analysis. The assumption that the system's components are confined inside an imaginary control container is the starting point for energy analysis. The laws of mass and energy conservation are then used to determine the energy interaction inside the control volume. An estimate of the system's performance is obtained by the energy analysis. Thermal efficiency is a common performance metric used in power cycles in energy analysis, whereas COP is used in cooling cycles. Energy analysis is helpful, but it cannot tell how much a system deviates

from its ideal or reversible performance limitations [18]. To address this limitation, exergy analysis, which is based on the second law of thermodynamics, is widely applied [19]. Exergy represents the maximum useful work that can be obtained from a system as it moves from a given state to a defined reference environment.

Whenever the characteristics of the system differ from those of the surrounding environment, there is a possibility for productive activity. However, when the system reaches a state of equilibrium with its environment, the amount of work required to extract potential or exergy becomes zero. At that moment, the system is said to be in a state of complete idleness, sometimes referred to as a "dead state." Exergy is considered to be the combined characteristic of both the system and its surroundings [20].

By identifying the source, location, and actual magnitude of energy loss, exergy analysis facilitates more efficient energy utilization. Consequently, exergy analysis is an exceptionally valuable method for upgrading an existing thermal system or devising and developing a new energy-efficient thermal system. In contrast to energy analysis, which assumes the conservation of energy, exergy analysis posits that exergy is inherently destructive. Exergy destruction occurs when irreversibilities are present in a system, such as heat transfer facilitated by a finite difference in temperature, fluid friction, chemical reactions, and so forth. An established method for improving the performance of a thermal system, exergy analysis identifies the primary locations of irreversibilities before modifying the operating and design parameters to reduce the irreversibilities.

Although exergy analysis is adequate for examining and enhancing the efficacy of a thermal system, it fails to consider economic considerations. An optimal thermal system should possess both high efficiency and cost-effectiveness. Although exergy analysis can improve the efficiency of a thermal system, it does not ensure that the system will remain cost-effective [22].

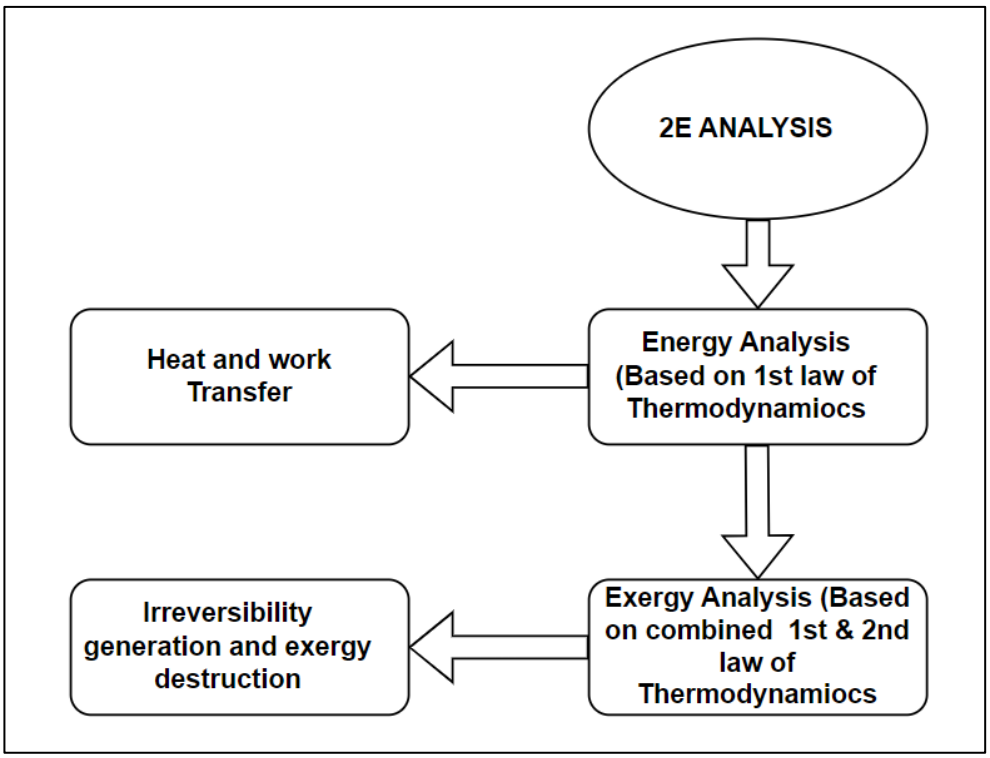

Fig. 1.4 A flow chart showing the steps of the 2E analysis

1.5 Outline of this Thesis

The thesis has six chapters, which are outlined as follows:

Chapter 1: Introduction

This chapter begins with a brief summary of how research into sustainable technologies, such as the ORC-VCR system, which transforms low- and medium-grade thermal energy into usable cooling power, has escalated due to the growing worldwide need for energy. This integrated system makes use of waste heat from renewable energy sources, automobile exhaust, and industrial processes. The refrigeration system may run with little to no reliance on grid electricity since the mechanical power generated by the ORC turbine is sent straight to the VCR compressor. As a result, overall energy utilization is improved while environmental emissions are reduced. This discussion proceeds with utilization of various components, followed by a summary of 2E analyses, which encompass Energy and Exergy assessments. Finally, this chapter finishes by providing an overview of the thesis.

Chapter 2: Literature Review

This chapter focuses on conducting a thorough review of the existing literature on combined ORC-VCR system, specifically exploring the concepts of energy and exergy and followed by multi-objective optimization. This chapter also explores the new methodology of advanced exergy analysis and its associated research. Furthermore, numerous literary works have also examined the performance-based parametric investigation to analyze the impact of different operating factors. Data and pertinent information were taken from various research papers in international journals and related theses. The findings from multiple Proceedings were also reviewed.

Chapter 3: System Description and Mathematical Modelling

This chapter discusses the description of various configurations of combined waste heat recovery cycle with cooling cycle. Moreover, the theoretical background of energy and exergy analyses along with their equations are also discussed. Also, the results based on an advanced exergy-based splitting of exergy destruction, and multi-objective optimization using a Genetic Algorithm (GA) are presented in this chapter.

Chapter 4: Model Validation

This chapter presents an overview of the significance of model validation in research or practical applications. The text discusses the need to validate models to ensure their reliability and effectiveness in addressing real-world issues. The mathematical models for the combined ORC-VCR system for single source and the combined ORC-VCR system with hybrid source have been validated by experimental data from various investigations.

Chapter 5: Results and Discussion

This chapter provides a comprehensive overview of the results achieved at each stage of the process. Furthermore, it examines the impact of source temperature, condenser temperature and evaporator temperature on performance of the system, as well as the multi-objective optimization analysis. The comparisons of the different scenarios are also presented.

Chapter 6: Conclusions and scope of future research

This chapter concludes the findings derived from the results gained through the various analyses conducted. Additionally, potential areas for further research have been suggested.

CHAPTER 2 LITERATURE REVIEW

2.1 Background

Due to growing environmental concerns and advancements in technology over the past decade, there has been a significant increase in both the need for and the potential to provide versatile energy solutions. In order to gain an understanding of the most recent developments in the optimisation and performance of the ORC-VCR, a succinct literature review was undertaken. This chapter presents the associated publications and research work, including their objectives, analytical methods, and concise findings. However, this chapter focuses on a comprehensive investigation of existing literature on the use of various waste heat source and optimization conducted on ORC-VCR configurations. Some researchers/authors concentrate on the operational parameters like Source temperature, Condenser temperature, evaporator temperature of the ORC system, while others optimize the working fluids.

The literature in this chapter is categorized into three primary sections: the impact of various operational factors on energy and exergy analysis, as well as multi-objective optimization. The main objective of this chapter is to pinpoint the research deficiency and concentrate on the specific domains of ORC-VCR systems.

2.2 Review based on energy and exergy analysis

2.2.1 Effect of Heat Source Temperature

Malwe et al. [22] presents a detailed analysis of how evaporator outlet temperature influences the performance of an ORC system operating with low-grade heat. This study highlights the significance of the evaporator, which plays a key role in heat absorption and influences the irreversibilities occurring within the cycle. The results show that an increase in evaporator outlet temperature improves thermal efficiency up to an optimum value by enhancing heat utilization. However, a further increase in temperature leads to a reduction in efficiency due to greater exergy losses. The findings also indicate that the evaporator and condenser are the major sources of irreversibility in the system, suggesting that their operating parameters should be selected carefully to achieve better performance. The authors conclude that there exists an optimal temperature range that balances cycle efficiency and minimizes exergy losses, confirming the ORC's potential

for efficient recovery of low-grade heat sources in renewable and industrial applications. Goyal et al.[23] study, a multi evaporator vapor-compression refrigeration (VCR) system driven by Organic Rankine Cycle (ORC) is proposed as a refrigeration system for supermarkets, restaurants, etc. The system is analyzed for its thermodynamic performance in terms of coefficient of performance (COPs) and exergetic efficiency (ηex). A zeotropic mixture of hexane and R245fa is used as working fluid over pure fluid to assess its impact on the thermodynamic performance of the system. Moreover, the system is optimized using an evolutionary algorithm called genetic algorithm (GA) to determine the optimal values of the operating parameters for the maximum exergetic efficiency of the system. The results indicate that COPs and ηex are maximum at the mass fraction of 0.5 of the zeotropic mixture. The maximum values of COPs and ηex are 0.425 and 31.1% respectively. The system can achieve an exergetic efficiency of 58% at the optimal set of operating parameters. The corresponding optimal values of the temperature of the ORC evaporator, VCR evaporator 1, VCR evaporator 2, and the condenser are 388 K, 268 K, 268 K, and 303 K respectively. Waste heat disposal in the form of hot gases in the environment is one of the main causes of global warming, and approximately 60% heat of primary industrial energy is lost during combustion and heat transfer. This waste heat is directly dumped into the environment even though it could be utilized to produce power or cooling effects. An extensive range of waste heat sources is readily accessible, including power plants, industries, and internal combustion engines. The combined cooling, heating and power (CCHP) system – a representative model of the decentralized energy system- has been garnered significant attention in both academia and industry in recent years. The growing interest stems from its notable advantages, including high overall system efficiency, enhanced economic performance, and substantial reductions in green gas (GHG) emissions when compared to conventional centralized energy system. Combined Cooling, Heating, and Power (CCHP) systems have gained considerable attention as an effective approach for improving energy utilization while reducing environmental impacts. This paper reviews the current research developments related to CCHP systems. It first discusses the basic operating principles, historical development, and common configurations of CCHP technology, followed by an examination of its advantages compared with conventional

energy systems. In addition, the major components of a CCHP system and their functions are briefly described to provide a foundation for understanding system operation and performance. In the second section, detailed attention is given to the prime movers—such as gas turbines, internal combustion engines, and fuel cells—followed by a discussion of thermally activated technologies, including absorption chillers and desiccant-based cooling systems. This part also emphasizes the role of innovative materials, advanced thermal management techniques, and emerging design strategies in improving the overall performance of Combined Cooling, Heating, and Power configurations.

A comprehensive screening of 43 refrigerants was conducted to identify suitable working fluids for both the Organic Rankine Cycle (ORC) and the Vapor Compression Refrigeration (VCR) cycle. Based on thermodynamic performance, environmental considerations, and safety characteristics, nine refrigerants were shortlisted for each cycle. The comparison showed that hydrofluoroolefins (HFOs), particularly R1234yf and R1234ze, offer a favorable balance between performance and environmental impact due to their negligible ODP and low GWP values. Among natural refrigerants, R717 (ammonia) exhibited superior thermodynamic performance under subcritical conditions, although its toxicity limits widespread adoption. The study also reported that for heat-source temperatures below 85°C, subcritical operation provides higher efficiency and more compact system design than supercritical operation. In addition, recommendations regarding expander and compressor dimensions were proposed to improve overall system performance [24,25].

In recent years, significant research attention has been directed toward ORC–VCR systems, with working-fluid selection emerging as one of the most important design considerations. Gonzalez et al. [26] investigated an ORC-driven VCR system powered by low- and medium-temperature renewable energy sources, including solar, geothermal, and waste heat. In this configuration, the ORC and VCR cycles are mechanically coupled through a common shaft while employing different working fluids to maximize efficiency. Eight refrigerants were evaluated, resulting in sixteen fluid-pair combinations. The analysis considered parameters such as compressor discharge temperature, VCR coefficient of performance (COP), and overall system

COP. Using the PC-SAFT equation of state to predict thermophysical properties, the study found that the combination of n-pentane in the ORC and R1233zd in the refrigeration cycle yielded the best overall performance. The results demonstrated that appropriate fluid selection can significantly improve system efficiency while reducing environmental impact.

Similarly, Bouneful et al. [27] reported that R600 exhibits favorable thermodynamic characteristics when evaluated using energy and exergy analyses. The study also emphasized the potential of waste heat recovery (WHR) from diesel engine exhaust gases, which typically range between 450°C and 550°C. Recovering this energy can reduce fuel consumption, improve system efficiency, and lower greenhouse gas emissions. Various WHR technologies, their classifications, applications, and implementation challenges were reviewed, together with potential solutions for overcoming existing barriers.

The review further highlighted recent developments in WHR systems, including applications in the food-processing and maritime sectors. Economic feasibility was assessed through payback-period analysis, demonstrating that waste heat utilization can provide substantial operational savings. Novel applications, such as using generator exhaust heat for agricultural product drying, were identified as promising opportunities for improving energy efficiency in agro-industrial operations. Overall, the findings suggest that effective waste heat recovery can reduce production costs while supporting environmental sustainability through lower carbon emissions [28].

The Organic Rankine Cycle is widely recognized as an effective technology for converting low-grade waste heat into useful power. Rather than relying on grid electricity, the mechanical power generated by the ORC can be directly used to drive a VCR system. Consequently, integrating ORC and VCR technologies offers an efficient approach for utilizing waste heat while simultaneously providing cooling. Saleh et al. [29] evaluated several hydrofluorocarbons, hydrocarbons, and HFO refrigerants, including R1234yf and R1234ze(E), in an ORC–VCR system operating with an ORC temperature range of 80–40°C and a VCR temperature range of 5–40°C. System performance was assessed using the overall coefficient of performance and the required mass flow rate per unit cooling capacity. The results indicated that high-boiling-point

refrigerants, particularly R245fa and R600, achieved superior performance. Among the fluids examined, R600 produced the highest overall coefficient of performance, reaching a value of 0.718 at a condenser temperature of 30°C, although its flammability remains a practical concern.

2.2.2 Effect of Condenser Temperature

Bounefour et al. [30] examined the effect of condenser temperature on the performance of ORC–VCR systems. The study reported that a reduction in condenser pressure, associated with lower condenser temperatures, influences the cycle pressure ratio and consequently affects the coefficient of performance (COP). It was further observed that condenser subcooling can improve system performance by increasing the refrigerating effect through a larger enthalpy difference across the evaporator. These findings underline the importance of condenser design and operating conditions in achieving higher cycle efficiency.

Iyengar et al. [31] investigated the impact of ambient conditions on ORC performance. Since the condenser operates in direct interaction with the surrounding environment, ambient temperature significantly influences cycle behavior. The results showed that higher ambient temperatures increase condenser temperature, leading to a decline in both thermal and exergetic efficiencies due to increased irreversibilities. In contrast, lower ambient temperatures improve heat rejection and enhance overall system performance. The study highlighted the importance of climatic conditions when designing ORC systems, particularly for regions with diverse weather patterns such as India. Recent research has also focused on advanced control strategies, optimization techniques, and system-sizing approaches for combined cooling, heating, and power (CCHP) systems. The integration of intelligent control algorithms, multi-objective optimization methods, and renewable energy sources has contributed to improved operational flexibility, reliability, and energy utilization. Furthermore, studies examining the deployment of CCHP technologies in different countries have emphasized the role of government policies, regulatory support, and market incentives in promoting adoption. Despite their advantages, challenges such as high capital costs, system integration complexity, and limited policy support continue to restrict widespread implementation [32].

The performance of Organic Rankine Cycles operating with working fluids such as benzene, ammonia, R11, R12, R113, and R134a has been investigated through several parametric studies. The results indicate that wet fluids generally exhibit improved efficiency at higher turbine inlet temperatures, whereas dry fluids tend to experience a reduction in efficiency under similar conditions. Isentropic fluids maintain relatively stable performance over a wide operating range, making them attractive candidates for low-temperature waste heat recovery applications. Comparative analyses of conventional refrigerants and their environmentally friendly substitutes have shown similar thermodynamic behavior, suggesting that sustainable alternatives can be adopted without significant performance penalties. These studies collectively demonstrate that working-fluid selection remains a key factor influencing ORC efficiency and system reliability [33]. A comprehensive review of hybrid cooling technologies integrating absorption, adsorption, and desiccant systems with conventional vapor-compression refrigeration has also been reported [34]. Hybrid absorption–compression systems have shown significant potential for reducing electricity consumption, with reported savings ranging from 45% to 88% compared with conventional refrigeration systems. Likewise, adsorption–compression configurations have demonstrated performance improvements through reduced condensation temperatures, although system dimensions and operating conditions strongly affect their effectiveness. Integrating vapor-compression cycles with solid or liquid desiccant systems has also enhanced cooling and dehumidification capabilities, particularly in multi-stage configurations. Additional developments involving ejector-assisted refrigeration systems [35] and ORC-based refrigeration technologies [36] have further expanded the range of thermally driven cooling solutions. Despite these advancements, each technology presents certain limitations. Sorption-based systems generally require large installation space and are constrained by relatively high evaporation temperatures. Ejector refrigeration systems often suffer from performance instability due to fixed ejector geometries. In comparison, Organic Rankine Cycle technology has attracted considerable interest because of its operational reliability and ability to utilize low-grade thermal energy effectively. By converting waste heat into mechanical power through an expander, ORC systems offer a practical route for energy recovery and utilization [37,38].

The increasing demand for cooling applications has encouraged the development of integrated ORC–VCR systems. One such approach involves the use of an Expander–Compressor Unit (ECU), which directly couples the power generated by the ORC to the refrigeration compressor. This arrangement eliminates the need for electrical energy conversion and allows thermal energy from waste heat or renewable sources to drive the cooling process directly. Considering that refrigeration and air-conditioning systems account for a substantial share of global electricity consumption, alternative cooling technologies based on thermal energy have gained significant attention.

In this context, a Thermo-Mechanical Refrigeration (TMR) system has been proposed for operation with low-temperature heat sources in the range of 60–100 °C. The system integrates an isobaric Expander–Compressor Unit with a vapor-compression refrigeration cycle, enabling direct conversion of thermal energy into mechanical work for refrigeration. The proposed configuration aims to simplify system architecture while improving the utilization of low-grade heat sources, thereby offering a sustainable alternative for future cooling applications.

Guopeng et al. [39] analyzed the ORC system employing diesel engine exhaust heat as the primary source for heating working fluid via an oil-gas heat exchanger and preheating working fluid via a diesel engine jacket water circuit. It was reported that a diesel engine (of capacity 258.3 kW) produced 0.2981 kg/s exhaust gas at a temperature of 808.15 K, which is used in ORC to generate 15.5 kW of power with a 9.1% thermal efficiency. Ghorbani et al. [40] simulated Transcritical Organic Rankine Vapor Compression (T-ORVC) using waste engine exhaust gas produced from a gasoline engine (of capacity 130 kW) as the heat source for an ORC cycle using as working fluids R134a, R245fa, R290, R600, and R1234yf. The system produced 20 kW of cooling capacity. The results demonstrate that the system can generate the necessary refrigeration capacity for cars and buses. The results also indicate that, among all the working fluids, R245fa and R600 has the highest heating COP values of 0.614 and 0.606, respectively. Ngangue et al. [41] reported the performance of a novel heat recovery cogeneration system integrating an Organic Rankine Cycle (ORC), a Vapor Absorption Cycle (VAC), and a Vapor Compression Cycle (VCC). The NH_3-NaSCN pair is employed as the working fluid in the VAC, while seven different refrigerants are

examined in the ORC–VCC to identify the most efficient option for tropical regions. The selected working fluids were chosen because of their low Global Warming Potential (GWP) and Ozone Depletion Potential (ODP). Thermodynamic simulations were carried out to determine appropriate operating conditions for the vapor absorption cycle (VAC). Energy and exergy analyses showed that R717 exhibited superior performance, achieving higher efficiency and improved system characteristics. Xia et al. [42] conducted a combined thermodynamic, economic, and environmental assessment and concluded that hydrocarbons are promising working fluids for ORC–VCR applications. Nevertheless, the literature does not identify a universally optimal working fluid for ORC–VCR systems. Reported results differ considerably due to variations in operating conditions and the limited range of fluids examined in individual studies. Moreover, most previous investigations have focused primarily on pure working fluids, leaving the potential of alternative fluid combinations relatively unexplored.

2.2.3 Effect of Evaporator Temperature

Goyal et al. [43] examined an Organic Rankine Cycle (ORC)-driven multi-evaporator vapor-compression refrigeration (mVCR) system intended for commercial refrigeration applications, including supermarkets and restaurants. To improve system performance, a zeotropic mixture of hexane and R245fa was employed as the working fluid. The system was evaluated using the overall coefficient of performance (COPs) and exergetic efficiency (ηex), while a genetic algorithm was applied to determine optimal operating conditions. The analysis showed that a mixture containing equal mass fractions of hexane and R245fa produced the best results, achieving a maximum COPs of 0.425 and an exergetic efficiency of 31.1%.

Bolaji et al. [44] assessed the performance of dimethyl ether (RE170) and its azeotropic blends, R510A and R511A, as alternatives to R134a in domestic refrigeration systems. The study demonstrated that these refrigerants provide higher thermal conductivity, greater refrigerating effect, improved volumetric cooling capacity, and better coefficients of performance than R134a. In addition, they require lower power input for the same cooling capacity. Owing to their favorable environmental characteristics and improved energy performance, RE170, R510A, and R511A were identified as promising substitutes for conventional refrigerants in refrigeration applications.

Solar energy can also be incorporated into the existing energy systems to enhance further efficiency of the system. Zheng et al. [45] analyzed a solar power ORC-VCR system with a source temperature range of 60°C to 120°C, using both pure and zeotropic mixtures of various refrigerants. The researchers studied R290, R161, R152a, R134a, R600a, R227ea, R1234yf, and R1234ze as working fluids. They discovered that R600a was the best among all pure working fluids, with an overall system efficiency of 22%. Additionally, they found that a mixture of R161/R600a was the best among all zeotropic mixtures, achieving an overall system efficiency of 31%, with a mass fraction of 0.25 for R161 and 0.75 for R600a. Bu et al. [46] analyzed the selection of various working fluids including R600, R600a, R123, and R245fa in an ORC-VCR system powered by solar heat. In terms of Pressure Ratio (PR) and COP of VCR, the refrigerants R600 and R600a were more suitable working fluids, while R123 was the most suitable working fluid for ORC/VCR in terms of the overall efficiency of the solar thermal ice maker and COP of the system. Zhang et al. [47] analyzed the ORC system is powered in series and parallel by three solar collectors and waste heat sources, with the following fuels utilized: R245fa, R1233zd, R245ca, R365mfc, R601a, R601, R141b, Iso-hexane, and Hexane. The temperature range of the sources is from 120°C to 150°C. The ORC system power and specific return period for a hexane working fluid and series arrangement are 80.85 kW and 2.88 years, respectively. Connecting heat exchangers in series is preferable when the temperature difference between the two heat sources exceeds 50°C. Aneke et al. [48] attempted to improve the efficiency of ORC using regeneration and reheating. Some studies examined the combined ORC system along with a vapor compression system and/or a vapor absorption refrigeration system (VARS) for generating both electricity and cooling. Compared to pure fluids, zeotropic mixtures can minimize irreversible losses during phase-change heat transfer processes due to their temperature glide properties. In addition, Ashwani et al. [49] found that an optimal mass fraction exists for the mixtures, with the ORC-VCR system achieving maximum COP at a Hexane mass fraction of 0.6 in the Hexane/R245fa mixture. Karellas and Braimakis [50] observed that as the VCR evaporation temperature increases, energy and exergy efficiency, COP, and electricity generation also rise, while the condensation temperature follows the opposite trend. Based on the research of Saleh [51] the system's COP

increased with rising heat source and evaporation temperatures but decreased as the condensation temperature increased. Nasir and Kim [52] reported that as the outdoor temperature increased from 30°C to 40°C, the total COP of the ORC-VCR system rose from 0.172 to 0.217. Yilmaz et al. [53] analyzed a T-ORVC refrigeration system using a single heat source i.e. engine exhaust as waste heat at 180°C - 200°C with wet refrigerant R134a and dry refrigerant R245fa. The optimum value for overall COP was 0.71 for R134a which was obtained at 180°C and 8 MPa and for R245fa the corresponding optimum value was 0.86 at 200°C and 8 MPa.

Ashwni et al. [54] analyzed a thermodynamic analysis of a hybrid heat source-driven Organic Rankine Cycle integrated with a Flash Tank Vapor Compression Refrigeration (ORC-FTVCR) system has been carried out using five different hydrocarbon working fluids, namely hexane, heptane, octane, nonane, and decane. The hybrid heat source comprises a solar collector and a biomass burner, thereby enabling the utilization of both renewable and sustainable energy resources. In this study, the system coefficient of performance (COPs) and overall exergetic efficiency (ηoex) are employed as the principal indicators of thermal performance. The influence of key operating parameters, such as solar radiation intensity, expander inlet temperature, VCR evaporator inlet temperature, compressor and expander isentropic efficiencies, and condenser saturation temperature, was examined to assess their impact on system performance. The analysis showed that the choice of working fluid has a significant effect on overall efficiency. Among the fluids considered, heptane exhibited the best performance, enabling the ORC–FTVCR system to achieve a coefficient of performance (COPs) of 0.551 and an overall exergetic efficiency of 4.21%. Exergy analysis further indicated that the solar collector and biomass burner were the major sources of irreversibility, accounting for nearly 88% of the total exergy destruction within the system. These findings suggest that performance improvements can be achieved by enhancing the design and operation of these components.

While theoretical studies provide valuable insights into the behavior of ORC-VCR systems, their predictions are often based on simplifying assumptions that may not fully represent actual operating conditions. As a result, experimental investigations are essential for validating theoretical models and assessing real-world performance.

Garland et al. [55] investigated a waste heat recovery (WHR) system designed to utilize exhaust heat from power-generation facilities. Such systems can be configured to produce power, cooling, or useful thermal energy, depending on application requirements. The study focused on a turbo-compression cooling system (TCCS), in which low-grade waste heat is used to vaporize a working fluid that drives a turbine operating within a recuperative Rankine cycle. The turbine is mechanically coupled to the compressor of a vapor-compression refrigeration cycle, enabling cooling production without the need for additional external power input. To evaluate system performance, the authors developed a mathematical model incorporating compressor and turbine efficiency maps together with a heat-exchanger UA-scaling approach. The model was validated experimentally using a 250 kWth TCCS operating under different ambient temperatures and cooling loads. A close agreement between experimental and predicted results was observed, with deviations not exceeding 2%. During testing, turbine mass flow rates varied from 0.35 to 0.50 kg s^{-1}, while refrigerant mass flow rates in the cooling cycle ranged from 0.65 to 0.85 kg s^{-1}. After validation, the model was applied to investigate the integration of the TCCS with a Natural Gas Combined Cycle (NGCC) power plant, demonstrating its potential for improving energy utilization in large-scale power-generation systems.

Grauberger et al. [56] a prototype of an ORC-VCR system utilizing R1234ze(E), featuring a rated COP of 0.56 and a cooling capacity of 264 kW. Sensitivity analysis indicated that, among the factors considered, the cooling medium in the condenser had the most significant influence on the system's COP. In an experimental evaluation of the ORC-VCR system. Wang et al. [57] presented findings on the effects of the working fluid flow rate and pump outlet pressure on system performance. The results indicated that both the expander power output and the recuperator effectiveness increased with a rise in the working fluid flow rate. The experimental research of Jiang et al. [5] indicated that power consumption of the compression process in air separation units can be effectively reduced by precooling the inlet air of compressors using a combined organic Rankine cycle and vapor compression cycle (ORC-VCR). While most existing research in this field has concentrated on thermodynamic modelling and performance analysis, this study presents an experimental evaluation of a mechanically coupled ORC-VCR

system for air separation units. The experimental study evaluated the performance of the gas-bearing fluid supply system and the motor cooling system, both of which operated reliably throughout the testing period. Additional experiments were conducted under dissimilar operating circumstances by varying the pressure ratio, mass flow rate, and evaporating pressures at mutually temperature levels. The results established a decreasing trend in COP with an increase in the ratio of the both evaporator pressures. During full-load operation, the system attained a refrigeration temperature of 287.6 K COP of 0.63, and a cooling capacity of 14.2 kW, at a rotational speed of 25,822 rpm. These observations validate the technical possibility of CHP based compression heat recovery systems and indicate their potential for enhancing energy utilization in air-separation processes. Liang et al. [7] through an experiment investigated an ORC–VCR system designed to improve waste heat from the cooling circuit of an internal combustion engine (ICE). Waste heat recovery has long been recognized as an effective method for refining the overall efficiency of engine-based energy systems. The anticipated configuration differs from conventional approaches by recovering thermal energy from engine cooling water and employing it to power a cooling cycle based on a coupled ORC-VCR arrangement. To verify the concept, a laboratory-scale model was established using commercially available gears. The power engendered by the ORC was conveyed to the VCR compressor through a belt-drive mechanism. The refrigerant R245fa was selected as the ORC working fluid, while the refrigerant R134a was used in the cooling cycle. An electric water heater simulated the engine cooling-water source, and a refrigerated chamber represented the cooling load. Experimental results demonstrated that, with a heat-source temperature of approximately 95 °C, the system produced nearly 1.8 kW of cooling at an evaporating temperature of −4 °C. The corresponding heat-to-cooling efficiency was approximately 0.18. The authors noted that further improvements could be achieved through component optimization, suggesting that the proposed system offers a practical solution for utilizing low-grade waste heat in transportation and marine refrigeration applications.

2.3 Research gaps

Based on the literature reviewed, several research gaps remain that require further investigation to improve the efficiency and operational performance of CHP systems. These gaps are elaborated below:

- The combination of diesel engine exhaust gas as the primary heat source and solar heating system as the secondary heat source for the ORC is scant.
- The study about thermo-environmentally optimal combinations of working fluids for the ORC-VCR integrated system is scant.
- Component-wise exergy analysis of the hybrid source CHP system is scant in existing literature.
- The performance of an integrated ORC-VCR system that employs both pure and blended refrigerants in Ultra-Low-grade heat (ULGH) conditions is scant.
- The multi-objective optimization considering the exergetic performance and cooling capacity for the aforesaid integrated system is scant in literature.

2.4 Research Objectives

In light of the identified gaps and insights gleaned from the literature review, the following research objectives are outlined as follows:

1. To identify CHP systems, in predetermined parameters
2. To formulate mathematical modelling of identified CHP systems.
3. To validate the model with experimental data/reporting data and carryout parametric investigation.
4. To evaluate the performance of CHP system.
5. To perform multi-objective optimization for the CHP systems.

Along with the utilisation of the energy, exergy, and optimisation methodologies described in the following chapters, an inlet air cooler has been implemented to achieve these objectives.

CHAPTER 3 SYSTEM DESCRIPTION AND METHODOLOGY

3.1 Introduction

This chapter focuses on the description of CHP configurations that have undergone multiple analyses, followed by the mathematical modelling of each analysis. This chapter also explores the context of multi-objective optimization, which is effective for identifying an optimal set of solutions (design variables) in order to obtain optimal design and conditions.

3.2 System Description

3.2.1 Cooling, Heating, Power system

The Organic Rankine Cycle–Vapor Compression Refrigeration (ORC-VCR) system efficiently utilizes low-grade heat sources to generate electricity, provide cooling, and deliver heating simultaneously. Functioning as a Cooling, Heating, and Power (CHP) system, it enhances overall energy utilization, reduces fuel consumption, and minimizes environmental impact, promoting sustainable and integrated energy solutions.

A. Organic Rankine Cycle (ORC)

The Organic Rankine Cycle (ORC) is a thermodynamic cycle that uses organic fluids with relatively low boiling temperatures to convert low- and medium-temperature heat into mechanical or electrical energy. In contrast to the orthodox steam power cycle (Rankine Cycle) the Organic power cycle (Organic Rankine Cycle) can successfully utilize heat from sources such as biomass, industrial waste streams, geothermal reservoirs, and solar thermal systems. The use of organic working fluids allows the system to operate at lower temperatures and pressures, resulting in improved operational flexibility and enhanced heat recovery. Owing to its ability to exploit low-grade thermal energy, ORC technology has gained considerable attention for applications including power generation, combined heat and power systems, and industrial waste heat recovery. The schematic layout of the ORC system is shown in Fig. 3.1.

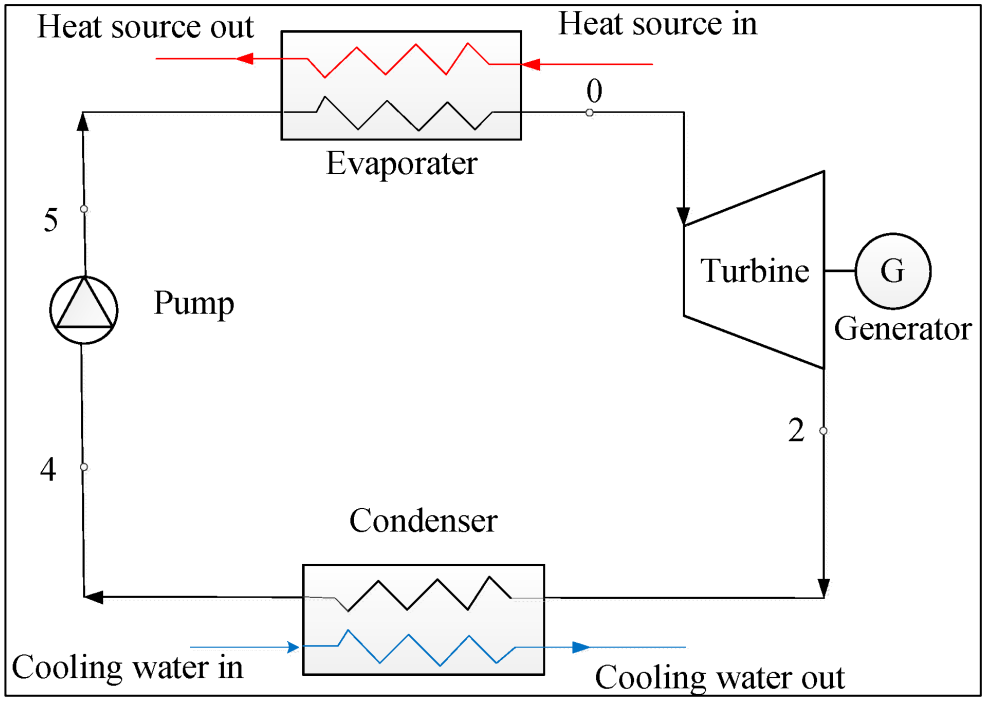

Fig. 3.1 Schematic diagram of ORC system

B. Vapor Compression Refrigeration (VCR) System

The Vapor Compression Refrigeration (VCR) system is one of the most commonly used refrigeration systems in residential, commercial, and industrial sectors. It works by circulating a refrigerant through a closed cycle, where the refrigerant absorbs heat from a low-temperature region and rejects it to the surroundings at a higher temperature. The system mainly consists of four components: a compressor, condenser, expansion valve, and evaporator. In the compressor, the refrigerant vapor is compressed to a high-pressure state before entering the condenser, where heat is released and the refrigerant changes into a liquid. The liquid refrigerant then passes through the expansion valve, which lowers its pressure and temperature. Finally, in the evaporator, the refrigerant absorbs heat from the space being cooled and evaporates, completing the cycle. Due to its simple design and dependable performance, the VCR system remains the preferred

choice for refrigeration and air-conditioning applications. Figure 3.2 shows the schematic diagram of the VCR system.

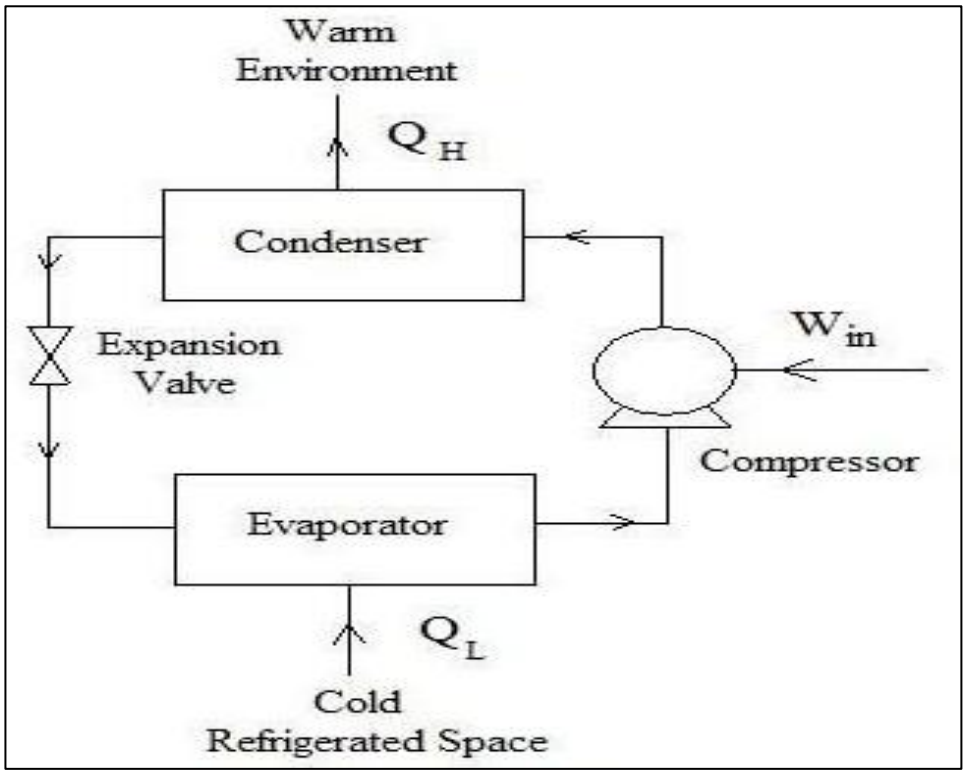

Fig. 3.2 Schematic diagram of VCR system

3.2.2 Ultra-Low-Grade Waste Heat Integrated ORC-VCR System

Figure 3.3 illustrates the layout and operating principle of the integrated ORC–VCR system. The system utilizes thermal energy supplied by an electric boiler, which is powered by a solar heating source. The solar heater delivers a constant heat input of 60 kW, providing sufficient energy to maintain the working fluid temperature within the required operating range and below its critical temperature.

In the ORC subsystem, the organic working fluid is first heated in the boiler. The high-pressure fluid then expands through the turbine (Process 2–3), producing mechanical power. During this expansion, the pressure and temperature of the fluid decrease while useful work is extracted. The fluid leaving the turbine enters the condenser, where heat is rejected to the surroundings (Process 3–4), resulting in condensation of the vapor into a liquid state.

After condensation, the liquid working fluid is pumped back to the boiler (Process 4–1). The pump increases the fluid pressure, allowing it to circulate continuously through

the cycle. This completes the ORC process and enables continuous power generation from the available thermal energy.

The VCR subsystem operates simultaneously to provide refrigeration. The refrigerant vapor is compressed in the compressor (Process 6–7), causing its pressure and temperature to rise. The high-pressure refrigerant then passes through the condenser (Process 7–8), where it releases heat to the surroundings and condenses into a liquid while maintaining nearly constant pressure.

The liquid refrigerant subsequently flows through the expansion valve (Process 8–5), where a reduction in pressure produces a corresponding drop in temperature. The low-pressure refrigerant then enters the evaporator (Process 5–6), absorbing heat from the cooling space and generating the desired refrigeration effect.

The integrated ORC–VCR system simultaneously generates power and cooling from a single energy source. The ORC converts thermal energy into mechanical work, while the VCR cycle produces refrigeration. This integration enhances overall energy utilization and is well suited for combined power and cooling applications.

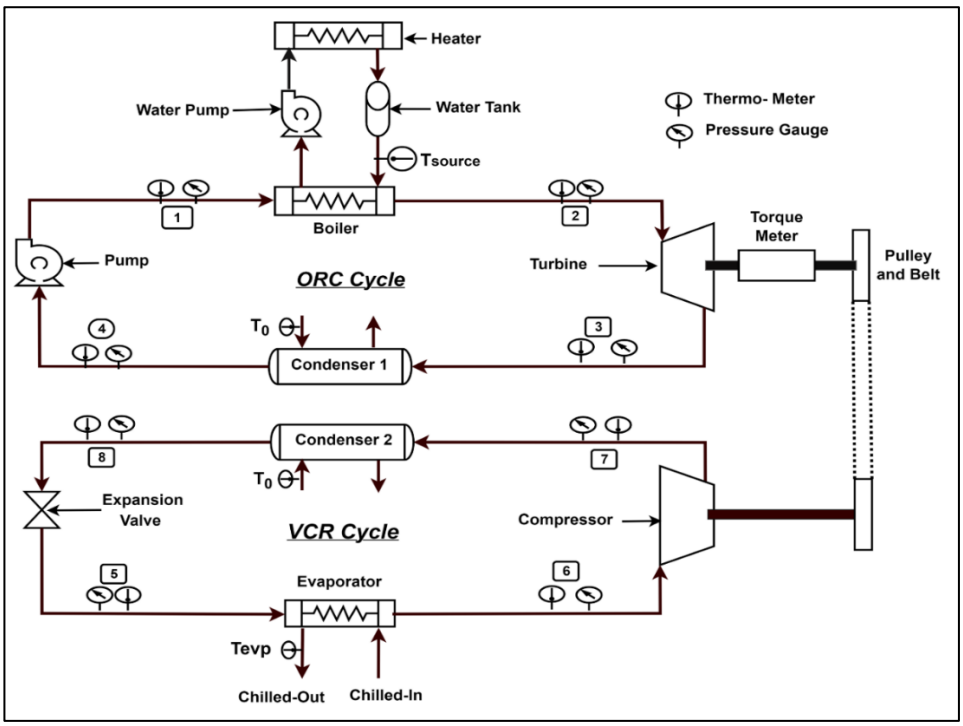

Fig. 3.3 Integrated coupled ORC-VCR system with Ultra Low-grade heat

A. OPERATING FLUIDS UTILIZED

12 The choice of working fluid plays an important role in determining the overall performance of the system. In addition to providing favorable thermodynamic performance, the fluid should meet current environmental requirements. Therefore, working fluids with low Global Warming Potential (GWP) and zero Ozone Depletion Potential (ODP) are preferred. Based on these considerations, R1234yf, R1233zd(E), and R600a were selected for the present study. These fluids offer suitable thermodynamic properties while having a comparatively lower environmental impact than many conventional refrigerants.

The key thermophysical properties, the environment, and health attributes of the selected refrigerants are summarized in Table 3.1 these properties strongly influence the cycle's thermodynamic behavior and help explain the performance differences discussed in the Results section and emphasizing their appropriateness for the ORC-VCR system. The study assesses the efficiency of these fluids in a variety of configurations within the system. Specifically, R1234yf, R1233zd(E), and R600a are employed in conjunction during the ORC and VCR cycles. The following nine configurations are investigated: *R1234yf-R1234yf, R1234yf-R1233zd(E), R1234yf-R600a, R1233zd(E)-R1234yf, R1233zd(E)-R1233zd(E), R1233zd(E)-R600a, R600a-R1234yf, R600a-R1233zd(E),* and *R600a-R600a*, as refrigerant pairs working fluids for ORC and VCR cycles, respectively.

Table 3.1 Characteristics of Refrigerants Used in the ORC-VCR System [58]

Working fluid	Chemical Formula	Thermo-Physical Properties						Environmental Data		
		M	NBP	h_{vap} at NBP	$T_{Critical}$	$P_{Critical}$	$V_{Critical}$	ODP	GWP	LFL %
		kg·mol^{-1}	K	kJ.kg^{-1}	K	kPa	m^3·kg^{-1}		100yr	
R1234yf	$C_3H_2F_4$	0.114	244.1	134	367.8	3380	0.00208	0	<1	6.2
R1233zd(E)	$C_3H_2ClF_3$	0.130	291.4	195	438.7	3573	0.00208	0	1	-
R600a	C_4H_{10}	0.058	261.4	366	407.8	3640	0.00439	0	<3	1.8
R134a	CH_2FCF_3	0.102	246.9	216	374.1	4059	0.00195	0	1430	0

3.2.3 Solar and diesel engine exhaust-driven ORC-VCR system

Fig. 3.4 shows a schematic diagram of the ORC-VCR system. It is operated by supplying heat from a hybrid source comprising of diesel engine exhaust gas and solar energy. The primary heat source, diesel engine exhaust gas is used to heat in the boiler of the Reheat ORC system which is supplied by a 4-cylinder heavy-duty diesel generator set with a rated output of 243 kW, air-fuel ratio of 19.7, and 1500 r.p.m. The temperature of diesel exhaust gas is between 690 K and 810 K, and the mass flow rate is between 0.099 kg/s and 0.38 kg/s [59].

The thermal oil cycle is added as a heat transfer medium to the boiler of the system, as depicted in Fig. 3.4 The oil tank is utilized as a cushion to reduce the impact of exhaust gas fluctuations. In addition, the thermal oil cycle maintains the working temperature of organic fluids below its critical temperature. Therminol 66 is selected as thermal oil due to its extremely high boiling point of 653 K and its non-corrosiveness towards metal [60].

The secondary heat source i.e. solar collector system is used to reheat the working fluids after they have been expanded by the High-Pressure Turbine (HPT) and before they are expanded by the Low-Pressure Turbine (LPT) in the ORC system. Due to environmental variability in solar radiation, the solar collector's heat gain varies. Consequently, a storage tank is used to store hot water for the continuous operation of the system by controlling the mass flow rate of solar water. Evacuated tube collector (ETC) [60]. system is used to maintain a temperature range of 433 K to 473 K in solar collector systems. In addition to tracking collectors, an ETC typically employs non-tracking collectors with an inclination chosen to maximize seasonal solar resource utilization.

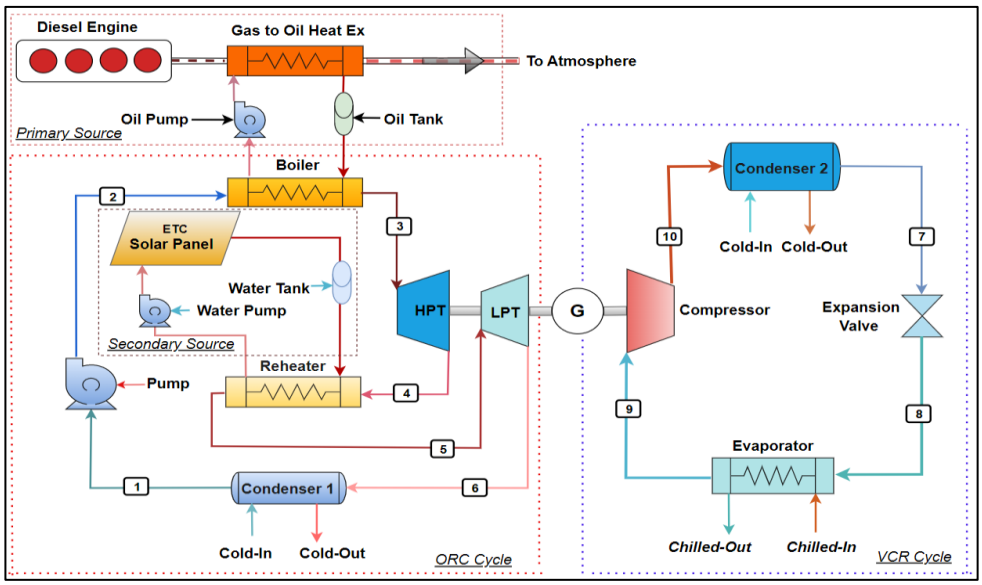

Fig. 3.4 Schematic diagram of diesel engine exhaust heat driven ORC-VCR system with solar reheat system

Fig. 3.5 represents the various processes occurring for Benzene-R1234yf working fluids utilized in the reheat ORC-VCR cycle. Process (3-4) represents actual expansion in the high-pressure turbine followed by reheating at constant pressure in the process (4-5). Process (5-6) represents the actual expansion in a low-pressure turbine. The process (6-1) represents heat transfer by the fluid to the surroundings in the condenser (cond) at constant pressure. Process (1-2) shows the pumping process in the pump. The heat is supplied to working fluids at constant pressure in the boiler from (2-3). The net-work produced by HPT and LPT is transferred to the VCR compressor via a generator.

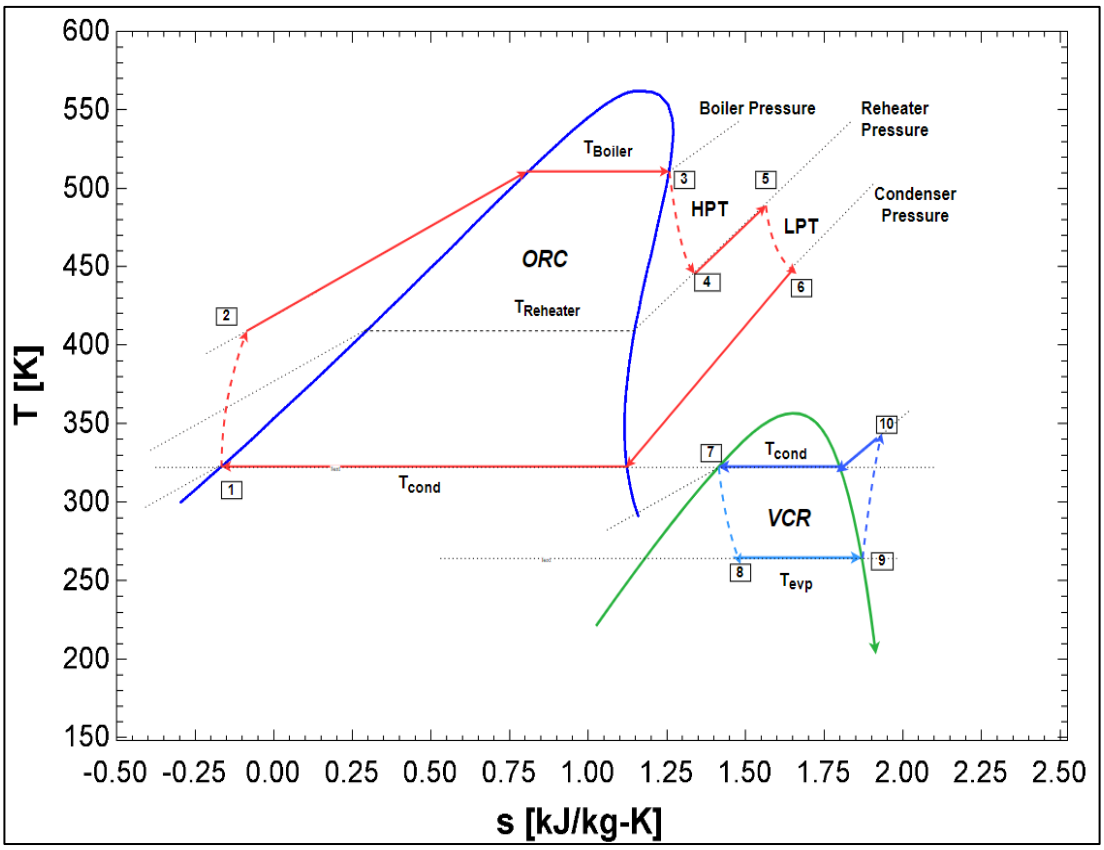

Fig. 3.5 Temperature-Entropy diagram for Benzene-R1234yf pair for reheat ORC-VCR system

In the VCR system, process (9-10) represents the actual work of the compressor, whereas process (10-7) depicts heat emission to the atmosphere at constant condenser pressure. The process represented by steps (7-8) is the isenthalpic expansion. The operation (8-9) illustrates the cooling effect of the VCR system.

This system seems advantageous, including the ability to generate electric power when cooling is not required.

A. Working fluids used in ORC-VCR system

The selection of working fluids for an ORC-VCR system is crucial, as it has a significant impact on system performance. A suitable working fluid should minimize environmental impacts while maximizing system performance. They have zero Ozone depletion potential (ODP) and exceedingly low Global warming potential (GWP) values, Hydrocarbons (HCs), Hydrofluorocarbons (HFCs), Hydrochlorofluoro-olefins (HCFOs), and Hydrofluoro-olefins (HFOs) have been considered as working fluids in this study. Table 3.2 depicts the physical, environmental, and safety data of the proposed

working fluids. Where M stands for Molar mass in kg.mol-1, NBP stands for Net boiling point in K, LFL stands for Lower flammability limit and $T_{critical}$, $P_{critical}$, and $V_{critical}$ stands for critical temperature, critical pressure, and critical volume respectively, of various refrigerants used in ORC-VCR system.

As working fluids, ORC employs Benzene and Cyclohexane and VCR utilizes R600a, R1234yf, R290, R601, and R1234zd. This is a result of the ORC operating at an exceptionally high temperature of around 550 K. Hence, within the specified parameters, only Benzene and Cyclohexane are viable working fluids; the remaining working fluids are employed in the VCR system on account of their relatively low boiling points. The investigation is focusing on different working fluid combinations, as indicated in Table 3.2 The working fluids do not undergo any mixing throughout the procedure. The combinations include Benzene-R600a, Benzene-R1234yf, Benzene-R290, Benzene-R601, Benzene-R1233zd, Cyclohexane-R600a, Cyclohexane-R1234yf, Cyclohexane-R290, Cyclohexane-R601 and Cyclohexane-R1233zd.

Table 3.2 Properties of refrigerants employed in the ORC-VCR [59]

Working fluid	**Chemical Formula**	**Physical Properties**					**Environmental Data**		
		M	**NBP**	**$T_{critical}$**	**$P_{critical}$**	**$V_{critical}$**	**ODP**	**GWP**	**LFL%**
		$kg \cdot mol^{-1}$	**K**	**K**	**kPa**	**$m^3 \cdot kg^{-1}$**		**100yr**	
Benzene	C_6H_6	0.078	353.3	562	4900	0.0032	0	LOW	1.2
Cyclohexane	C_6H_{12}	0.084	353.9	553.6	4075	0.00368	0	LOW	1.33
R600a	C_4H_{110}	0.058	261.3	408	3600	0.00436	0	3	1.8
R1234yf	$C_3H_2F_4$	0.114	243.6	370.7	3381	0.00209	0	<1	6.2
R290	C_3H_8	0.072	309	469.5	3370	0.0045	0	4	2.1
R601	CH_3-3(CH_2)-CH_3	0.044	315.1	369.7	42.5	0.00431	0	3	1.4
R1233zd	$C_3H_2ClF_3$	0.130	292	438.5	35.7	0.00208	0	1	-

3.3 Mathematical Modelling

This chapter also focuses on the mathematical model development of energy systems utilizing thermodynamics principles including the concept of exergy and economic analysis.

The thermodynamics assessment of an energy system consists of mass balance, energy balance, entropy balance, and exergy balance as detailed below.

3.3.1 Mass balance

The principle of mass conservation is a vital concept in the analysis of all thermodynamics systems. The principle is termed for a control volume, as illustrated in Fig. 3.4 in the following manner [61]:

$$\sum_k \dot{m}_i - \sum_k \dot{m}_e = \frac{dm_{CV}}{dt} \quad 3.1$$

In equation 3.1, m and $\dot{m}$ represent the mass and mass flow rate, correspondingly. The subscripts e and i indicate the exit and inlet of the control volume, respectively. The term "subscript cv" denotes the control volume.

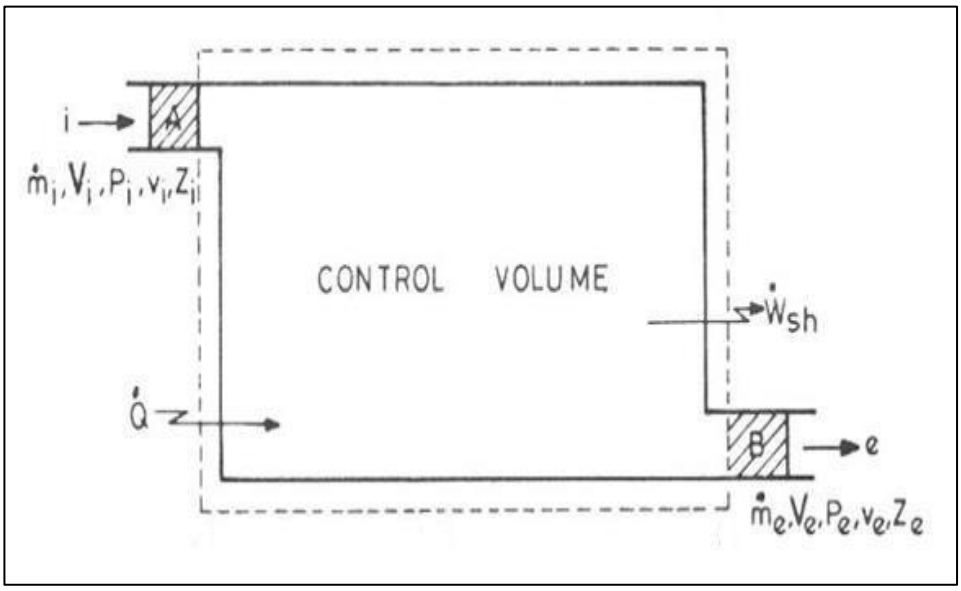

Fig. 3.6 A control volume for mass and energy balance

3.3.2 Energy Balance

The energy balance of a control volume (as shown in Fig. 3.6) pertains to the total energy inputs and outputs of a specified control volume. The 1st law of thermodynamics, also referred to as the concept of energy conservation, is described as [62]:

$$\dot{Q} - \dot{W} + \sum_i \dot{m}_i \left(h_i + \frac{V_i^2}{2} + gZ_i\right) - \sum_e \dot{m}_e \left(h_e + \frac{V_e^2}{2} + gZ_e\right) = \frac{dE_{CV}}{dt} \quad 3.2$$

Where E_{cv} represents the energy of the control volume. Q and W represent the rates at which heat and work are transferred, respectively, and t represents the time. The symbols

V, g, Z, and h represent the velocity, gravitational acceleration, elevation, and specific enthalpy, respectively.

3.3.3 Entropy Balance

Entropy in a physical system is linked to the quantification of energy that cannot be utilized (i.e., losses). These are referred to as entropy generation from a thermodynamics standpoint. The entropy generation rate ($S_{gèn}$) for a control volume can be expressed as [63]:

$$\dot{S}_{gen} = \sum_e \dot{m}_e - \sum_i \dot{m}_i s_i - \sum_k \frac{\dot{Q}}{T_k} + \frac{dS_{CV}}{dt} \tag{3.3}$$

Where s is the specific entropy and T is the temperature in Kelvin.

3.3.4 Exergy Analysis

Exergy analysis is a method of evaluating a system in a rational manner by applying the principles of the 1st and 2nd laws of thermodynamics [64]. It allows for the assessment and comparison of processes and identifies areas for improvement by reducing irreversibility on a component level [65]. The exergy of a substance is frequently classified into discrete element. The two most prevalent forms of exergy are chemical and physical. The two additional forms of exergy, kinetic and potential energy, are considered insignificant in this context due to the minor changes in elevation and comparatively low speeds [66]. The physical exergy is the highest amount of useful work that can be obtained when a system interacts with an equilibrium state. Moreover, the chemical equilibrium. It is particularly relevant in processes that include burning and other chemical transformations. Comprehensively, the exergy balance equation in control volume is written as:

$$\frac{dE_{CV}}{dt_j} = \Sigma \left(1 - \frac{T_0}{T_i}\right) \dot{Q}_i - \left(\dot{W} - P_0 \frac{dV_{CV}}{dt}\right) + \sum_i \dot{m}_i e_i - \sum_e \dot{m}_e e_e - \dot{E}x_D \tag{3.4}$$

if there is no energy exchange across the control volume. The above equation can be derived as follows [62]:

$$\dot{Ex}_Q + \sum_i \dot{m}_i e_i = \sum_e \dot{m}_e e_e + \dot{Ex}_W + \dot{Ex}_D \tag{3.5}$$

where e is the exergy and $\dot{Ex}_D$ is the rate of exergy destruction in kW.

$$\dot{Ex}_D = T_0 S_{gen} \tag{3.6}$$

$$\dot{E}x_Q = \left(1 - \frac{T_0}{T_i}\right) \dot{Q}_i \tag{3.7}$$

$$\dot{E}x_W = \dot{W} - P_0 \frac{dV_{CV}}{dt} \quad (3.8)$$

$$e_{ph} = (h - h_0) - T_0(s - s_0) \quad (3.9)$$

Where, e_{ph} is the physical exergy function to determine the exergy of any inlet or outlet stream of any component of the CHP.

3.3.5 Optimization

Optimization aims to identify the optimal values for variable that maximize or minimize a multivariate objective function while adhering to a certain set of constraints. Constraints provide the boundaries of a search space, sometimes referred to as the feasible region, in the initial step in every optimization problem. It is necessary to incorporate all subsystems that have an impact on the performance of the system. When the system becomes excessively intricate, it is frequently preferable to breakdown it into smaller subsystems. The objective function, constraints, and decision variable are all vital components of an optimization problem [67].

A. Objective Function

In mathematical optimization problems, the objective function is a real-valued function that must be maximized or minimized with respect to the set of feasible alternatives. The objective function is determined by the decision maker's desire or goal. Considering the energy systems, the objective function can be based on the performance (Energy or exergy efficiency and COP), Cost (Cost of exergy destruction, investment cost, and total cost), and environmental standpoint (emissions, fuel utilization), etc. [68].

When there are more than objective functions that are to be maximized or minimized utilizing the same constraints, this type of problem is known as multi-objective optimization [69].

B. Decision variables and constraints

Another crucial aspect in defining an optimization problem is the choice of independent decision variables that accurately represent the potential design possibilities. In order to choose these decision variables, it is crucial to incorporate all significant parameters that might impact the system's performance and cost factor, and exclude variables that have less relevance.

The constraints in a specific design challenge are imposed by limitations on the ranges of the operating parameters, the need to satisfy basic conservation principles, and other limitations. The optimization problems are also addressed by utilizing the restrictions in the form of the search space of operational parameters [70].

C. Optimization Techniques

There are several techniques to solve the optimization problems as described below:

i. Classical Techniques

The classical optimization method is a basic problem-solving technique for continuous and differentiable functions. It is convenient in the determination of the maximum and minimum of unconstrained differentiable functions. However, these methods have limited use in practical applications as in real life the continuous functions are not so frequent [71].

ii. Numerical Methods

There are several numerical methods based on optimization techniques described below:

iii. Linear programming

Optimization problems where the objective function is linear and the solution space is defined by linear equalities and inequalities.

iv. Integer programming

Optimization problems where the solution set has at least one integer in it.

v. Nonlinear programming

Optimization problems in which the objective function or constraints or both encompass nonlinear terms of decision variables.

vi. Stochastic programming

Optimization problems in which some of the constraints depend on random variables.

D. Evolutionary algorithms

An evolutionary algorithm employs methodologies that draw inspiration from biological processes such as selection, mutation, recombination, and reproduction [72]. Candidate solutions to the optimization problem are represented as members of a population, and their "living environment" is determined by the fitness function. Fuzzy logic, genetic algorithms (GAs), and artificial neural networks (ANNs) are all examples of

evolutionary algorithm methodologies [73]. These methods are elaborated upon in greater detail below.

E. Genetic algorithms (GA)

A genetic algorithm is a search methodology that utilizes evolutionary principles, such as inheritance, learning, selection, and mutation, to find an ideal answer. The process starts by establishing a group of potential solutions referred to as people. It then advances through successive generations, with the evaluation of each individual's fitness. Fitness is determined by the goal function. After, many individuals are chosen from the present generation according to their fitness and altered to create a fresh population. The subsequent iteration utilizes this updated population, enabling the algorithm to advance toward the intended optimum point [74].

3.3.6 Multi-objective optimization

The selection of optimum operating conditions depends on the objective function considered in the analysis. This technique is very useful for the optimization of operating parameters. In real-world applications, however, multiple performance standards are usually taken into account simultaneously. The progress of thermal and energy systems usually focuses on refining efficiency, enhancing output and production capacity, preserving product superiority, and maximizing heat-transfer effectiveness while simultaneously lessening energy consumption, operating spending, and environmental influences. The objective function for a problem can be any of these, however, it is typically more relevant and valuable to consider several objectives. A single-objective optimization issue involves finding the optimal value for a single objective function. Multi-objective optimization refers to the process of optimizing several objective functions. A popular method for minimizing or maximizing numerous goal functions is to merge them into a single function. For illustration, maximizing heat transfer rate is important when designing heat exchangers and cooling systems for electronic equipment [75]. Nevertheless, this leads to increased fluid flow rates and pressure losses due to friction. In recent years, there has been significant attention directed toward multi-objective optimization as an additional approach. This method involves the consideration of two or more relevant objective functions for a given

problem, followed by developing a strategy to balance or trade-off each objective function in relation to the others [76].

3.4 Analysis of the CHP System

The CHP system has undergone energy and exergy analysis, further, the Multi objective optimization has also been performed to evaluate avoidable and unavoidable cost factors of system.

3.4.1 Assumptions

- The system operates in a steady state
- The loss of heat from connecting pipelines and components (except heat exchangers) and changes in potential and kinetic energy are regarded as insignificant.
- The fluid that operates from the condenser (both ORC & VCR) exits in saturated liquid state.

3.4.2 Analysis of Ultra-Low-Grade Waste Heat Integrated ORC-VCR System

A. ENERGY ANALYSIS

In accordance with the stated assumptions [77], each component of the system is represented by its balance equations for energy and mass rate in Table 3.3. Equation (3.10) represents the balanced mass flow rate, while Equation (3.11) represents the energy balance.

$$\sum \dot{m}_{in} = \sum \dot{m}_{out} \tag{3.10}$$

$$\dot{Q} + \dot{W} = \sum \dot{m}_{out}\, h_{out} - \sum \dot{m}_{in}\, h_{in} \tag{3.11}$$

B. EXERGY ANALYSIS

Compared to first-law analysis, exergy-based analysis provides a more sophisticated and efficient methodology for improving thermal energy conversion systems. Through the identification of significant energy losses, exergy analysis contributes to the enhancement of both individual components and overall system performance [78]. Table 3.4, based on the assumptions previously stated, delineates the exergetic balance equations for each component within the system. Two primary indicators used to assess the system's exergetic performance are the exergy destruction rate ($\dot{E}x_d$) and the exergetic efficiency ($\dot{\eta}_{ex}$) [79]. A thorough exergy balance must be conducted on each component of the system in order to ascertain these metrics [80].

Equations (3.12) through (3.15) present the formulations used to calculate exergy destruction and exergetic efficiency.

$$\dot{E}x_d = \sum \dot{m}_{in} e_{in} - \sum \dot{m}_{out} e_{out} - \dot{E}x_w + \dot{E}x_Q \quad (3.12)$$

In equation (3.12), $\dot{E}_d$ represents the exergy destruction rate [81] in kW, while, e_{in} and e_{out} denote the inlet and outlet specific exergy in kJ/kg, respectively. Similarly, $\dot{m}_{in}$ and $\dot{m}_{out}$ correspond to the mass flow rates at the inlet and outlet, respectively. Furthermore, $\dot{E}_Q$ and $\dot{W}$ represent across the control volume boundaries, the exergy rates associated with heat transfer and work is measured in kW.

$$\dot{E}x_Q = \sum \left(1 - \frac{T_0}{T_{in}}\right) \dot{Q}_{in} \quad (3.13)$$

In equation (3.13), $\dot{E}x_Q$ represents the rate of exergy associated with the transfer of heat in kW, T_0 denotes the ambient temperature in K, and T_{in} refers to the temperature at the component boundary in K. Additionally, $\dot{Q}_{in}$ Signifies the rate of heat transfer to the system in kW.

Physical, potential, chemical, and kinetic exergies are the four components of specific exergy. Nevertheless, the kinetic and potential exergies are negligible. Additionally, the chemical exergy term is neglected due to the absence of chemical material transfer between the system and its environment [82]. Accordingly, this analysis accounts only for physical exergy. The precise exergy of any given point i, Ex_i, has the following definition:

$$Ex_i = (h_i - h_0) - T_0(s_i - s_0) \quad (3.14)$$

In equation (3.14), s_i and h_i Is the specific entropy and enthalpy at point i, respectively. The total Irreversibility of the ORC-VCR system ($\dot{E}x_{Total,system}$), can be determined using equation (3.15).

$$\dot{E}x_{Total,system} = \sum_i \dot{E}x_d \quad (3.15)$$

In equation (3.16), where, $\dot{E}x_{product}$ and $\dot{E}x_{in}$ Can be calculated from the equations (3.16) & (3.17) below:

$$\dot{E}x_{product} = \dot{Q}_{evp} \times \left[\left(\frac{T_0}{T_{evp}}\right) - 1\right] \quad (3.16)$$

$$\dot{E}x_{in} = \dot{Q}_{boiler} \times \left[1 - \left(\frac{T_0}{T_{boiler}}\right)\right] \quad (3.17)$$

The exergetic efficiency of the system can be calculated from equation (3.18) as given below.

$$\dot{\eta}_{ex,system} = \frac{\dot{E}x_{product}}{\dot{E}x_{in}} \quad (3.18)$$

The exergetic efficiency and exergetic performance of the ORC-VCR system are evaluated by applying the aforementioned equations to its various components. In order to evaluate the influence of numerous operational parameters on the ORC-VCR system's functionality, a simulation study was implemented.

The analysis examines the impact of these configurations on the thermodynamic performance of the system. The study endeavours to determine the most environmentally sustainable and efficient combination by evaluating the interaction between the working fluids in the ORC and VCR cycles. This thorough assessment is indispensable for the development of the viability of the CHP systems in a variety of applications, thereby encouragement both ecological accountability and operational efficiency.

Table 3.3 Designed equations for energy for all parameter

Parameter	Equations
Boiler Heat	$\dot{Q}_{boiler} = \dot{m}_{ORC} \times (h_2 - h_1)$ $= \dot{m}_{water} \times c_{p,water} \times (t_{water,in} - t_{water,out})$
Pump Work	$\dot{W}_{pump} = \dot{m}_{ORC} \times (h_1 - h_4)$
Turbine Work	$\dot{W}_{Tur} = \dot{m}_{ORC} \times (h_2 - h_3)$
ORC condenser Heat	$\dot{Q}_{ORC,cond} = \dot{m}_{ORC} \times (h_3 - h_4)$
VCR condenser Heat	$\dot{Q}_{VCR,cond} = \dot{m}_{VCR} \times (h_7 - h_8)$
Compressor work	$\dot{W}_{comp} = \dot{W}_{Tur} - \dot{W}_{pump}$
Expansion Valve enthalpy	$h_5 = h_8$
Evaporator Heat	$\dot{Q}_{evp} = \dot{m}_{VCR} \times (h_6 - h_5)$
COP_{system}	$COP_{system} = \frac{\dot{Q}_{evp}}{(\dot{Q}_{boiler})}$
Power cycle efficiency (η_{pl})	$\eta_{pl} = \frac{\dot{W}_{Tur} - \dot{W}_{pump}}{\dot{Q}_{boiler}}$
COP_{VCR}	$COP_{VCR} = \frac{\dot{Q}_{evp}}{\dot{W}_{comp}}$
BWP	$BWP = \frac{\dot{W}_{pump}}{\dot{W}_{Tur}}$

Table 3.4 The exergy equations of each component in the system

Components	Equations
Boiler	$\dot{E}x_{d,boiler} = \dot{E}x_1 - \dot{E}_2 + \dot{E}_{Q,boiler}$
Compressor	$\dot{E}x_{d,comp} = \dot{E}x_6 - \dot{E}x_7 + \dot{E}x_{W,comp}$
Turbine	$\dot{E}x_{d,Tur} = \dot{E}x_2 - \dot{E}x_3 - \dot{E}x_{W,Tur}$
ORC Condenser	$\dot{E}x_{d,cond,ORC} = \dot{E}x_3 - \dot{E}x_4 - \dot{E}x_{Q,cond,ORC}$
VCR Condenser	$\dot{E}x_{d,cond,VCR} = \dot{E}x_7 - \dot{E}x_8 - \dot{E}x_{Q,cond,VCR}$
Pump	$\dot{E}x_{d,pump} = \dot{E}x_4 - \dot{E}x_1 + \dot{E}x_{w,pump}$
Expansion Valve	$\dot{E}x_{d,exp} = \dot{E}x_8 - \dot{E}x_5$

Evaporator	$\dot{E}x_{d,evp} = \dot{E}x_5 - \dot{E}x_6 + \dot{E}_{Q,evp}$

C. MULTI-OBJECTIVE OPTIMIZATION USING GENETIC ALGORITHM (MOGA)

Obtaining the best solution in a multi-objective optimization problem is often challenging because several performance goals must be considered at the same time. The complexity and nonlinear characteristics of such problems make metaheuristic algorithms suitable and dependable tools of optimization. Amid these, the Multi-Objective Genetic Algorithm (MOGA) is broadly used because of its ability to handle multiple and often contradictory objectives efficiently [83]. In many engineering applications, refining one objective may adversely affect another, making it difficult to identify a single best solution. So, optimization studies commonly generate a set of Pareto-optimal solutions. A solution is classified as non-dominated when improving one objective predictable result in a reduction in the performance of at least one of the remaining objectives. The Pareto front provides decision-makers with several possible alternatives, allowing them to select a solution that best satisfies their specific design requirements and priorities [84].

A computational model was developed in MATLAB to evaluate the system performance based on the principles of the first and second laws of thermodynamics. The program was used to calculate and analyze the relevant thermodynamic parameters under different operating conditions. For a consistent analysis, the input data provided in Table 3.5 were utilized to calculate the exergy-based performance metrics of each component as well as the overall ORC-VCR system, which was subsequently subjected to further optimization.

Table 3.5 Simulation input parameters

Parameter	Value
Refrigerant ORC	R1234zd(E)
Refrigerant VCR	R1234zd(E)
Heater load (Q_{heater}) (kW)	60
Heater outlet temperature (K)	348
Heater inlet Temperature (K)	343
Turbine inlet Temperature T_2 (K)	343
Boiler outlet Temperature T_2 (K)	343
Boiler inlet Temperature T_1 (K)	305
Isentropic efficiency of Pump (%)	80
Isentropic Efficiency of Turbine (%)	90
Isentropic Efficiency of Compressor (%)	70
Effectiveness of heat exchanger (%)	95
Evaporator temperature T_{evp} (K)	273
Condenser temperature T_4, T_8 (K)	305
Condenser Outlet quality	Liquid (x=0)
Evaporator Outlet quality	Saturated vapor (x=1)
Ambient Temperature T_0 (K)	300
Ambient Pressure (kPa)	101.3

3.4.3 Solar and diesel engine exhaust-driven ORC-VCR system

A. Exergy analysis

The exergy-based analysis of any thermal energy conversion system is a more advanced and effective method for the improvement of the system than the first law-based analysis than the first law-based analysis. Exergy analysis identifies areas where significant energy degradation is taking place. Therefore, it assists in improving the exergetic performance at the component level as well as of the entire system [85]. Table 3.6 provides the exergy equations for each component of the ORC-VCR system based on the assumptions mentioned above. Exergy destruction rate ($\dot{E}x_d$) and exergetic system

efficiency ($\dot{\eta}_{ex}$) [86] are the two most important factors for evaluating the exergetic performance of an ORC-VCR system. To evaluate exergy destruction and exergetic efficiency these exergy terms, and exergy balance must be performed for each component of the system [87].

Table 3.6 Exergy equations of each component in the ORC-VCR system

Components	Equations
Compressor	$\dot{E}x_{d,comp} = \dot{E}x_9 - \dot{E}x_{10} + \dot{E}x_{W,comp}$
Boiler	$\dot{E}x_{d,boiler} = \dot{E}x_2 - \dot{E}_3 + \dot{E}_{Q,boiler}$
Reheater	$\dot{E}x_{d,reheater} = \dot{E}x_4 - \dot{E}x_5 + \dot{E}x_{Q,reheater}$
High Pressure Turbine	$\dot{E}x_{d,HPT} = \dot{E}x_3 - \dot{E}x_4 - \dot{E}x_{W,HPT}$
Low-pressure Turbine	$\dot{E}x_{d,LPT} = \dot{E}x_5 - \dot{E}x_6 - \dot{E}x_{W,LPT}$
ORC Condenser	$\dot{E}x_{d,cond,ORC} = \dot{E}x_6 - \dot{E}x_1 - \dot{E}x_{Q,cond,ORC}$
VCR Condenser	$\dot{E}x_{d,cond,VCC} = \dot{E}x_{10} - \dot{E}x_7 - \dot{E}x_{Q,cond,VCC}$
Pump	$\dot{E}x_{d,pump} = \dot{E}x_1 - \dot{E}x_2 + \dot{E}x_{w,pump}$
Expansion Valve	$\dot{E}x_{d,exp} = \dot{E}x_7 - \dot{E}x_8$
Evaporator	$\dot{E}x_{d,evp} = \dot{E}x_8 - \dot{E}x_9 + \dot{E}_{Q,evp}$

B. Multi-objective Optimization for Solar and diesel engine exhaust-driven ORC-VCR system

To function effectively, the operating and design parameters of the system utilizing the ORC-VCR must be optimized. The $T_{HPT,in}$, $T_{LPT,in}$, T_{evp}, and T_{cond} are experiential to affect both the energy and exergy performance of ORC-VCR based on the above parametric investigation. Moreover, the cooling capacity and exergetic efficiency are the chosen performance parameters. These performance parameters were chosen because cooling capacity is an indicator of the design requirement of the refrigeration plant and exergetic efficiency is preferred to provide a thermodynamics viewpoint of the system. An increase in both aforementioned parameters is desirable. Therefore, both have to be maximized to obtain optimality.

To obtain the summarized actual equations for cooling capacity and exergetic efficiency, the Design Expert software [86] is utilized to conduct the regression analysis. The regression analysis input variables and their respective ranges are $T_{HPT,in}$ (450 K to 550 K), $T_{LPT,in}$ (423 K to 463 K), T_{cond} (308 K to 323 K), and T_{evp} (268 K to 283 K). The software Design Expert was used to test three distinct regression models: linear, 2FI, and quadratic [87]. In addition, each regression model employs three terms: predicted R^2 (R_p^2), adjusted R^2 (R_a^2), and adequate precision (AP). The greater the difference between (R_p^2) and (R_a^2), the greater the AP value, which indicates a more accurate regression model. If a model's AP value is less than 4, further examination is not recommended [88]. As demonstrated in Table 3.7, the quadratic model is superior for regression analysis, as its accuracy is the highest among all models.

Table 3.7 Statistical information regarding various regression models [89]

Performance Factor	Linear			2FI			Quadratic		
	R_a^2	R_p^2	AP	R_a^2	R_p^2	AP	R_a^2	R_p^2	AP
Cooling capacity (Q_c)	0.93	0.92	37.29	0.96	0.92	31.51	0.99	0.98	61.88
Exergetic Efficiency (η_{ex})	0.96	0.94	41.63	0.95	0.89	25.56	0.99	0.99	178.71

Based on the selected quadratic regression model, a pair of equations ((Eqs. 3.19) and (Eqs. 3.20)) are derived for both performance parameters.

$$\begin{aligned} Q_c = &-170.499 + 0.129843 \times T_{HPT,in} + 0.248833 \times T_{LPT,in} - 1.26053 \times T_{cond} \\ &+ 2.24539 \times T_{evp} - 0.000030 \times T_{HPT,in} \times T_{LPT,in} \\ &- 0.000713 \times T_{HPT,in} \times T_{cond} + 0.001073 \times T_{HPT,in} \times T_{evp} \\ &- 0.001067 \times T_{LPT,in} \times T_{cond} + 0.00075 \times T_{LPT,in} \times T_{evp} \\ &- 0.037244 \times T_{cond} \times T_{evp} - 0.000155 \times T_{HPT,in}^2 \\ &- 0.000092 \times T_{LPT,in}^2 + 0.018459 \times T_{cond}^2 + 0.016837 \times T_{evp}^2 \end{aligned} \quad (3.19)$$

$$\begin{aligned}\eta_{ex} = {} & 822.49780 + 0.802289 \times T_{HPT,in} - 0.138538 \times T_{LPT,in} \\ & - 10.54080 \times \mathrm{T_{cond}} + 5.96932 \times \mathrm{T_{evp}} \\ & - 0.000077 \times T_{HPT,in} \times T_{LPT,in} - 0.001053 \times T_{HPT,in} \times \mathrm{T_{cond}} \\ & - 0.000627 \times T_{HPT,in} \times \mathrm{T_{evp}} + 0.000317 \times T_{LPT,in} \times \mathrm{T_{cond}} \\ & + 0.000267 \times T_{LPT,in} \times \mathrm{T_{evp}} - 0.001333 \times \mathrm{T_{cond}} \times \mathrm{T_{evp}} \\ & - 0.000223 \times T_{HPT,in}^2 - 0.000015 \times T_{LPT,in}^2 + 0.016852 \times \mathrm{T_{cond}^2} \\ & - 0.010193 \times \mathrm{T_{evp}^2}\end{aligned} \tag{3.20}$$

These equations are subsequently implemented for optimization. Cooling capacity and exergetic efficiency comprise the objective function. The aforementioned concern is then resolved by employing multi-objective optimization by using a genetic algorithm (MOGA) [90]. MOGA is a metaheuristic technique that generates a large variety of solutions that seek to provide all possible trade-offs between two or more objective functions. Consequently, Pareto optimality has been achieved. During the execution of the genetic algorithm [83] the following parameters were selected: population size of 200, crossover probability of 0.8, and Pareto front population percentage of 0.35. In addition, the used selection function is 'tournament' with a size of 2 and 'intermediate' crossover functions.

CHAPTER 4 MODEL VALIDATION

4.1 Introduction

Validating the numerical model for this system is essential to avoid discrepancies and attain trust in the precision of the results. The study results have been validated by prior experimental experiments that have been published. The CHP model have been validated by experimental and analytical findings from several studies.

4.2 Validation of Ultra-Low-Grade Waste Heat Integrated ORC-VCR System

Fig 4.1 illustrates the block layout of an actual ORC-VCR system. The system comprises two cycles, one is Organic Rankine Cycle and second is Vapour Compression Cycle, to ensure accuracy and eliminate uncertainties, it is imperative to verify the numerical model that was created for the system. For this purpose, the ORC-VCR model is compared to the experimental results reported by Sleiti et al. [58]. Their experimental setup consisted of an integrated ORC-VCR unit powered by a 60-kW heat input at 348 K, employing R134a as the working fluid in both cycles. The experimental setup consisted of a turbine, compressor, boiler, condenser, and evaporator arranged in a configuration similar to that used in the present study. This work was selected for model validation because it examined the performance of an ORC–VCR system operating with ultra-low-grade heat sources under conditions comparable to those considered in the current analysis. As a result, it provided a suitable reference for assessing the accuracy of the numerical model. The validation is conducted under identical operating conditions, including a heat input of 60 kW, mass flow rate of water is taken as 2.86 $kg.s^{-1}$ in heater, a heat source temperature in the range of 338 K to 358 K, a condenser outlet temperature of 298 K, an evaporator pressure of 200 kPa, and an evaporator outlet fluid dryness fraction (X) of 1. Furthermore, the validation is conducted using the same working refrigerant pair (R134a-R134a) and consistent isentropic efficiencies for the pump (80%), turbine (90%), and compressor (70%).

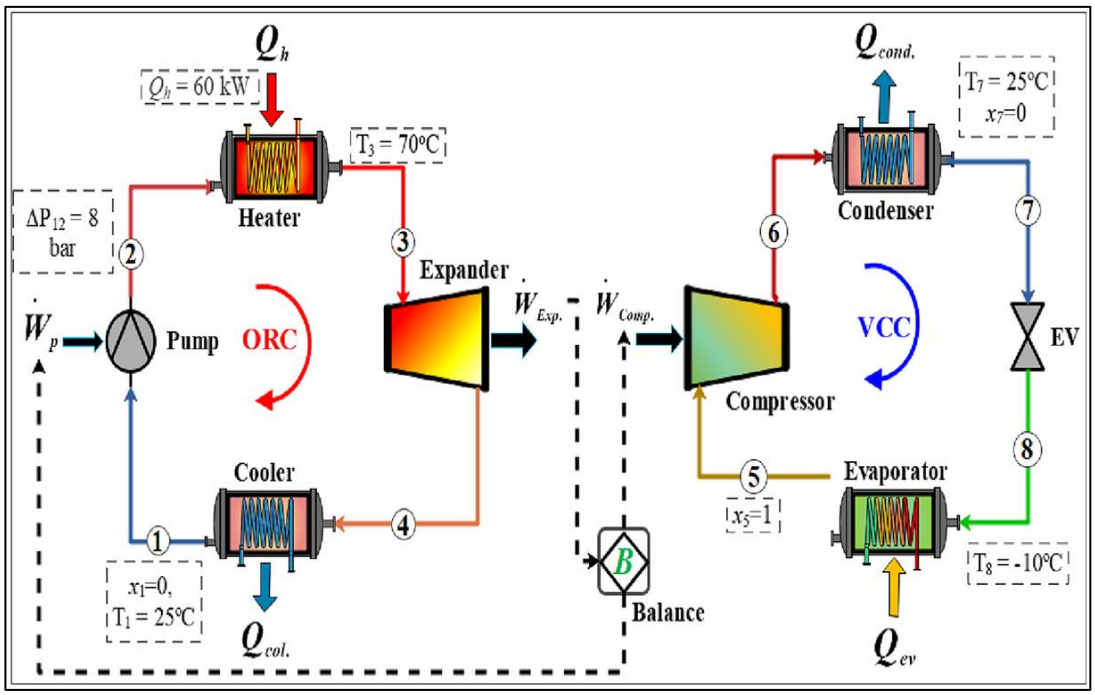

Fig. 4.1 Experiment setup of Ultra-Low-Grade Waste Heat Integrated ORC-VCR System

Fig. 4.2 illustrates the comparison between the results obtained from the present model and the experimental findings of Sleiti et al. [24]. The calculated energy efficiency (Power loop efficiency, η_{pl})(Color: Black), Co-efficient of performance of VCR system (COP_{VCR}) (Colour: Red) and Back Work Ratio (BWR) (Colour: Green) of system demonstrate strong agreement with the results of Sleiti et al. [24], with minimum deviance of 3.97 % in power loop efficiency at 75 °C source temperature and maximum deviance of 19.48 % in the BWR at 85 °C source temperature. Theoretical results deviate from experimental findings due to assumptions and ideal conditions considered during analysis.

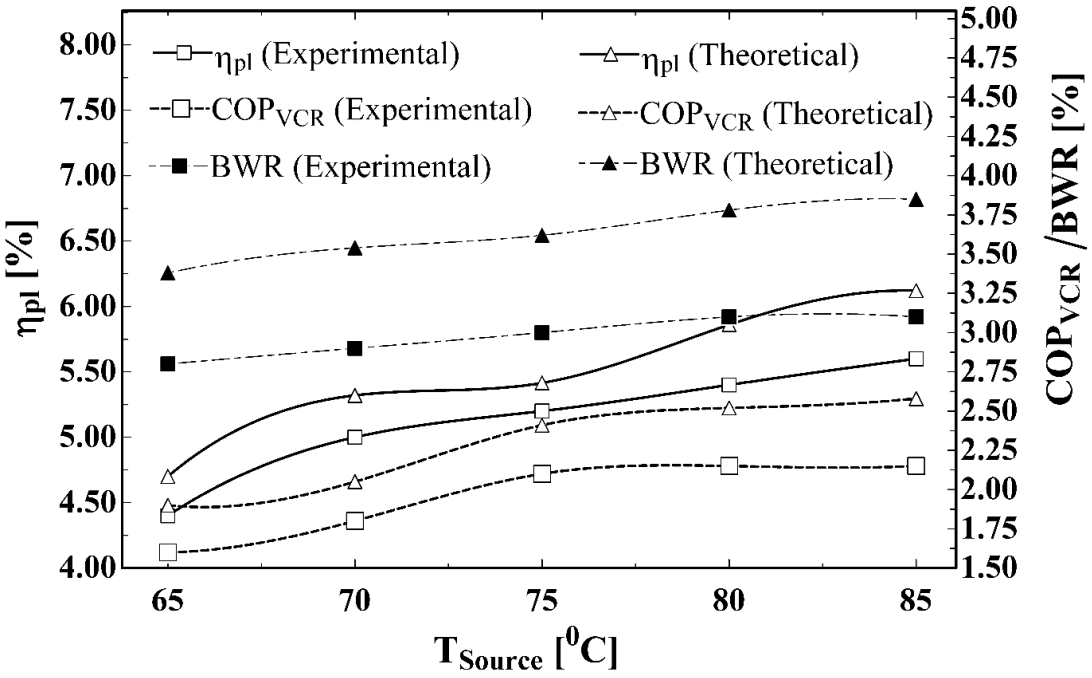

Fig. 4.2 Comparison of the results of the current investigation with those of Sleiti et al.[58]

4.3 Validation of Solar and diesel engine exhaust-driven ORC-VCR system

Fig 4.3 illustrates the block layout of a theoretical ORC-VCR system. The system comprises two cycles, one is Organic Rankine Cycle and second is Vapour Compression Cycle, to ensure accuracy and eliminate uncertainties, it is imperative to verify the numerical model that was created for the system. For this purpose, the ORC-VCR model is compared to the It is essential to compare the numerical model developed for the ORC-VCR system to eliminate ambiguities and instill confidence in the accuracy of the results. The ORC-VCR model examined in this study is compared with the previously reported results of Bao et al. [91], for the same operating conditions (i.e. heat supplied to the system = 4852 kW, heat source temperature of 413 K, condenser temperature of 308 K, and evaporator temperature of 278 K), the identical working fluid (R290), and the identical isentropic efficiencies of the pump, turbine, and compressor (85%, 85%, and 80%, respectively).

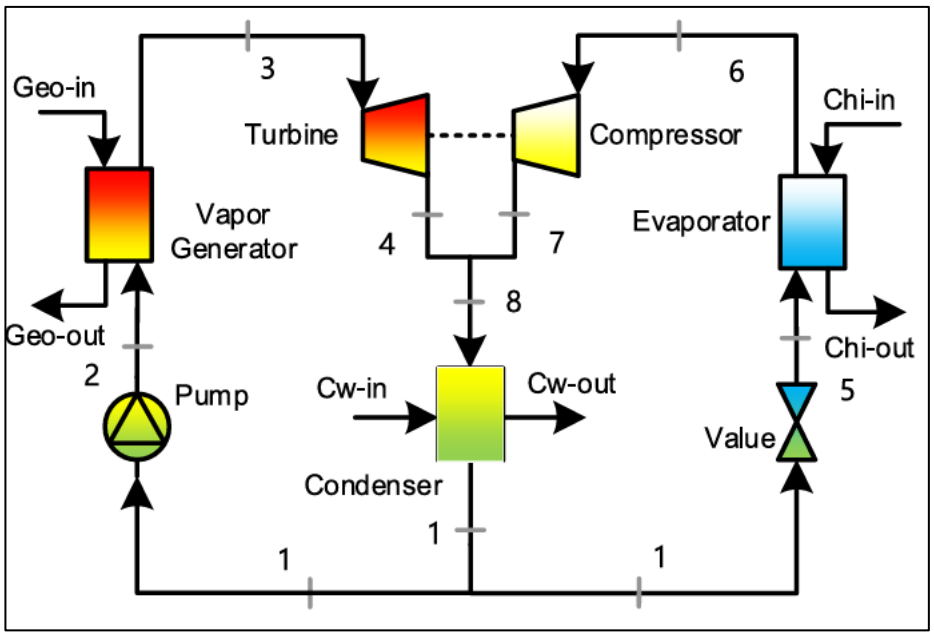

Fig. 4.3 Schematic diagram of ORC-VCR system proposed by Bao et al. [91]

Error! Reference source not found..1 shows the comparison of results obtained from the present model with those of Bao et al. [24]. The COP_{sys}, exergetic efficiency, and heat absorbed by the evaporator calculated for the present system exhibit a good agreement with the results of Bao et al. [24] with a maximum deviation of 1.82% in exergetic efficiency.

Table 4. 1 Comparison of results for present work with the results of Bao et al [91].

Parameter	Current study	Bao et al.[24]	Relative Error (%)
COPsys	0.3428	0.34	0.82
η_{ex} **(%)**	21.61	22	(-)1.82
Qevp (kW)	1651	1650	0.1

4.4 Discussion on Model Reliability

The validation study validates that the numerical model can consistently estimate the performance of the CHP system under different operating conditions. The close correspondence between the foreseen results and the available experimental and

published data supports the accuracy of the model and confirms its suitability for subsequent parametric investigations and optimization analyses.

4.5 Summary

This chapter focused on validating the developed Cooling, Heating, and Power numerical model by comparing its predictions with available reference data. The satisfactory agreement obtained through the validation process demonstrates the reliability of the model and supports its use for further performance analysis and optimization of the system.

CHAPTER 5 RESULTS AND DISCUSSION

5.1 Introduction

To enhance understanding of the system's performance, it is essential to conduct numerous investigations to evaluate how the performance of CHP varies under different operating conditions. This chapter provides an explanation of the results pertaining to energy, exergy, sustainability, and multi-objective optimization. Exergy analysis is employed to investigate different thermal processes, particularly exergetic efficiency in the CHP system, and can provide valuable insights for devising strategies and guidelines to enhance energy efficiency and effectiveness. The exergy analysis involves calculating the rate at which exergy is being destroyed and the exergy efficiency of each section in the CHP. It also estimates the total exergy efficiency of the CHP system. Exergy analysis is convenient for determining and measuring the origin of inefficiencies in the systems, specifically related to each component. The exergy-based sustainability assessment of the system evaluates and analyses various sustainability indicators of a standalone CHP and an integrated CHP to determine fuel utilization. In addition, the exergo-economic analysis demonstrates the use of the exergy costing approach to evaluate the rate at which exergy is destroyed, as well as the cost of investment for each component and how it changes with different operational parameters.

By utilizing optimization, the most advantageous compromises between the CHP system's numerous operating parameters can be determined. The presence of COP_{sys} and efficiency in the systems renders a single objective optimization strategy incapable of generating an exact optimal solution. An outcome of this is the implementation of a multi-objective optimization strategy on the system.

This chapter explores several output key parameters. The performance parameters include COP_{sys}, overall exergy efficiency, and total exergy destruction rate, and evaporator heat. In addition, a thorough parametric analysis is undertaken to improve the comprehension of the system's performance. This study examines the effects of varying various key design parameters on the system's performance. The use of a multi-

objective genetic algorithm optimisation technique allows for the determination of the most optimal design parameters by establishing specific objective functions.

5.2 PARAMETRIC ANALYSIS

We present the results of a parametric investigation that is based on energy and exergy, and it is based on the modulation of several operating parameters. Parameters that are assessed include the temperature of the source (T_{source}), Ambient temperature (T_0) and Evaporator Temperature (T_{evp}).

5.2.1 Ultra-Low-Grade Waste Heat Integrated ORC-VCR System

The input data used for simulation is presented in Table 5.1. In two sections, the outcomes of the energy and exergy analyses are presented: (i) parametric investigation and (ii) multi-objective optimization. In order to conduct a systematic assessment of a variety of performance indicators, a program was created using Engineering Equation Solver (EES), which implements the first and second thermodynamic laws. Utilizing the input data, which has been furnished in 5.1, the energy- and exergy-related performance metrics of the ORC-VCR system were calculated. It is also important to note that, as specified in Table 5.1, the condensers of both cycles are designed to operate at the same temperature.

Table 5.1 Input data used for analysis for ULGH integrated ORC-VCR system

Parameter	Value
Refrigerant ORC	R1234zd(E)
Refrigerant VCR	R1234zd(E)
Heater load (Q_{heater}) (kW)	60
Heater outlet temperature (K)	348
Heater inlet Temperature (K)	343
Turbine inlet Temperature T_2 (K)	343
Boiler outlet Temperature T_2 (K)	343
Boiler inlet Temperature T_1 (K)	305
Isentropic efficiency of Pump (%)	80
Isentropic Efficiency of Turbine (%)	90
Isentropic Efficiency of Compressor (%)	70
Effectiveness of heat exchanger (%)	95
Evaporator temperature T_{evp} (K)	273
Condenser temperature T_4, T_8 (K)	305
Condenser Outlet quality	Liquid (x=0)
Evaporator Outlet quality	Saturated vapor (x=1)
Ambient Temperature T_0 (K)	300
Ambient Pressure (kPa)	101.3

Using the baseline input data for the VCR cycle, the cooling capacity for the refrigerant pair R1234zd(E)-R1234zd(E) is calculated to be 16.02 kW (equivalent to 4.56 TR). The VCR cycle achieves a coefficient of performance (COP) of 4.45, while the efficiency of the power loop is found to be 7.00%. In the combined ORC-VCR system, the heater absorbs heat from waste heat sources, notably a solar heater. As a result, the system's operational costs are minimal and can be considered negligible.
In contrast, the same level of heat absorption could be achieved with a conventional vapor compression refrigeration system, but the associated electricity expenses would be substantial.

Table 5.2 shows the exergy destruction rates for the different components of the ORC-VCR system under the given input conditions. The turbine exhibits the highest exergy destruction (4.47 kW), followed by the evaporator (3.17 kW) and the ORC condenser (1.77 kW). The significant exergy losses in the turbine are primarily attributed to irreversibilities associated with expansion processes, such as isentropic inefficiency and pressure losses. Similarly, high exergy destruction in the evaporator results from heat transfer across a large temperature difference, which inherently increases irreversibility.

The ORC condenser signifies another source of exergy destruction, due to the thermal discrepancy between the refrigerant and the ambient conditions. Contrariwise, the pump and expansion valve shows relatively insignificant exergy destruction, with values of 0.01 kW and 0.24 kW, respectively, demonstrating their findings highlight the potential for improving the overall exergetic efficiency over optimized turbine design and improved heat-transfer performance in the evaporator.

Table 5. 2 Components-wise exergy destruction rate for ORC-VCR system

Components	Rate of Exergy Destruction (kW)
Expansion Valve	0.24
Turbine	4.47
VCR condenser	0.65
Pump	0.01
Boiler	1.38
Compressor	1.42
Evaporator	3.17
ORC condenser	1.77

A. EFFECT OF SOURCE TEMPERATURE

Figure 5.1 illustrates the variation of exergetic efficiency with source temperature for different refrigerant combinations. A decreasing trend in exergetic efficiency is observed for all refrigerant pairs as the source temperature increases. This behavior occurs because the exergy supplied to the system increases more rapidly than the useful exergy output, leading to a reduction in the overall exergetic efficiency. The decrease is primarily associated with the increase in source-temperature-related exergy input, which has a greater influence on the system than other factors such as boiler heat input and ambient conditions. Therefore, though the system output may rise with temperature, the corresponding rise in input exergy is proportionally higher, resulting in lower exergetic efficiency.

At a source temperature of 338 K, the refrigerant pair R1233zd(E)-R1233zd(E) gains the maximum exergetic efficiency among all the proposed refrigerant pairs, whereas, the refrigerant pair R600a-R1234yf exhibits the less value of exergetic efficiency. This

difference can be attributed to the thermodynamic properties of the refrigerants, predominantly the latent heat of vaporization in the CHP system's component "evaporator". The R1233zd(E)-R1233zd(E) pair has a higher enthalpy of vaporization (165.4 kJ/kg) than the R600a-R1234yf pair (120.1 kJ/kg), contributing to its greater exergetic performance. The larger difference in enthalpy allows the refrigerant pair R1233zd(E)-R1233zd(E) to deliver more evaporator heat, leading to higher efficiency.

Across the source temperature range from 338 K to 356 K, the exergetic efficiency of the refrigerant pair R1233zd(E)-R1233zd(E) reduces from 36.9% to 33.63% and for the refrigerant pair R600a-R1234yf drops from 29.94% to 24.55%. Even though the refrigerant pair R1233zd(E)-R1233zd(E) experiences greater total exergy destruction. Its higher enthalpy of vaporization enables it to attain better performance than R600a-R1234yf. At 338 K, the system reaches its maximum exergetic efficiency of 36.9% with R1233zd(E)-R1233zd(E), while the lowest efficiency of 24.55% is observed for R600a–R1234yf at 356 K.

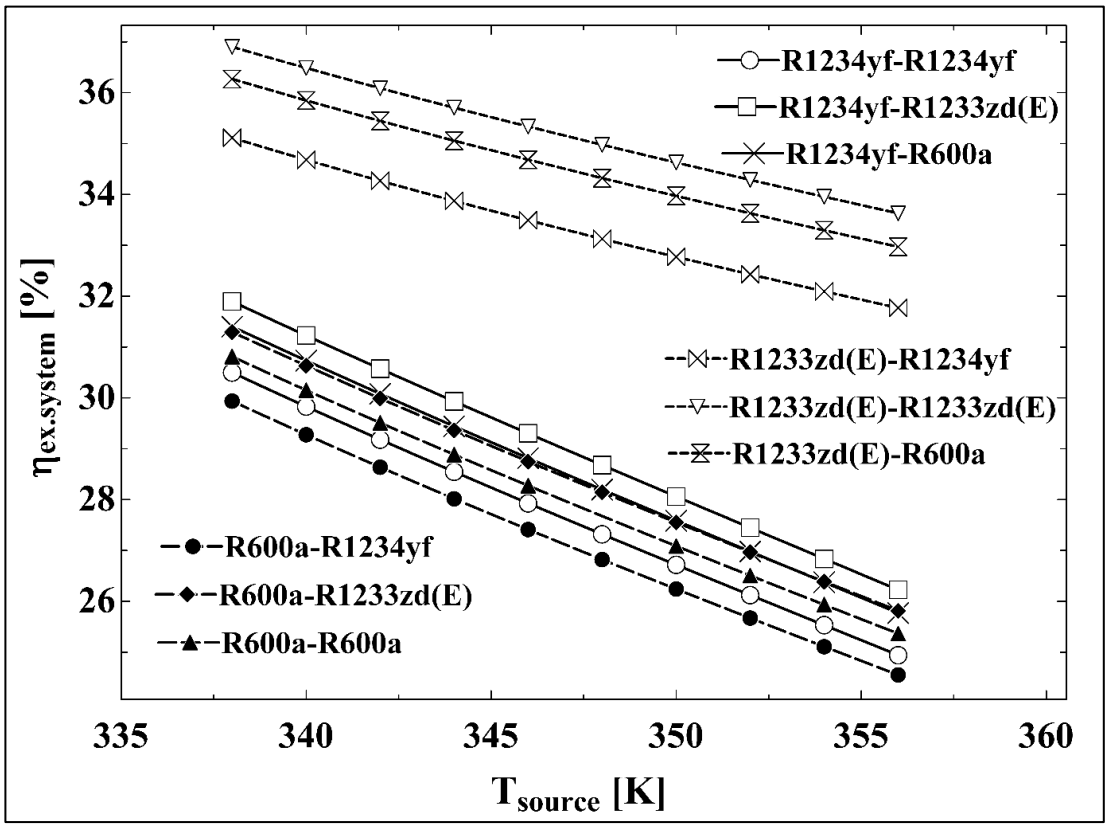

Fig. 5.1 Effect of T_{source} on $\eta_{ex.system}$ at T_0 is 300 K , T_{evp} is 273 K and Q_{boiler} = 60 kW

16

Fig. 5.2 illustrates the relationship between the system's coefficient of performance (COP) and the source temperature. The COP of the system is defined as the ratio of the heat absorbed in the evaporator to the heat supplied from the source. Since the source heat is fixed at 60 kW, the system COP depends directly on the amount of heat absorbed in the evaporator. This evaporator heat is primarily influenced by the enthalpy of vaporization, which is higher for the R1233zd(E)-R1233zd(E) pair compared to the R600a-R1234yf pair. Therefore, the refrigerant pair R1233zd(E)-R1233zd(E) demonstrates better overall performance than the other tested refrigerant groupings.

As the source temperature increases, the coefficient of performance (COP) increases for all the proposed refrigerant combinations in this research. An increase in source temperature delivers more thermal energy to the system, which improves the heat absorption capacity of the evaporator and, therefore, increases the cooling effect.

Within the examined temperature range of 338 K to 356 K, the refrigerant pair R1233zd(E)-R1233zd(E) displays the highest Coefficient of performance, with values changes from 0.21 to 0.30. In other contrast, the refrigerant pair R600a–R1234yf delivers the lowest coefficient of performance, ranging from 0.14 to 0.19. The higher the coefficient of performance value of the refrigerant pair R1233zd(E)-R1233zd(E) can be attributed to its favourable thermodynamic properties, which enable greater heat absorption for a given heat input.

The refrigerant pair R1233zd(E)-1233zd(E) obtained maximum COP of 0.30 at a source temperature of 356 K, whereas the minimum value of COP is 0.14, observed for the refrigerant pair R600a–R1234yf at 338 K. Furthermore, the increase in COP with source temperature is more noticeable for systems using R1233zd(E) than for those employing R1234yf or R600a. This tendency suggests that R1233zd(E) responds more effectively to improved thermal conditions, resulting in better overall refrigeration performance across the studied operating range.

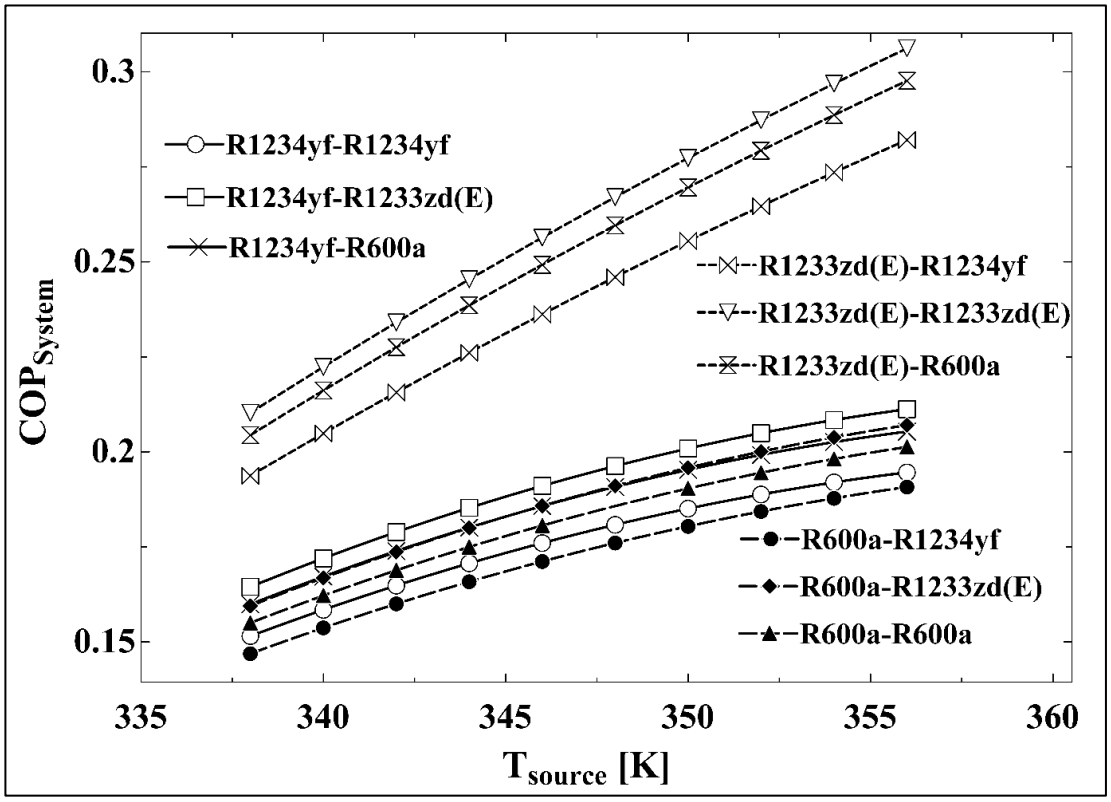

Fig. 5.2 Effect of T_{source} on COP_{system} at T_0 is 300 K, T_{evp} is 273 K and Q_{boiler} = 60 kW

Fig. 5.3 shows the relation between the source temperature and evaporator heat. As the source temperature rises from 338 K to 356 K, the heat absorbed by the evaporator also rises because the higher rate of change of enthalpy of vaporization allows the evaporator to absorb more heat at the same evaporator temperature.

Among the all proposed refrigerant pairs evaluated, the refrigerant pair R1233zd(E)-R1233zd(E) exhibits the highest evaporator heat values, ranging from 12.62 kW to 18.37 kW, while the refrigerant pair R600a-R1234yf presents the lowest evaporator heat, changes between 8.81 kW and 11.45 kW. This difference arises from the higher enthalpy of vaporization of R1233zd(E) in the VCR cycle at the fixed evaporator temperature of 273 K. Therefore, the highest evaporator heat of 18.37 kW is achieved with the refrigerant pair R1233zd(E)-R1233zd(E) at 356 K, whereas the minimum of 8.81 kW is attained with the refrigerant pair R600a–R1234yf at 338 K.

It is also observed that the rate of increase in evaporator heat with rising source temperature is steeper for R1233zd(E) operating in the ORC compared to R1234yf and

R600a. This discrepancy is attributed to the superior thermal properties of R1233zd(E), which enable more efficient heat absorption and transfer under the same operating conditions. As a result, the R1233zd(E)-R1233zd(E) pair consistently demonstrates better evaporator performance than the other refrigerant combinations considered.

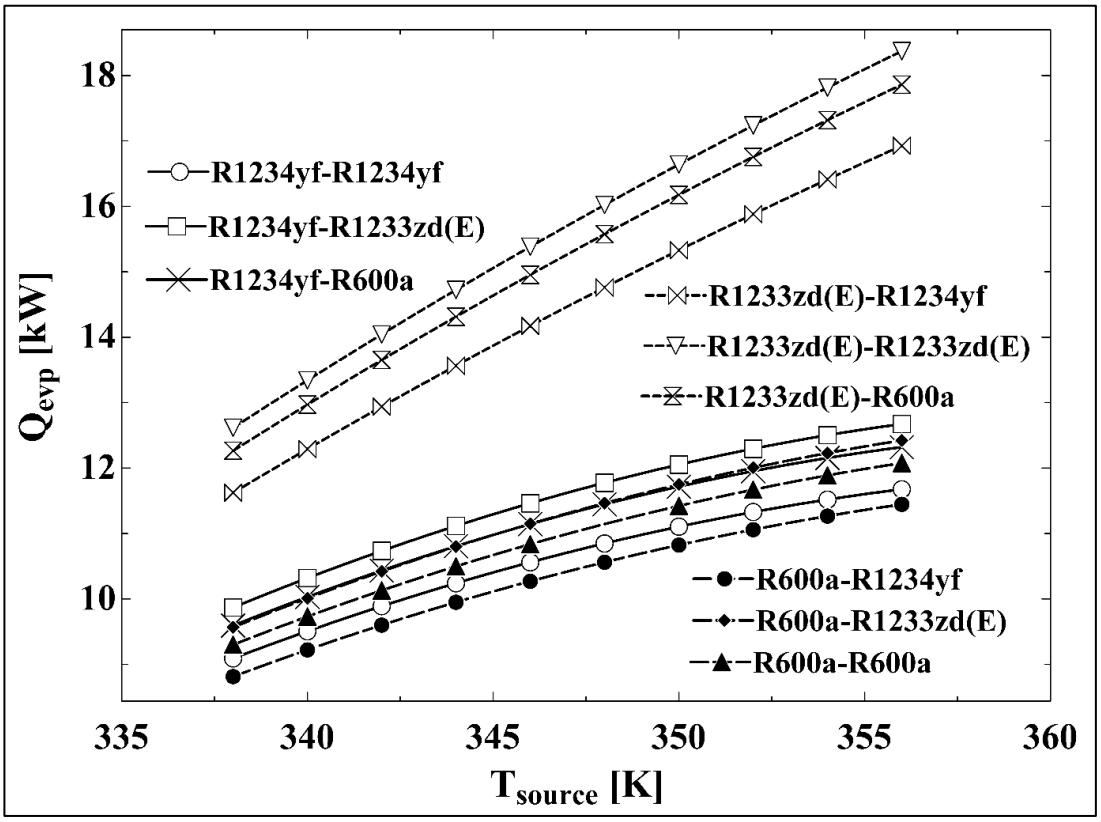

Fig. 5.3 Effect of T_{source} on Q_{evp} at T_0 is 300 K, T_{evp} is 273 K and Q_{boiler} = 60 kW

B. EFFECT OF AMBIENT TEMPERATURE

Figure 5.4 illustrates the effect of ambient temperature on the exergetic efficiency of the system. A gradual rise in exergetic efficiency is observed as the ambient temperature increases from 300 K to 314 K for all refrigerant combinations. This improvement is associated with the relative deviations in the exergy supplied to the system and the valuable exergy obtained from it. With increasing ambient temperature, both fuel exergy and product exergy decrease. However, the decline in fuel exergy is greater than that of product exergy, resulting in a higher ratio of useful exergy output to exergy input. Therefore, the rise in overall exergetic efficiency. The reduction in product exergy is

mostly related to the condensation process, where the enthalpy change during condensation reduces as the ambient temperature increases.

Among the all proposed refrigerant pairs considered, the refrigerant pair R1233zd(E)-R1233zd(E) shows the best performance across the entire ambient temperature range, with exergetic efficiency values changes from 34.98% to 35.65%.

In contrast, on the other side the refrigerant pair R600a–R1234yf records the lowest results, varies between 26.82% and 27.38%. The highest exergetic efficiency of 35.65% is attained by the refrigerant pair R1233zd(E)-R1233zd(E) and lowest efficiency of 26.82% is obtained for the R600a–R1234yf pair at temperature of 314 K and 300 K respectively. The higher efficiency of the R1233zd(E)-R1233zd(E) refrigerant combination can be attributed to its ability to deliver greater useful exergy under the similar operating conditions, making it more effective than the other refrigerant pairs evaluated in this research.

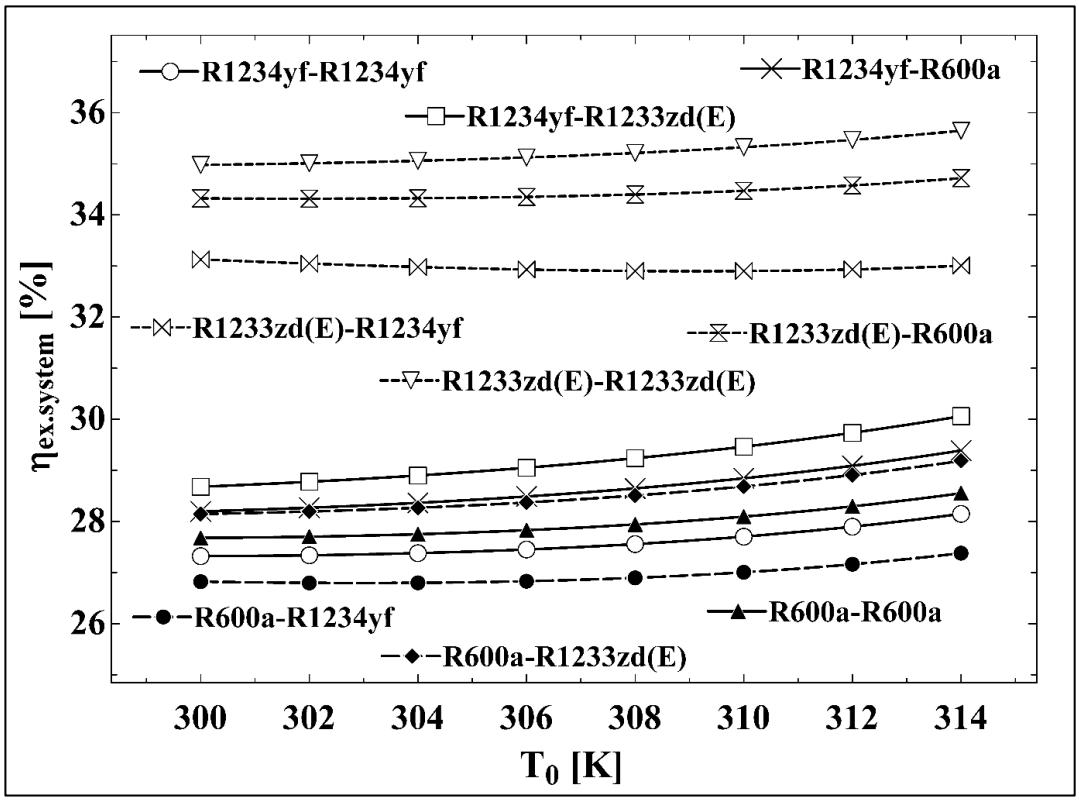

Fig. 5.4 Effect of T_0 on $\eta_{ex.system}$ at T_{source} is 348 K, T_{evp} is 273 K and Q_{boiler} = 60 kW

Figure 5.5 shows the effect of ambient temperature on the coefficient of performance (COP) of the system. A decreasing trend in COP is observed for all refrigerant pairs as the ambient temperature increases from 300 K to 314 K. On the same boiler heat input, the reduction is mainly attributed to the decrease in the cooling effect. On increasing of the ambient temperature, the condenser runs at a higher pressure, which decreases the enthalpy difference across the evaporator. Therefore, the amount of heat absorbed in the evaporator decreases, leading to a lower cooling capacity and a reduction in COP. Among the all proposed refrigerant pairs investigated, the refrigerant pair R1233zd(E)-R1233zd(E) attains the highest COP throughout the studied temperature range, with values decreasing from 0.26 to 0.11. The enhance performance can be attributed to the higher latent of vaporization, which advances the refrigerant's ability to absorb heat within the evaporator.

The R600a-R1234yf combination displays the lowest COP values, ranging from 0.17 to 0.06 at temperature ranges from 300 K to 314 K. The comparatively limited heat absorption capability results in a lower cooling effect, which adversely affects the overall system performance. The lowest COP of 0.06 is observed for the R600a-R1234yf pair at 314 K, whereas highest COP of 0.26 is obtained with the R1233zd(E)-R1233zd(E) pair at an ambient temperature of 300 K. These findings indicate that increasing ambient temperature adversely affects the performance of the ORC-VCR system, while the R1233zd(E)-R1233zd(E) combination maintains comparatively better performance over the entire operating range.

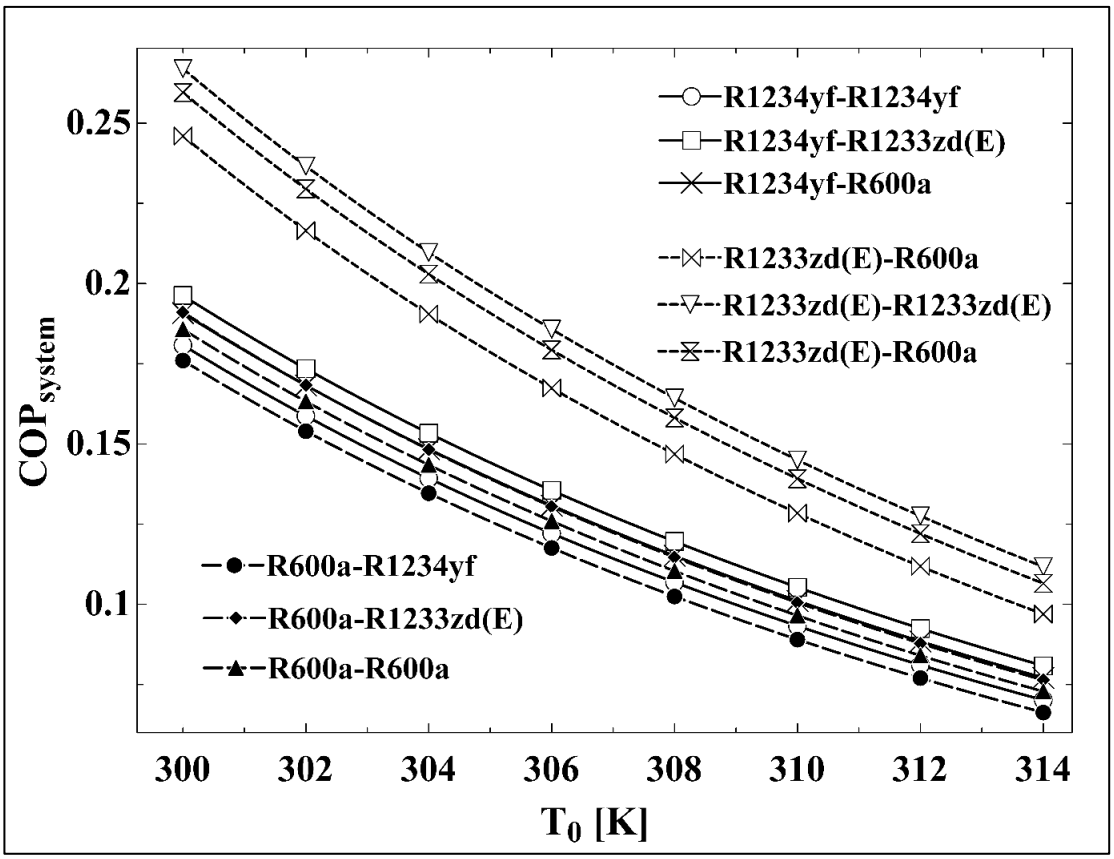

Fig. 5.5 Effect of T_0 on COP_{system} at T_{source} is 348 K, T_{evp} is 273 K and Q_{boiler} = 60 kW

Fig. 5.6 illustrates that the evaporator heat changes with changes in ambient temperature. When the ambient temperature increases from 300 K to 314 K, the heat absorbed in the evaporator decreases for all refrigerant pairs. This trend is mainly caused by the rise in condenser pressure at higher ambient temperatures. The rise in condenser pressure decreases the enthalpy change during the evaporation process, which therefore lowers both the refrigeration effect and the evaporator heat absorption. Among the refrigerant pairs studied, the R1233zd(E)-R1233zd(E) combination provides the highest evaporator heat, with values decreasing from 16.02 kW at 300 K to 6.70 kW at 314 K. On the other hand, the R600a-R1234yf combination exhibits the lowest evaporator heat, ranging from 10.56 kW to 3.97 kW over the same temperature range. The superior performance of the R1233zd(E)-R1233zd(E) pair is attributed to its higher latent heat of vaporization, which enables greater heat absorption during the evaporation process. In comparison, the lower latent heat characteristics of the R600a–R1234yf combination limit its cooling capacity. The maximum evaporator heat of 16.02 kW is obtained with

the R1233zd(E)–R1233zd(E) refrigerant pair at an ambient temperature of 300 K, whereas the minimum value of 3.97 kW is recorded for the R600a–R1234yf pair at 314 K. These results indicate that higher ambient temperatures reduce the cooling potential of the system, although the R1233zd(E)–R1233zd(E) combination continues to deliver the highest evaporator heat among the refrigerants investigated.

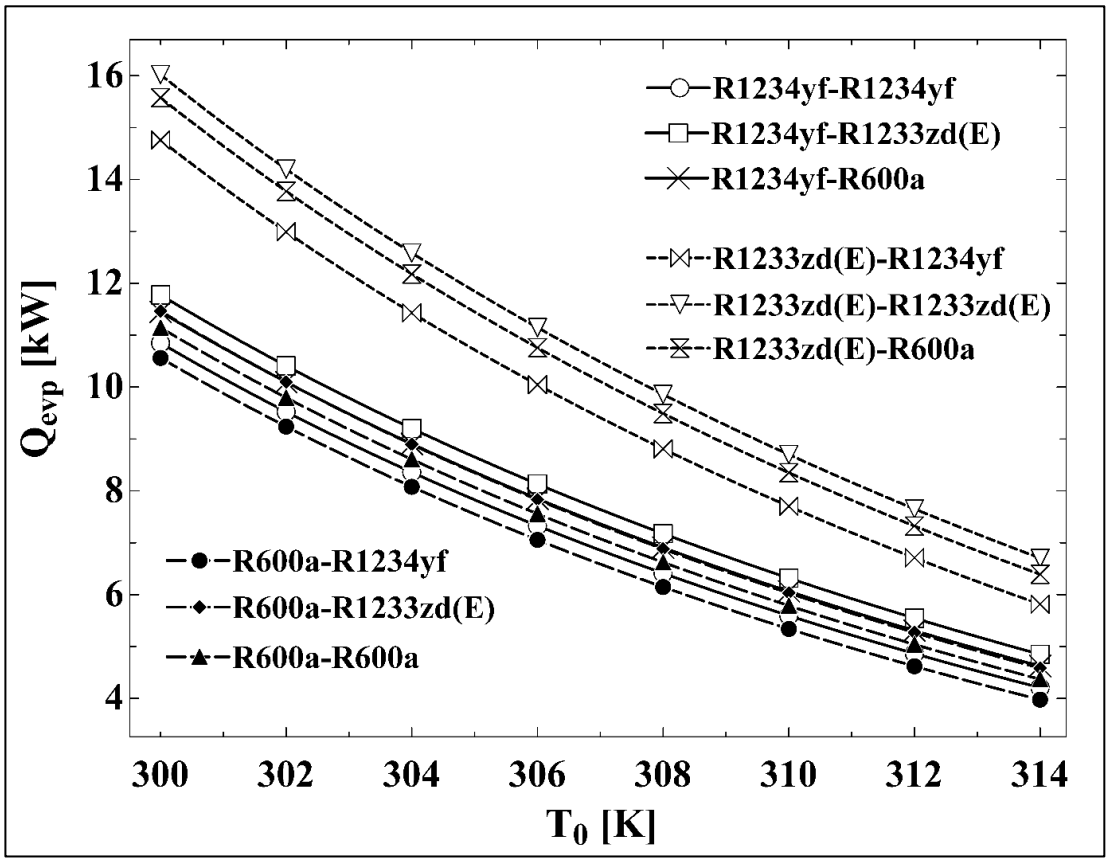

Fig. 5.6 Effect of T_0 on Q_{evp} at T_{source} is 348 K, T_{evp} is 273 K and Q_{boiler} = 60 kW

C. INFLUENCE OF EVAPORATOR TEMPERATURE

Figure 5.7 presents the variation of exergetic efficiency with evaporator temperature. An increase in evaporator temperature from 268 K to 284 K leads to an improvement in exergetic efficiency for all refrigerant combinations considered. This behavior is associated with the enhanced heat absorption capability of the refrigerants at higher evaporator temperatures, which increases the useful exergy produced by the system. Higher evaporator temperatures result in a greater refrigeration effect and improved utilization of the available energy, thereby contributing to an increase in overall exergetic efficiency.

Among the all proposed refrigerant pairs investigated, the R1233zd(E)-R1233zd(E) pair shows better performance throughout the operating range. The exergetic efficiency of the refrigerant pair of R1233zd(E)- R1233zd(E) increases from 26.42% to 35.87% as the evaporator temperature rises from 268 K to 284 K. In comparison, the refrigerant pair R600a-R1234yf attains lower efficiency values under the same conditions. The better performance exhibited by the R1233zd(E)-R1233zd(E) combination is mainly due to its higher useful exergy generation under identical operating conditions. As a result, this refrigerant pair delivers greater thermodynamic effectiveness than the other combinations examined in the study. The maximum exergetic efficiency of 35.87% is obtained with R1233zd(E)-R1233zd(E) at an evaporator temperature of 284 K, while the minimum efficiency of 27.65% is observed with R600a-R1234yf at 268 K. These results confirm that raising the evaporator temperature enhances system performance and that R1233zd(E)-R1233zd(E) is the most favourable pair among those considered, due to its superior thermal and exergetic properties.

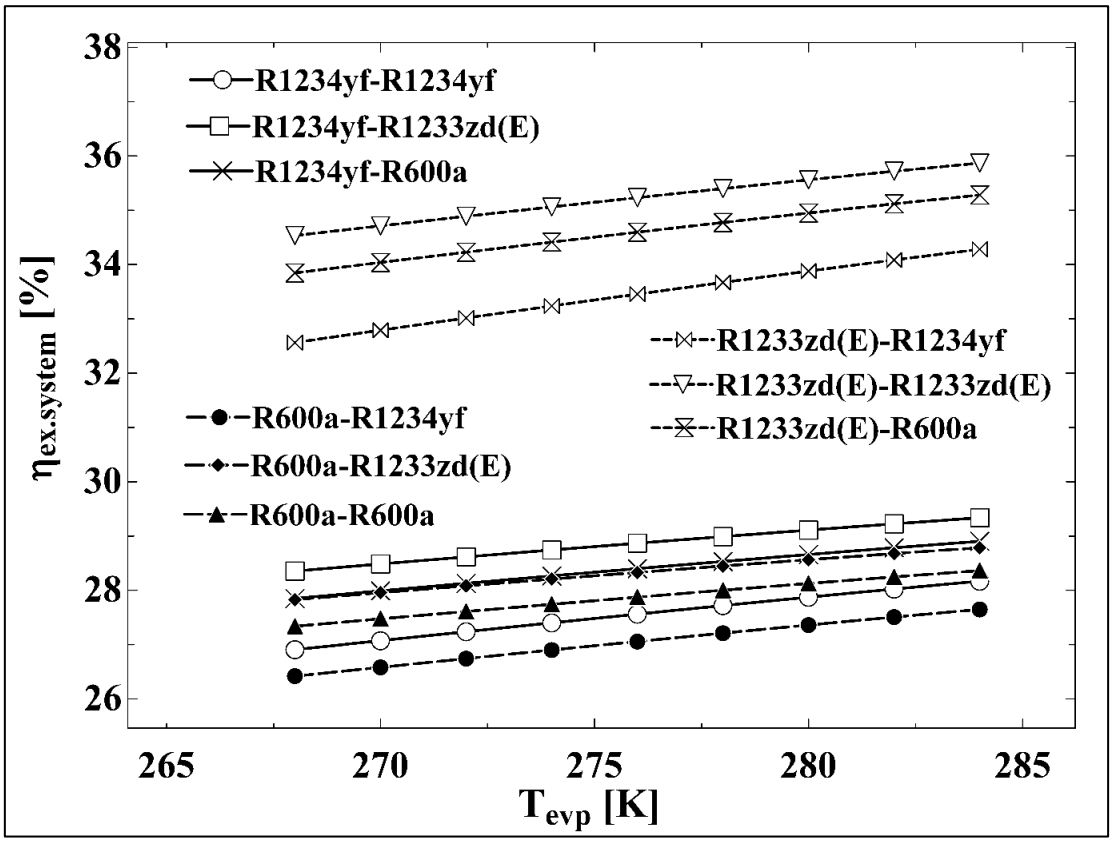

Fig. 5.7 Effect of T_{evp} on $\eta_{ex.system}$ at T_{source} is 348 K, T_0 is 300 K and Q_{boiler} = 60 kW

Fig. 5.8 shows the correlation between the system's COP and the evaporator temperature. As the evaporator temperature rises from 268 K to 284 K, the COP of the system increases. This improvement is due to the increase in evaporator heat with higher evaporator temperatures, even though the system's heat input remains constant.

Among the refrigerant pairs evaluated, R1233zd(E)-R1233zd(E) achieves the highest COP values, varying between 0.22 and 0.44. In contrast, the R600a-R1234yf pair shows the lowest COP values, ranging from 0.14 to 0.29. This difference is primarily attributed to the greater evaporator heat absorbed by the R1233zd(E)-R1233zd(E) pair compared to R600a-R1234yf.

The system reaches its highest COP of 0.41 with the refrigerant pair R1233zd(E)-R1233zd(E) at an evaporator temperature of 284 K, while the lowest COP of 0.14 occurs with the R600a-R1234yf pair at 268 K, within the evaporator temperature range of 268 K to 284 K.

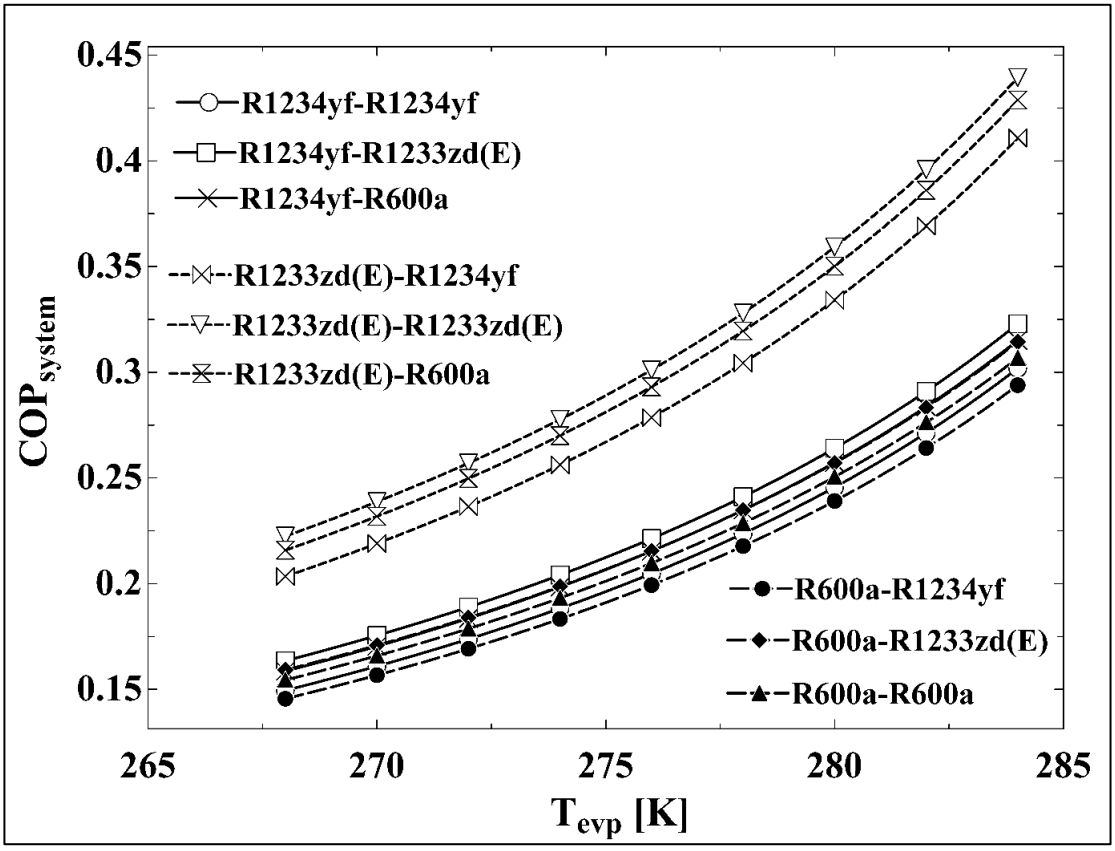

Fig. 5.8 Effect of T_{evp} on COP_{system} at T_{source} is 348 K, T_0 is 300 K and Q_{boiler} = 60 kW

Figure 5.9 shows the variation of evaporator heat with evaporator temperature. An increase in evaporator temperature from 268 K to 284 K results in a corresponding increase in the heat absorbed by the evaporator. This trend is mainly due to the increase in the latent heat associated with the evaporation process, which enhances the refrigerant's ability to absorb heat.

Among the refrigerant combinations considered, the R1233zd(E)-R1233zd(E) pair delivers the highest evaporator heat throughout the investigated range, with values increasing from 13.35 kW to 26.36 kW. The latent heat of vaporization reaches at 162.2 kJ/kg at an evaporator temperature of 268 K cause higher performance is related to its higher latent heat of vaporization. The R600a-R1234yf pair exhibits comparatively lower evaporator heat, changing from 8.73 kW to 17.64 kW over the same temperature range. This behavior is associated with its lower latent heat of vaporization, measured at 116.8 kJ/kg at 268 K.

The highest evaporator heat value of 26.36 kW is obtained with the R1233zd(E)-R1233zd(E) pair at an evaporator temperature of 284 K, while the lowest value of 8.73 kW is observed for the R600a-R1234yf pair at 268 K. These findings indicate that evaporator performance is strongly influenced by both operating temperature and refrigerant properties. The results also suggest that the R1233zd(E)-R1233zd(E)

combination is more effective in absorbing heat and therefore offers better thermal performance within the proposed ORC-VCR system.

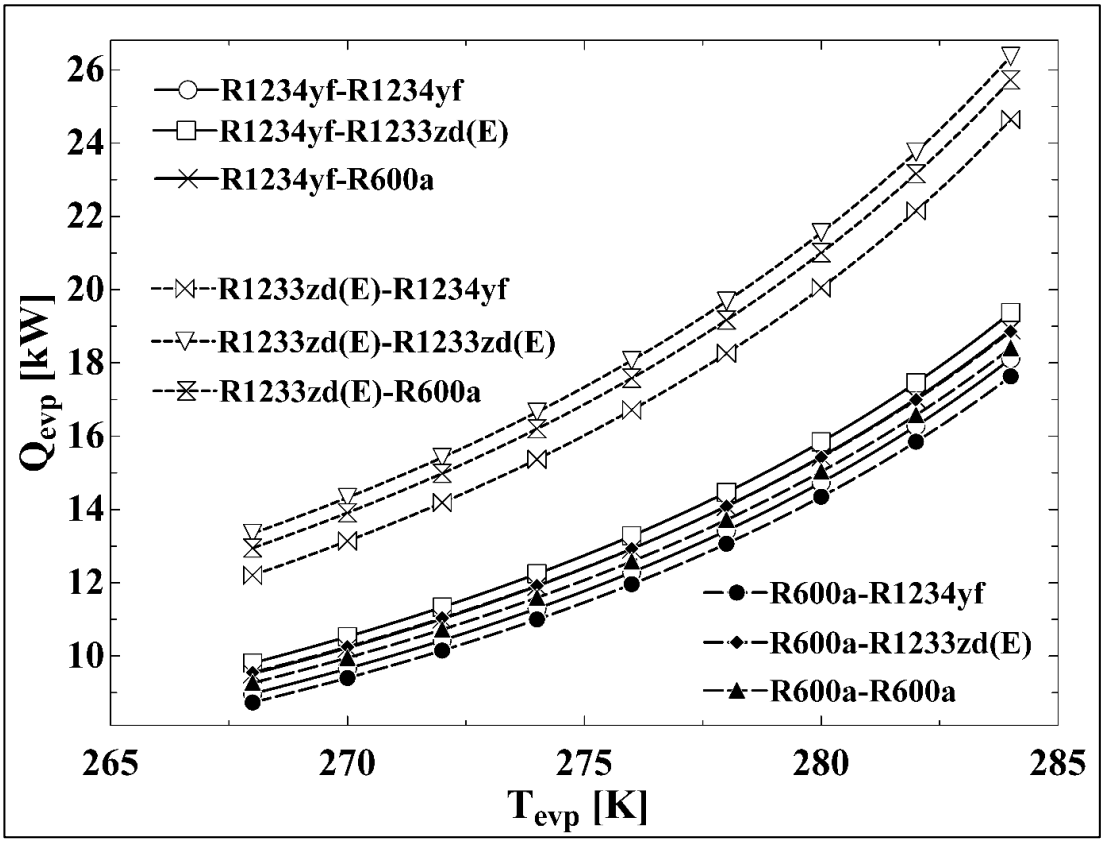

Fig. 5.9 Effect of T_{evp} on Q_{evp} at T_{source} is 348 K, T_0 is 300 K and Q_{boiler} = 60 kW

D. MULTI-OBJECTIVE OPTIMIZATION

Efficient operation of the ORC-VCR system requires careful selection of both design variables and operating conditions. The results of the parametric analysis indicate that source temperature (T_{source}), evaporator temperature (T_{evp}), and ambient temperature (T_0) have a significant influence on the energy and exergy characteristics of the system. Therefore, source temperature, evaporator temperature and ambient temperature were selected as the main variables for further optimization and performance evaluation. The selected performance indicators for optimization are the coefficient of performance (COP) and system's exergetic efficiency. The COP reflects the refrigeration system's effectiveness, while exergetic efficiency provides a deeper thermodynamic insight into

system behaviour. Improving both parameters is desirable; therefore, the optimization process aims to maximize them simultaneously to achieve optimal system performance. Regression analysis was performed using Design Expert software [92] to obtain empirical equations representing the system's COP and exergetic efficiency. The input parameters for the analysis and their respective ranges were: source temperature (T_{source}) ranging from 338 K to 356 K, evaporator temperature (T_{evp}) from 268 K to 284 K, and ambient temperature (T_0) from 300 K to 314 K. Three regression models: linear, two-factor interaction (2FI), and quadratic were assessed using the software. Each model was evaluated based on three statistical metrics: adequate precision (AP), adjusted R^2 (R_a^2), and predicted R^2 (R_p^2). A higher AP value, particularly when the difference between R_p^2 and R_a^2, is significant, indicates a more accurate model. However, if the AP value falls below 4, the model is generally considered unreliable for further analysis [92].

Based on the selected quadratic regression model, a pair of equations ((Eqs. 5.1) and (Eqs. 5.2)) are derived for both performance parameters. It should be noted that both Equations (5.1) and (5.2) are derived and validated only for the R1233zd(E)–R1233zd(E) refrigerant pair. These correlations are therefore not generalized to all refrigerant combinations but are presented here to demonstrate the performance trends of this specific pair, as also reflected in Fig. 5.10.

$$\mathrm{COP}_{system} = 0.743616 - 0.000540512 \times T_{source} - 0.0257168 \times T_0 + 0.0259607 \times \mathrm{T_{evp}} - 4.2859 \times 10^{-5} \times T_{source} \times T_0 + 0.000128566 \times T_{source} \times \mathrm{T_{evp}} - 0.000600267 \times T_0 \times \mathrm{T_{evp}} - 2.39588 \times 10^{-5} \times T_{source}^2 + 0.000314519 \times T_0^2 + 0.000219484 \times \mathrm{T_{evp}^2} \quad (5.1)$$

$$\eta_{\mathrm{ex.system}} = 21.3347 + 0.0687269 \times T_{source} + 0.00502045 \times T_0 + 0.135799 \times \mathrm{T_{evp}} - 0.00708555 \times T_{source} \times T_0 + 0.00124681 \times T_{source} \times \mathrm{T_{evp}} - 0.00131621 \times T_0 \times \mathrm{T_{evp}} + 0.00221987 \times T_{source}^2 + 0.00469125 \times T_0^2 - 0.000145743 \times \mathrm{T_{evp}^2} \quad (5.2)$$

The developed equations were subsequently used for system optimization, with the coefficient of performance (COP) and exergetic efficiency selected as the objective

functions. The implementation of a Multi-Objective Genetic Algorithm (MOGA) [93] facilitated the identification of the optimal operating parameters.

The MOGA is an evolutionary optimization method based on the principles of natural selection and genetic. It is capable of handling multiple conflicting objectives simultaneously. It is widely used to optimize complex engineering systems with multiple conflicting objectives by generating a diverse set of Pareto-optimal solutions that represent different compromises between the selected objectives. In the present study, the algorithm was executed using a population size of 200, a Pareto fraction of 35%, and a crossover fraction of 0.8. Tournament selection with a tournament size of 2 was adopted, while the intermediate crossover operator was employed to generate new candidate solutions.

Figure 5.10 shows the Pareto front obtained from the optimization process. The analysis highlights the conflicting relationship between the exergetic efficiency and coefficient of performance. Solutions with higher exergetic efficiency generally correspond to lower COP values, whereas higher COP values are associated with reduced exergetic efficiency. To scrutinize this behavior in detail, three typical solutions were selected from the Pareto front: an intermediate point, denoted as B and two extreme points, denoted as C and A. Most of the optimal solutions are focussed near the upper limit of the evaporator temperature range, around 283 K.

The optimization results designate that point A yields the highest Coefficient of performance of 0.44, related with an exergetic efficiency of 35.1% at this point the equivalent cooling capacity is 26.64 kW. The ambient temperature at this operating condition is roughly 300.07 K (26.92°C) and remains nearly unaffected up to point B. Between points A and B, the system's performance characteristics are largely controlled by changes in the source temperature. At point B, the COP decreases to 0.33, while the exergetic efficiency increases to 37.74%. The cooling capacity at this condition is 20.25 kW. Compared with point A, the COP decreases by 25%, whereas the exergetic efficiency increases by 7.52% and at the point cooling capacity also drops by 23.98%.

At point C, the system reaches its highest exergetic efficiency of 39.24%, but the COP reduced to 0.10 and at same point the equivalent cooling capacity is 6.22 kW. Relative to point B, the COP decreases by 69.69%, while the improvement in exergetic efficiency

is limited to 3.97% and in addition, the cooling capacity is decreased considerably by 87.70%.

The findings indicate that the most suitable operating region lies between points A and B, in particular near point B, as it delivers a more composed trade-off between exergetic efficiency and coefficient of performance. Even though point C offers the highest exergetic efficiency, it is convoyed by substantial drops in both cooling capacity and COP. The results indicate that the operating condition with the highest exergetic efficiency is not inevitably the most effective. Subsequently, a compromise between the competing performance objectives is required to optimize overall system operation.

Among all input parameters, ambient temperature has the greatest impact on the thermodynamic efficiency of the ORC-VCR system. In the A-B region, the performance parameters are largely influenced by the source temperature, making it a crucial design variable. However, once the ambient temperature exceeds 300 K, the system's exergetic efficiency begins to rise and whereas the cooling capacity and COP of the system reduce. This scenario presents an operating condition where the total irreversibility of the system reduces.

As discussed earlier, point A provides a higher COP than point B, making it advantageous to operate the ORC–VCR system near point A when a greater cooling effect is required for the same heat input. On the other hand, point B exhibits a higher exergetic efficiency than point A. Therefore, operating the system near point B is more beneficial in scenarios where the heat source temperature is on the lower side of ultra-low. Point B also represents lower exergy losses, thereby indicating more efficient utilization of the source energy. Extracting the heat at a higher rate from a waste heat or solar energy source can match the cooling capacity at point A at a lower COP value. This also avoids affecting the environment negatively. Thus, it is a better option to design a system corresponding to operating parameters at point B, as it gives better exergetic efficiency.

It is important to note that while the optimization focused on thermodynamic performance parameters, the selection of working fluids also considered environmental sustainability. In particular, the R1233zd(E)–R1233zd(E) pair, which demonstrated the best balance of COP and exergy efficiency, has an ODP of zero and a very low GWP ≈

1. Thus, this refrigerant combination not only performs well thermodynamically but also aligns with long-term environmental regulations and sustainability goals.

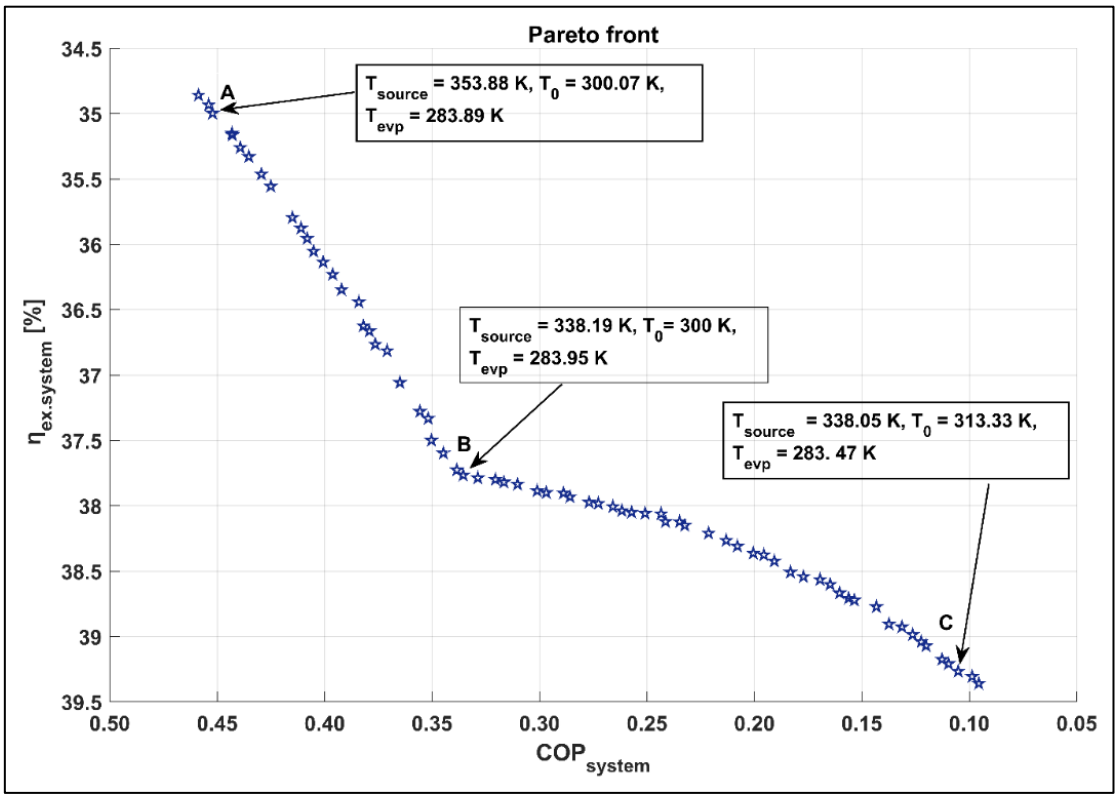

Fig. 5.10 The exergetic efficiency of the CHP and the Pareto front for the COP_{system} were calculated using MOGA for the R1234zd(E)-R1234zd(E) refrigerant pair

5.2.2 Solar and diesel engine exhaust-driven ORC-VCR system

The results of energy and exergy-based analysis are divided into two subsections, i.e. (i) parametric investigation, and (ii) multi-objective optimization.

Using the first and second laws of thermodynamics, a program was developed in Engineering Equation Solver (EES) to systematically analyze the various performance-based parameters. The input data presented in **Error! Reference source not found.** are used in the calculation for energy-exergy-based performance parameters for the entire ORC-VCR system, followed by further optimization for a rational approach. Further, it is important to mention here that both ORC and VCR condensers are assumed to operate at the same temperature as mentioned in Table 5.3

Table 5.3 Input parameters used for simulation.

Parameter	Value	Range
Diesel engine exhaust gas input temperature [K]	690	690-810
Diesel engine exhaust gas outlet pressure [kPa, absolute] [25]	121.32	-
Thermal oil (Theminol 66) input temperature [K]	613	-
Inlet Temperature of High-Pressure Turbine ($T_{HPT,in}$) [K]	550	450-550
ETC solar water temperature [K]	473	433-473
Inlet Temperature of Low-Pressure Turbine ($T_{LPT,in}$) [K]	463	423-463
Pressure drop in Boiler and condenser	5%	
Condenser temperature T_{cond} [K] (Both ORC and VCR)	313	308-323
Evaporator temperature, T_{evp} [K]	273	268-283
Effectiveness of heat exchangers	0.8	-
η_{tur} [3]	87%	-
η_{comp} [26]	80%	-
η_{pump} [26]	85%	-

The cooling capacity of the refrigerant pair, Benzene-R601, is determined to be 19.85 TR, using the base input data for the VCR cycle. The ORC-VCR system generates cooling capacity through the utilization of waste heat, specifically exhaust heat from diesel engines and solar energy. Hence, the operational expenses of this system (ORC-VCR system) are negligible and can be disregarded. Alternatively, if we require the same amount of cooling from a conventional vapor compression refrigeration system, we would have incurred substantial electricity costs. Comparing the present system to an air conditioning system under the aforementioned input conditions listed in Table 5, the net compressor power to be delivered for the refrigerant R601 is 14.41 kW. The electricity consumption for this compressor would amount to approximately $1,621 over a 1500-hour period of operation, assuming the price of electricity of 0.075 $.kW^{-1}.hr^{-1} [94].

Table 5.4 shows the total exergy destruction rate for each component of the ORC-VCR system at input condition. It shows that the evaporator has the highest value of exergy destruction and the condenser of VCR has the lowest value of exergy destruction, where the energy results for the system correspond to the base value given in Table 5.4.

Table 5. 4 Components-wise exergy destruction rate for ORC-VCR system

Components	Rate of Exergy Destruction (%)
Compressor	9.293
VCR condenser	0.005
ORC condenser	4.29
Pump	0.23
Boiler	31.11
Reheater	2.711
Expansion Valve	6.653
Evaporator	40.262
HPT	3.053
LPT	2.39

A. Effect of Temperature of High-Pressure Turbine

Fig. 5.11 depicts the variation between the COP of the system with variation in $T_{HPT,in}$. The results show that with the increase in $T_{HPT,in}$, the COP of system increases as well for all the refrigerants. Though the COP of the system increases with an increase in $T_{HPT,in}$, the marginal increment in the COP decreases continuously over the specified range of $T_{HPT,in}$. The reason is that the mass flow rate of refrigerant ($\dot{m}_{ref}$) flow in VCR increases quite marginally. For the base conditions (Given in **Error! Reference source not found.**), the COP of the system is higher (0.93-1.17) for the Benzene-R601 among all the combinations of refrigerants and the lower (0.76-0.97) is for the Cyclohexane-R1234yf. The COP for Benzene-R601 is observed to be 17.5% higher than

Cyclohexnane-R1234yf, because of a higher cooling effect in the case of Benzene-R601, as compared to Cyclohexane-R1234yf for the same energy input.

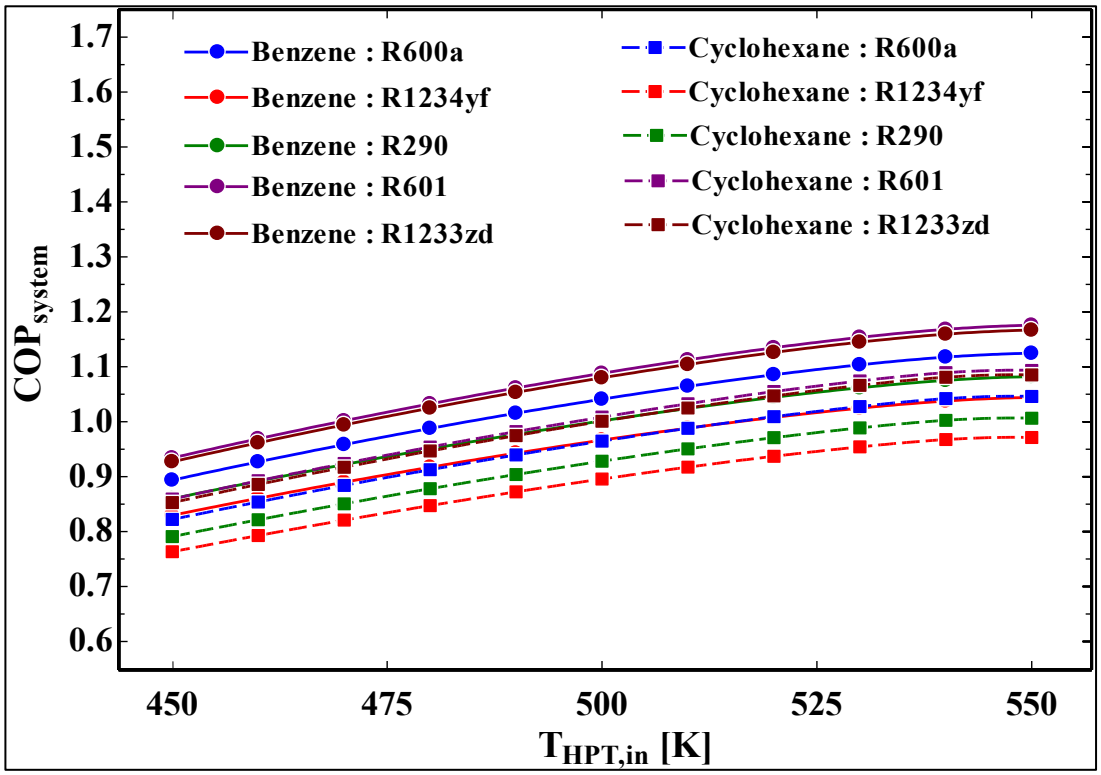

Fig. 5.11 Effect of $T_{HPT,in}$ on the COP of the system at $T_{LPT,in}$ is 463 K, T_{cond} is 313 K and T_{evp} is 273 K

Fig. 5.12 depicts the variation between the exergetic efficiency of the system with variation in $T_{HPT,in}$. The exergetic efficiency for all the refrigerants increases with an increase in the $T_{HPT,in}$. The refrigerant pair of Benzene-R601 is showing better results among all refrigerant pairs and the refrigerant pair of Cyclohexane-R1234yf is showing the least exergetic efficiency with an increase in $T_{HPT,in}$. Though the exergetic efficiency of the system increases with an increase in $T_{HPT,in}$, the marginal increment in the exergetic efficiency decreases continuously over the specified range of $T_{HPT,in}$. The reason is that the $\dot{m}_{ref}$ flow in the VCR system, increases quite marginally. The exergetic efficiency for Benzen-R601 is (16.9-21.1%) and for Cyclohexane-R1234yf is (13.8-17.3%). At the base input parameters (given in **Error! Reference source not found.**), the value of exergetic efficiency of ORC-VCR for Benzen-R601 is 18% higher than Cyclohexane-R1234yf, is so, because the exergy of product for the system ORC-

VCR is higher for Benzen-R601 pair, as compared to Cyclohexane-R1234yf for same energy input.

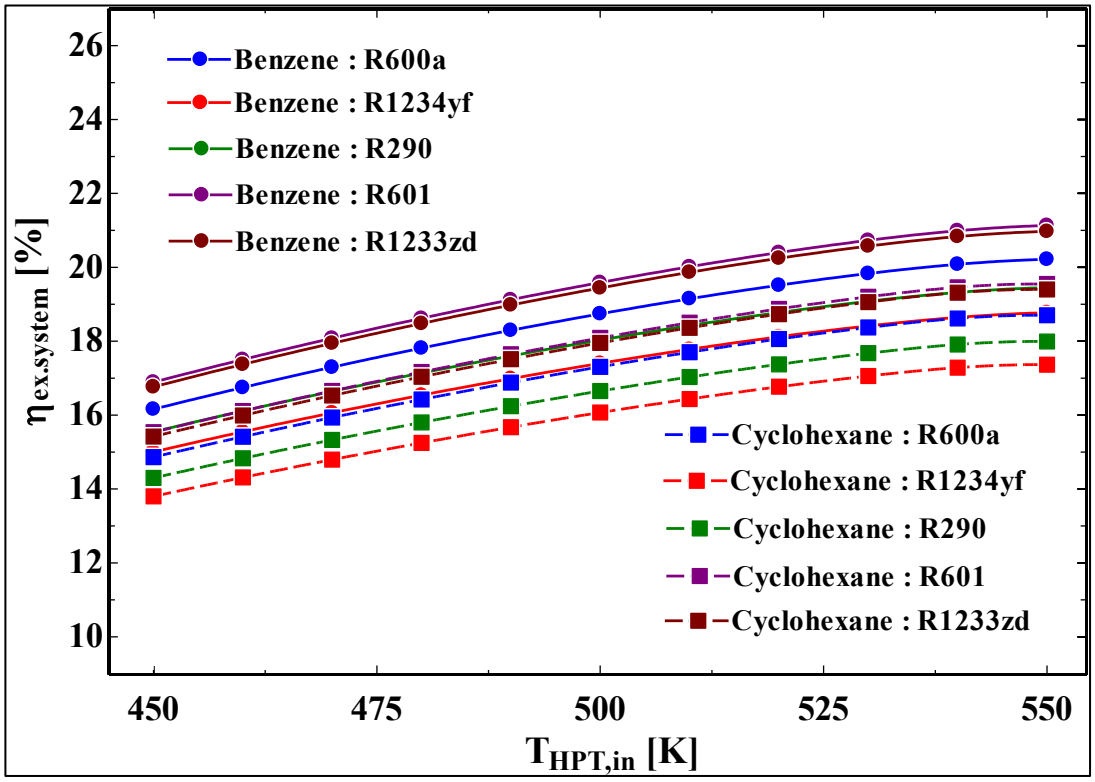

Fig. 5.12 Effect of $T_{HPT,in}$ on exergetic efficiency of the ORC-VCR system at $T_{LPT,in}$ is 463 K, T_{cond} is 313 K and T_{evp} is 273 K

Fig. 5.13 illustrates the correlation between the cooling capacity of VCR and the variation in the $T_{HPT,in}$. The cooling capacity of all refrigerants increases as the $T_{HPT,in}$ increases. However, the incremental increase in cooling capacity consistently rises within the prescribed range of the $T_{HPT,in}$. The reason is that the $\dot{m}_{ref}$ in the VCR system, increases with the increase in $T_{HPT,in}$. The cooling capacity of Benzen-R601 ranges from 16.86-19.85 TR, while the same for Cyclohexane-R1234yf ranges from 13.75-15.48 TR. For the base case (input data given in **Error! Reference source not found.**), the cooling capacity of the Benzen-R601 group is 20.15% higher than that of the Cyclohexane-R1234yf group. It is so because the evaporator heat is higher for the Benzene-R601 combination compared to the Cyclohexane-R1234yf, for the same amount of energy input.

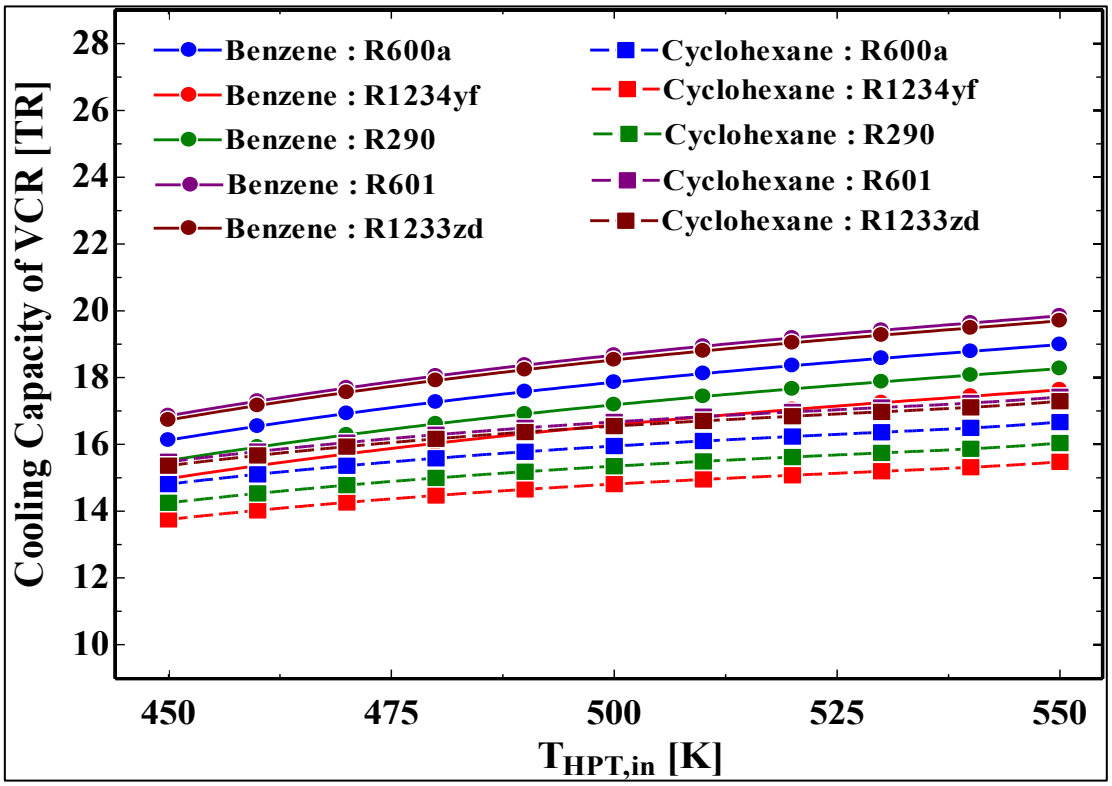

Fig. 5.13 Effect of $T_{HPT,in}$ on Cooling capacity of the VCR system at $T_{LPT,in}$ is 463 K, T_{cond} is 313 K and T_{evp} is 273 K

B. Effect of Temperature of Low-Pressure Turbine

Fig. 5.14 illustrates the variation on the COP of the system with the variation in $T_{LPT,in}$. As the $T_{LPT,in}$ increases the COP of the system reduces. The reason is that the COP of the system is a combined effect of evaporator cooling in VCR and heat supplied in ORC. In this scenario, the cooling effect in the VCR is less vulnerable to changes in the quantity of heat delivered, particularly within the set range of the $T_{LPT,in}$. Among the refrigerant pairs that have been proposed, Benzene-R601 exhibits the highest COP at 1.23-1.17, while Cyclohexane-R1234yf demonstrates the lowest COP at 1.04-0.97. With the same energy input and base input parameters (**Error! Reference source not found.**), the COP of the Benzene-R601 system is 17.09% greater than that of the Cyclohexane-R1234yf system. This is because the cooling effect of Benzene-R601 is greater.

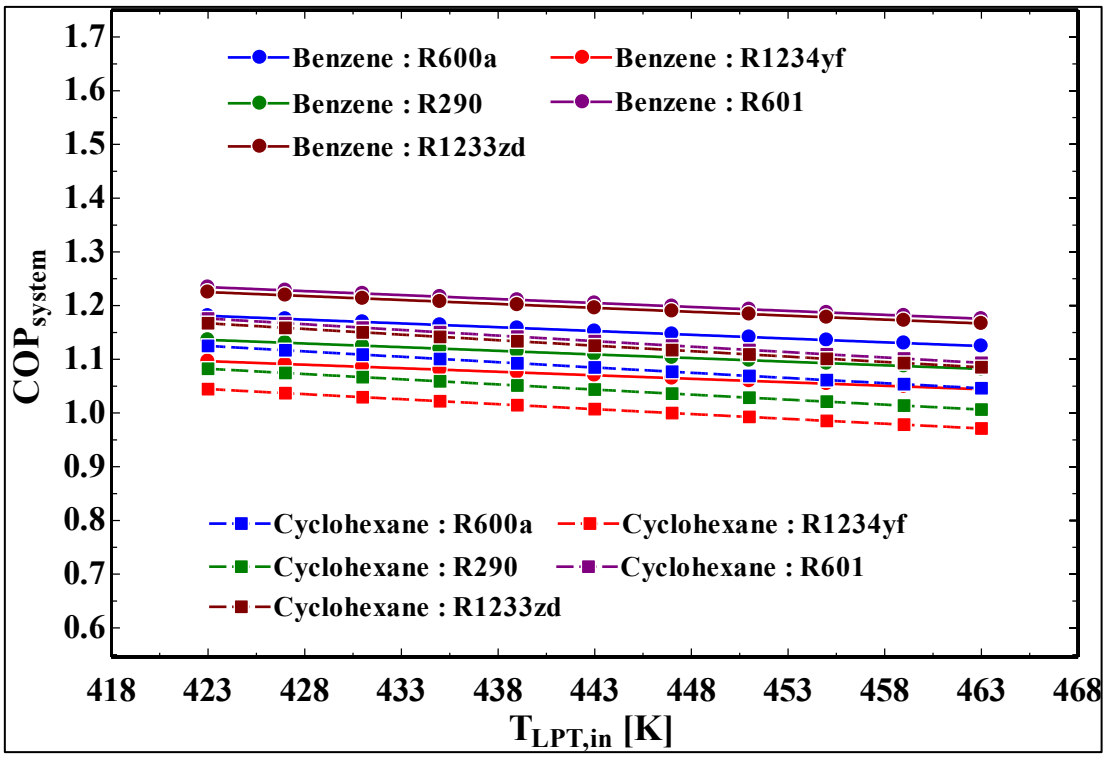

Fig. 5.14 Effect of $T_{LPT,in}$ on the COP of the system at $T_{HPT,in}$ is 550 K, T_{cond} is 313 K and T_{evp} is 273 K

Fig. 5.15 illustrates the variation on exergetic efficiency of the ORC-VCR system with the variation in $T_{LPT,in}$. The exergetic efficiency decreases with increasing the $T_{LPT,in}$. The Benzene-R601 refrigerant pair demonstrates the highest exergetic efficiency, ranging from 21.13% to 21.99%, while the Cyclohexane-R1234yf refrigerant pair exhibits the lowest, ranging from 17.36% to 18.45%. When comparing the rates of exergetic efficiency decrease in the Benzene and Cyclohexane groups, it is evident that the cyclohexane group shows clearly a decrease in efficiency that is considerably more pronounced. This can be attributed to the fact that the total irreversibility of the system increases more rapidly in the cyclohexane group. In the base

case, as indicated by the input data in **Error! Reference source not found.**, the Benzene-R601 system exhibits a 16.56% improvement in exergetic efficiency over the Cyclohexane-R1234yf system. This can be attributed to the reduced total irreversibility of the Benzene-R601 system.

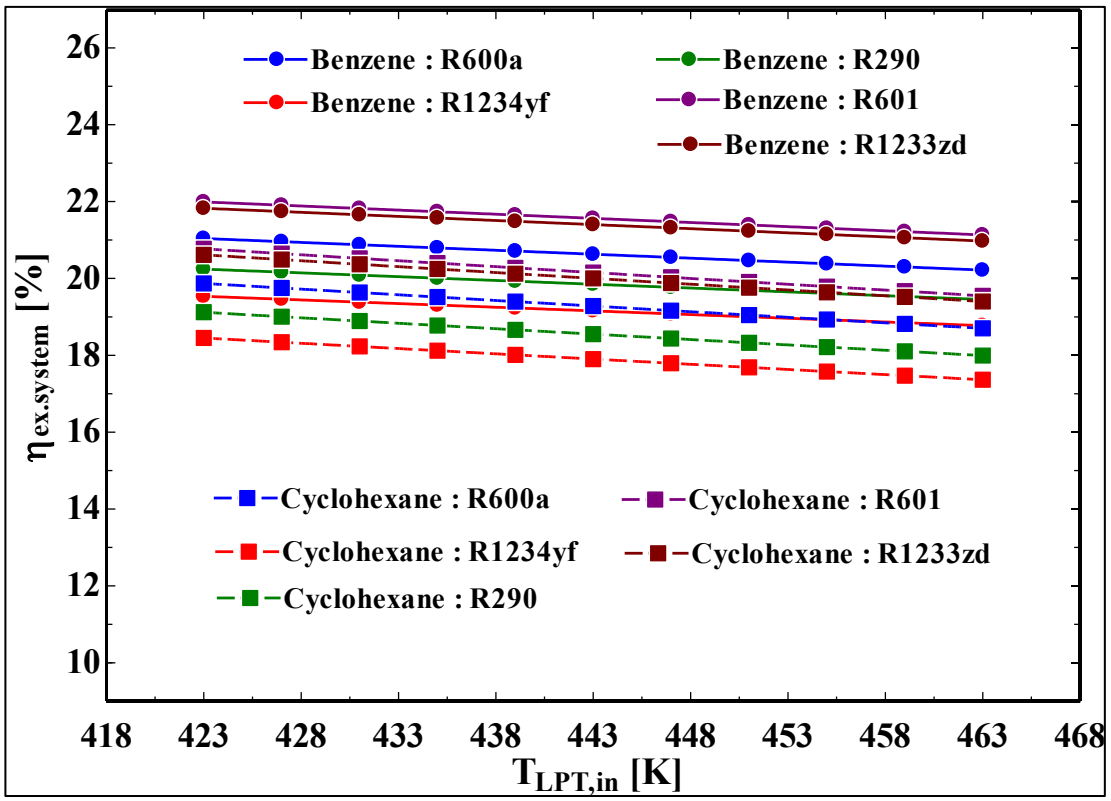

Fig. 5.15 Effect of $T_{LPT,in}$ on exergetic efficiency of the system at $T_{HPT,in}$ is 550 K, T_{cond} is 313 K and T_{evp} is 273 K

Fig. 5.16 illustrates the variation of the cooling effect in VCR system and the $T_{LPT,in}$. The cooling capacity rises with the increase of the $T_{LPT,in}$. The cooling capacity of the pair Benzene-R601 is 18.98 - 19.85TR, which is the highest among all the refrigerant pairs, whereas for the pair Cyclohexane-R1234yf is 14.8 - 15.48 TR, which is the lower one. The reason for this increment in cooling capacity is, the increase in $\dot{m}_{ref}$ in the VCR system, the resultant evaporator heat arises. For the base case (input data given in **Error! Reference source not found.**), In comparison to the Cyclohexane-R1234yf system, the Benzene-R601 system exhibits a variance of 22.01% in cooling capacity. This is because the $\dot{m}_{ref}$ of the VCR system of Benzene-R601 is higher.

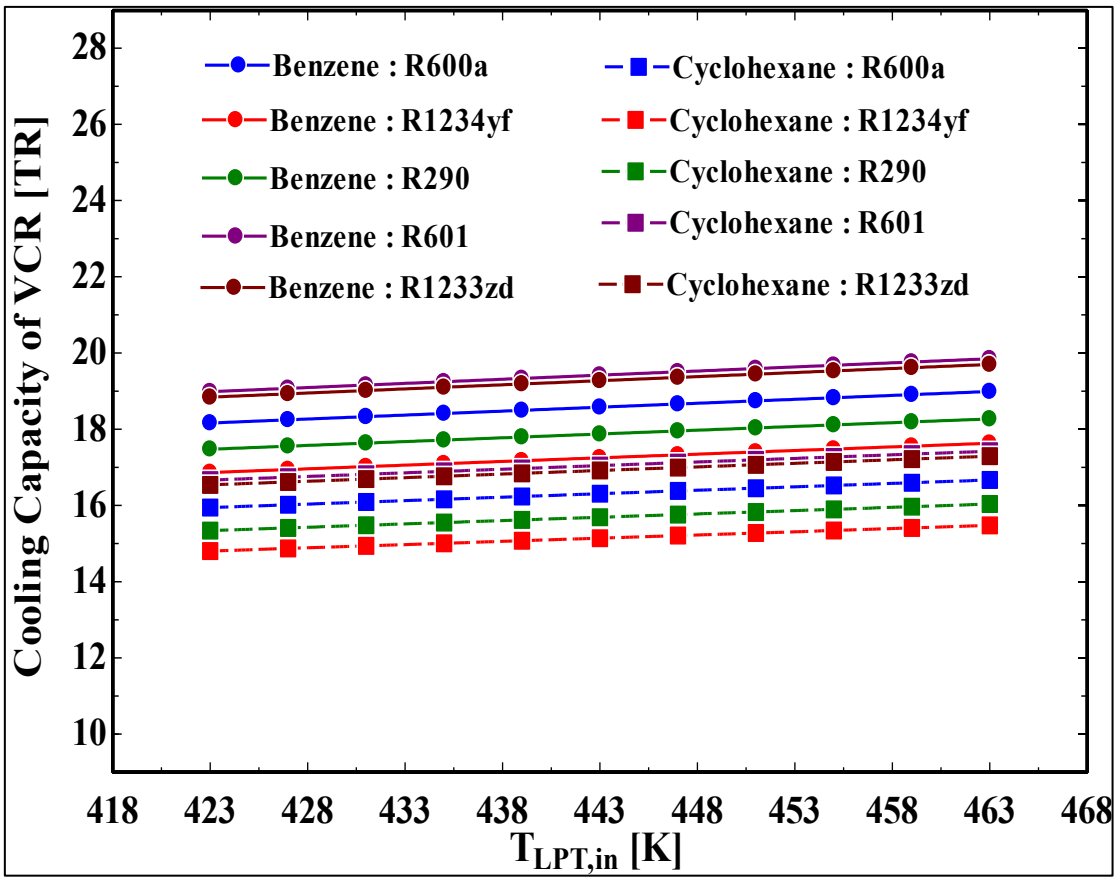

Fig. 5.16 Effect of $T_{LPT,in}$ on the cooling capacity of VCR at $T_{HPT,in}$ is 550 K, T_{cond} is 313 K and T_{evp} is 273 K

C. Effect of Evaporator Temperature

Fig. 5.17 depicts the variation of COP of the system with a change in T_{evp}. Though the COP of the system increases with an increase in T_{evp}, the marginal increment in the COP increases continuously over the specified range of T_{evp}. The reason is that the $\dot{m}_{ref}$ increases quite marginally. Among all the refrigerant pairs, the Benzene-R601 pair shows the COP in the range of 0.99 to 1.69, which is the highest, and the Cyclohexane-R1234yf pair is shown in the range of 0.81 to 1.41, which is least. For base input parameters (**Error! Reference source not found.**), the COP of the Benzene-R601 system is 20.16% greater than that of the Cyclohexane-R1234yf system. This is because the cooling effect of Benzene-R601 is greater.

Fig. 5.18 depicts the variation of the cooling capacity of VCR with a change in T_{evp}. As the T_{evp} increases the cooling capacity increases. It is so, the $\dot{m}_{ref}$ increases quite

marginally. Among all the combinations of refrigerant pair, the Benzene-R601pair shows a cooling capacity in the range of 16.85 – 28.49 TR, which is the highest, and the Cyclohexane-R1234yf shows in the range of 13.02 – 22.58 TR, which is least. For the base case (input data given in **Error! Reference source not found.**), The Benzene-R601 system exhibits a 23% growth in cooling capacity when compared to the Cyclohexane-R1234yf system. This is because the $\dot{m}_{ref}$ of the system of Benzene-R601 is higher.

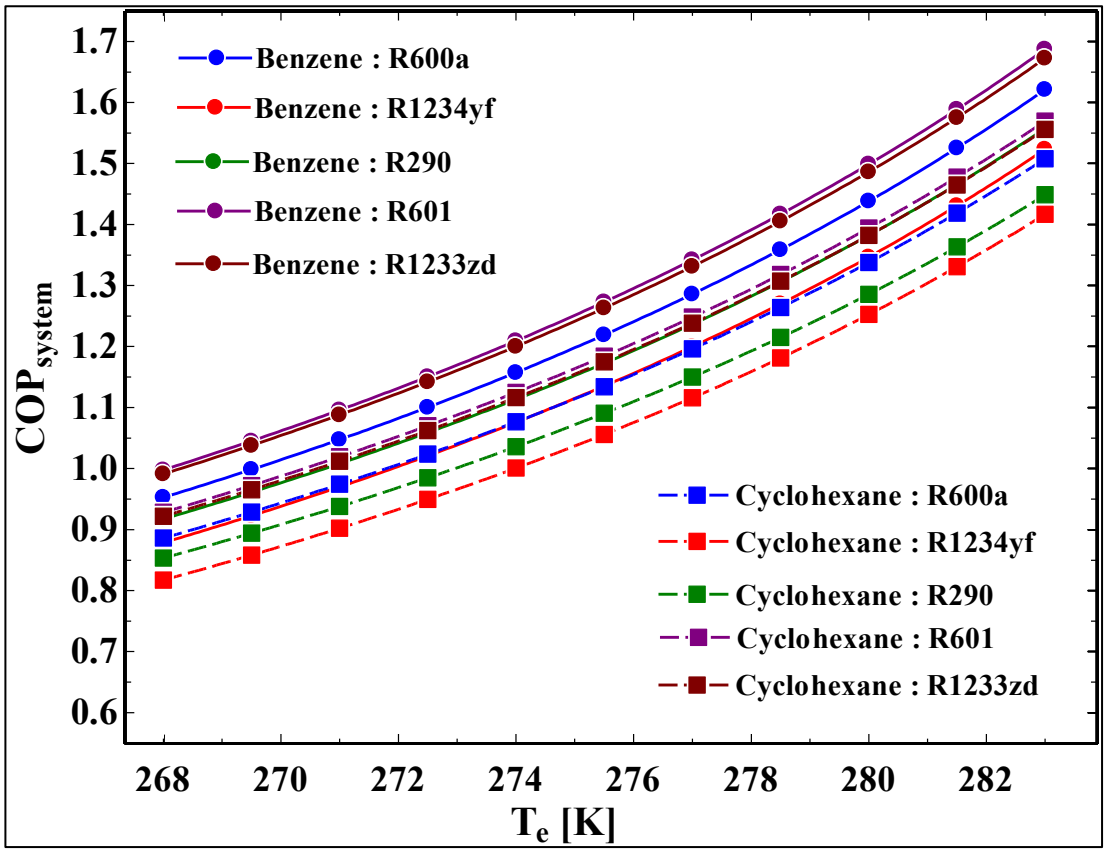

Fig. 5.17 Effect of T_{evp} on COP of the system at $T_{HPT,in}$ is 550 K, $T_{LPT,in}$ is 463 K and T_{cond} is 313 K

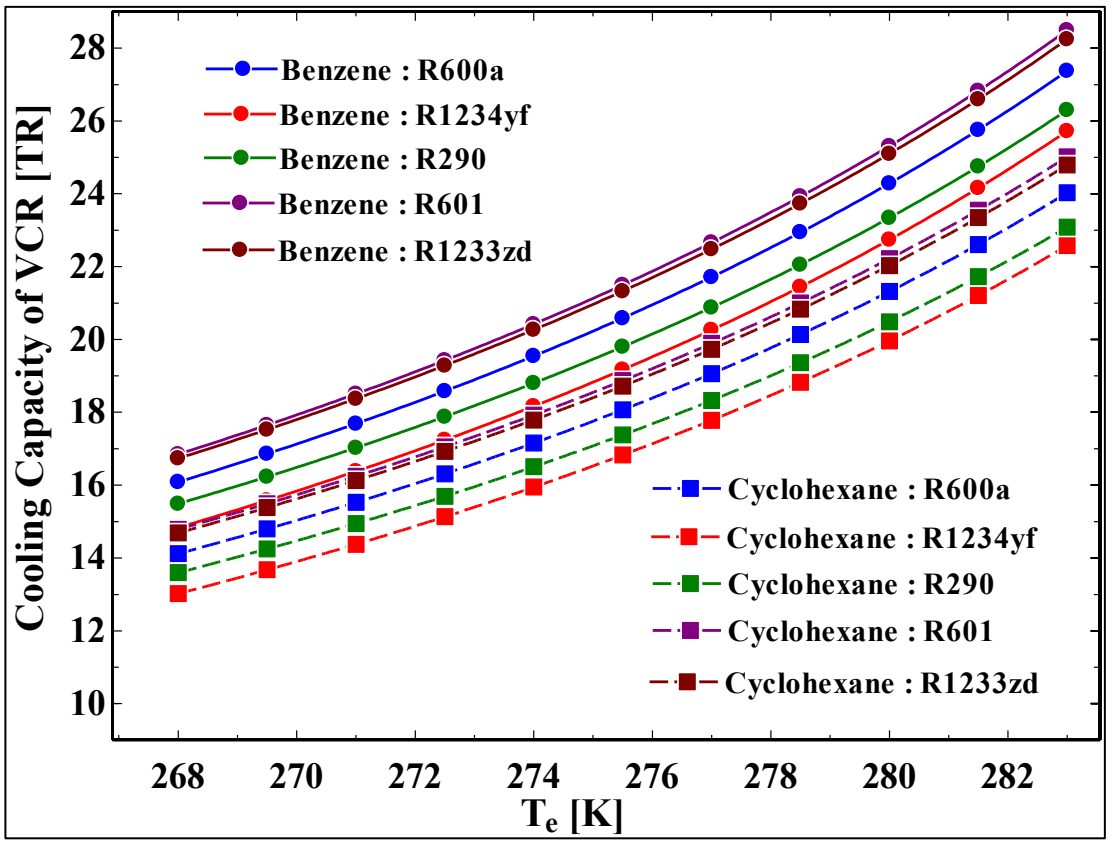

Fig. 5.18 Effect of T_{evp} on cooling capacity of VCR at $T_{HPT,in}$ is 550 K, $T_{LPT,in}$ is 463 K and T_{cond} is 313 K

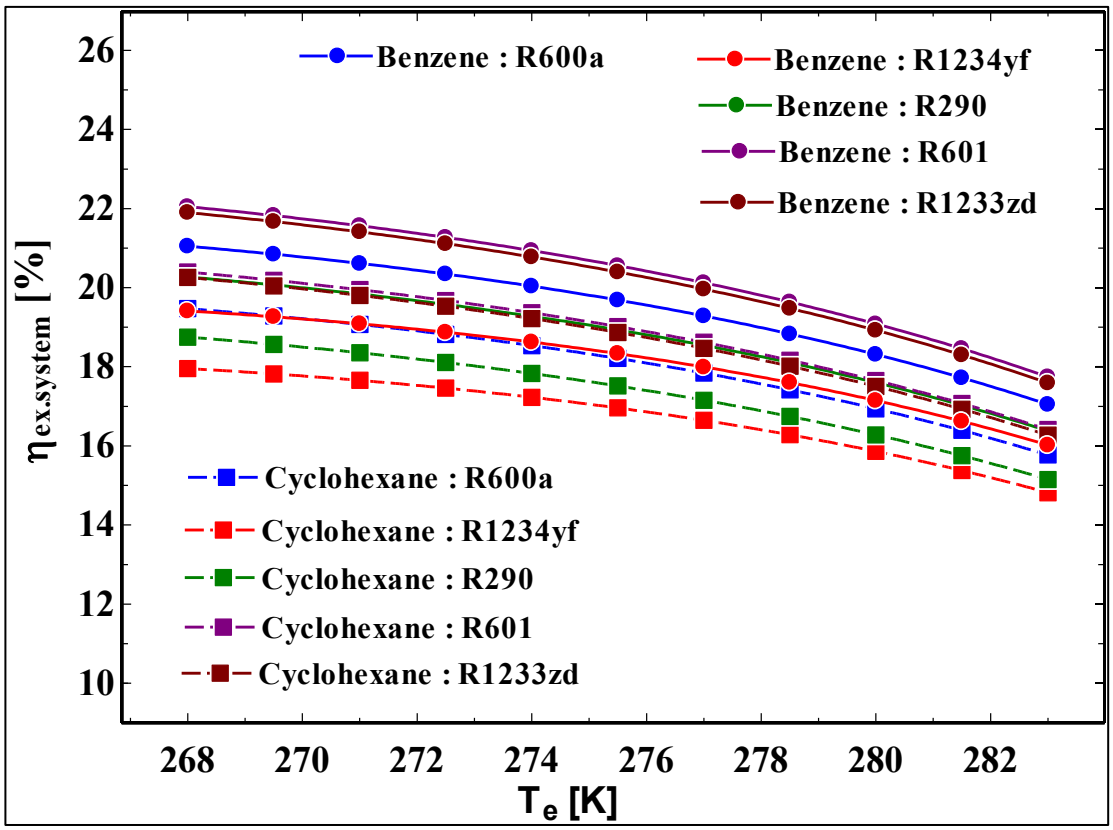

Fig. 5. 19 Effect of T_{evp} on exergetic efficiency of the system at $T_{HPT,in}$ is 550 K, $T_{LPT,in}$ is 463 K and T_{cond} is 313 K

Fig. 5.19 illustrates the variation between the exergetic efficiency of the system and the T_{evp}. The exergetic efficiency decreases with the increase of T_{evp}, it is so, that the total irreversibility of the system increases with increasing of T_{evp}. The refrigerant pair of Benzene-R601 shows exergetic efficiency in the range of 40.67% to 42.79%, which is the highest and the Cyclohexane-R1234yf pair shows in the range of 34.8% to 37.22%, which is the least. For the base case (input data given in **Error! Reference source not found.**), the exergetic efficiency of the Benzene-R601 system is 13.98% greater than that of the Cyclohexane-R1234yf system. This is because the total irreversibility of the system of Benzene-R601 is lower.

D. Effect of Condenser Temperature

Fig. 5.20 illustrates the variation of the COP of the system with variations in the T_{cond}. The COP of the system decreases with increases in T_{cond}. As T_{cond} rises after throttling, the liquid component drops, requiring less heat to fully vaporize. This reduces the

cooling effect of the system. Furthermore, the compressor's work increases as the pressure ratio grows. Consequently, the system's COP decreases. Also, as we compare all the refrigerant pairs, the Benzene-R601 is showing the COP in the higher range of 1.418 to 0.838 and the Cyclohexane-R1234yf pair is showing in the lower range of 1.196 to 0.657. For base input parameters (**Error! Reference source not found.**), the COP of the Benzene-R601 system is 16.10% greater than that of the Cyclohexane-R1234yf system. This is because the cooling effect of Benzene-R601 is greater.

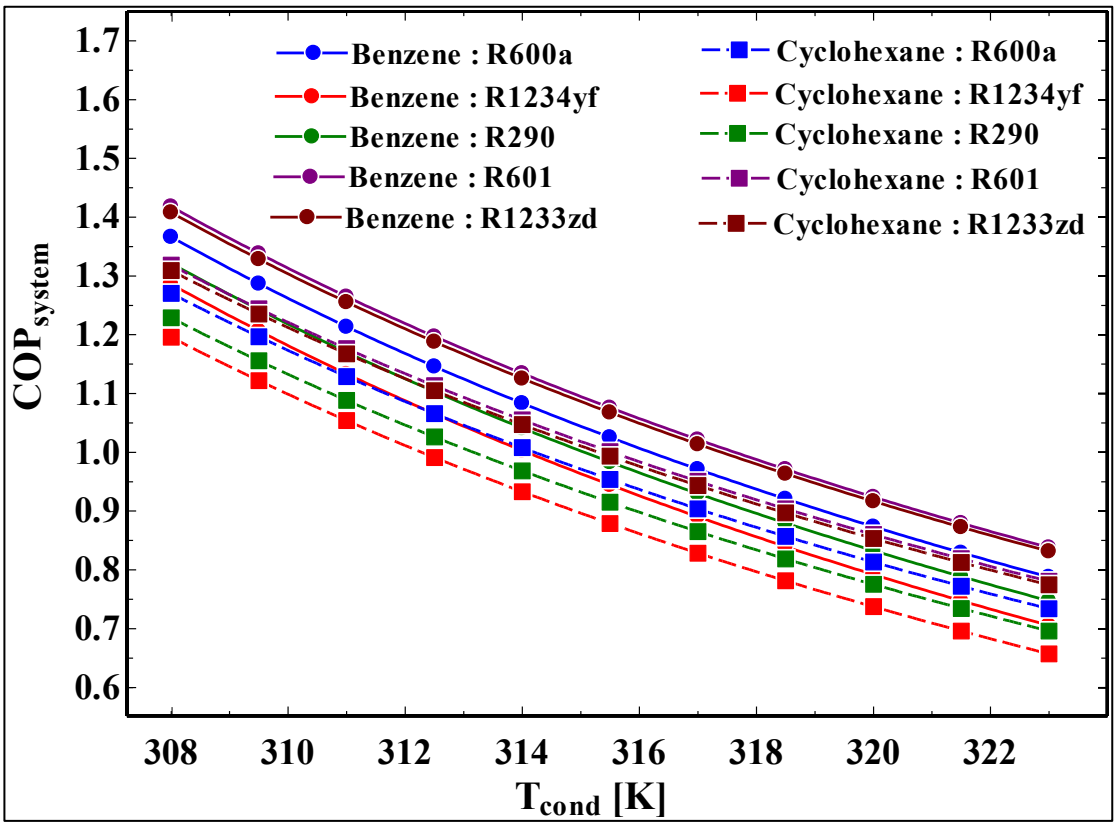

Fig. 5. 20 Effect of T_{cond} on COP of the system at $T_{HPT,in}$ is 550 K, $T_{LPT,in}$ is 463 K and T_{evp} is 273 K

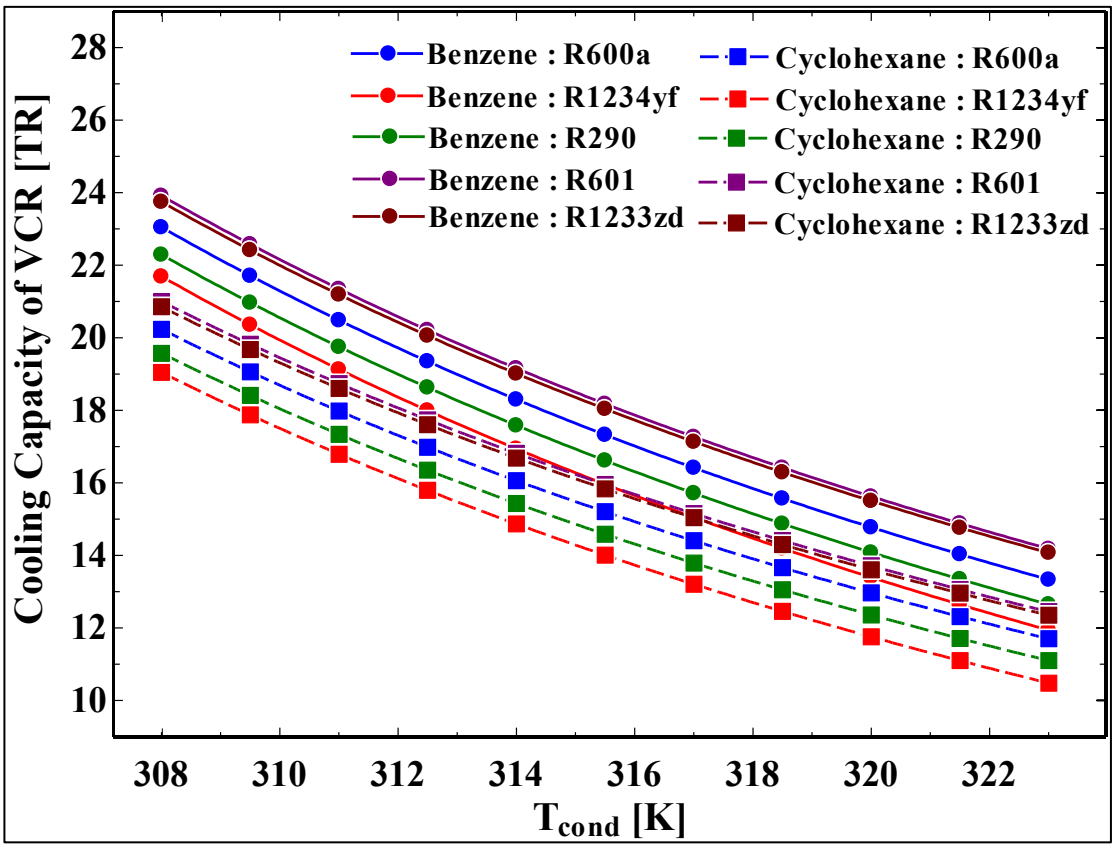

Fig. 5. 21 Effect of T_{cond} on cooling capacity of VCR at $T_{HPT,in}$ is 550 K, $T_{LPT,in}$ is 463 K and T_{evp} is 273 K

Fig. 5.21 illustrates the variation of the cooling capacity of VCR with variations in the T_{cond}. The cooling capacity of the VCR system decreases with increases in T_{cond}. Among all the combinations of refrigerant pair, the Benzene-R601 shows a cooling capacity in the range of 23.92 TR to 14.18 TR, which is the highest and the Cyclohexane-R1234yf pair shows in the range of 19.05 TR to 10.48 TR, which is least. The Benzene-R601 system exhibits a cooling capacity that is 20.51% more substantial than that of the Cyclohexane-R1234yf system.

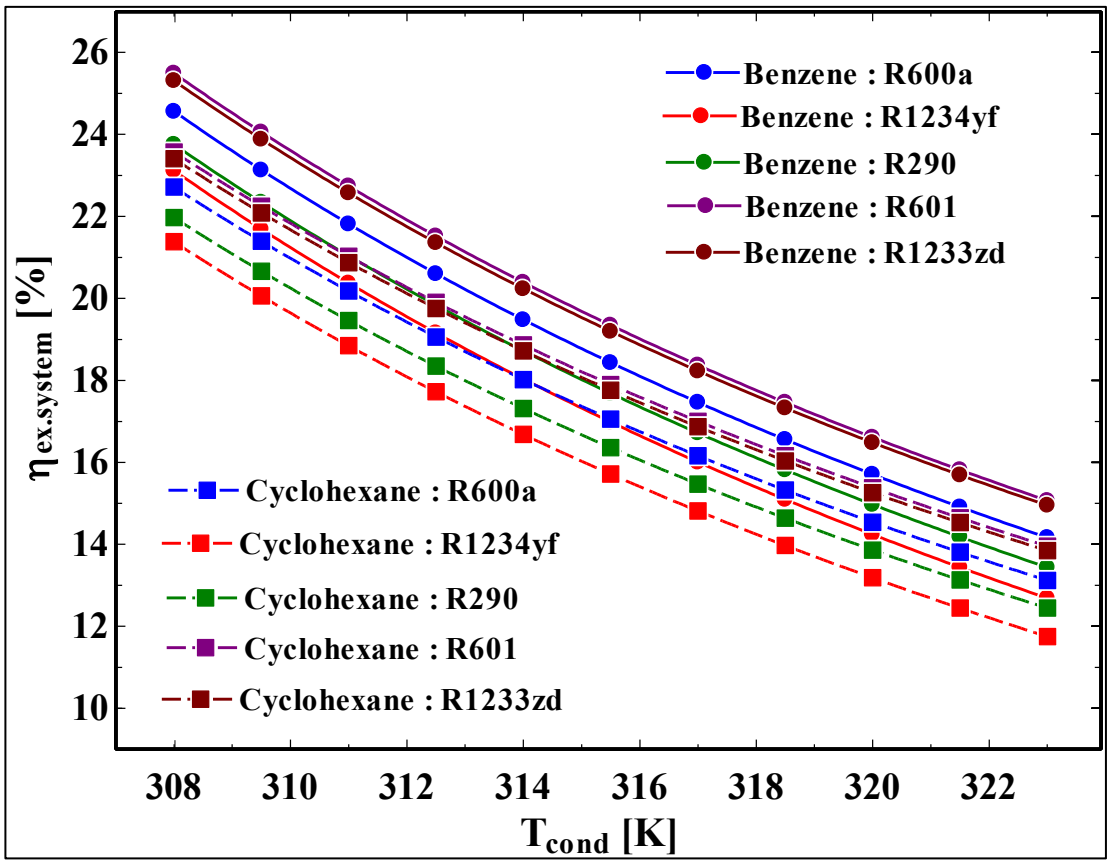

Fig. 5.22 Effect of T_{cond} on exergetic efficiency of the system at $T_{HPT,in}$ is 550 K, $T_{LPT,in}$ is 463 K and T_{evp} is 273 K

Fig. 5.22 illustrates the variation of the exergetic efficiency and T_{cond}. The exergetic efficiency decreases with increasing T_{cond}. The reason is, that the total irreversibility of the system increases with the rise of the T_{cond}. The refrigerant pair of Benzene-R601 shows exergetic efficiency in the range of 25.49% to 15.07%, which is the highest and the pair of Cyclohexane-R1234yf shows in the range of 21.38% to 11.75%, which is the least. For the base case (input data given in **Error! Reference source not found.**), the exergetic efficiency of the Benzene-R601 system is 19.04% greater

than that of the Cyclohexane-R1234yf system. This is because the total irreversibility of the system of Benzene-R601 is lower.

E. Multi-objective Optimization

To function effectively, the operating and design parameters of the system utilizing the ORC-VCR must be optimized. The $T_{HPT,in}$, $T_{LPT,in}$, T_{evp}, and T_{cond} are experiential to affect both the energy and exergy performance of ORC-VCR based on the above parametric investigation. Moreover, the cooling capacity and exergetic efficiency are the chosen performance parameters. These performance parameters were chosen because cooling capacity is an indicator of the design requirement of the refrigeration plant and exergetic efficiency is preferred to provide a thermodynamics viewpoint of the system. An increase in both aforementioned parameters is desirable. Therefore, both have to be maximized to obtain optimality.

To obtain the summarized actual equations for cooling capacity and exergetic efficiency, the Design Expert software [87] is utilized to conduct the regression analysis. The regression analysis input variables and their respective ranges are $T_{HPT,in}$ (450 K to 550 K), $T_{LPT,in}$ (423 K to 463 K), T_{cond} (308 K to 323 K), and T_{evp} (268 K to 283 K). The software Design Expert was used to test three distinct regression models: linear, 2FI, and quadratic. In addition, each regression model employs three terms: predicted R^2 (R_p^2), adjusted R^2 (R_a^2), and adequate precision (AP). The greater the difference between (R_p^2) and (R_a^2), the greater the AP value, which indicates a more accurate regression model. If a model's AP value is less than 4, further examination is not recommended [92]. As demonstrated in Table 5.5, the quadratic model is superior for regression analysis, as its accuracy is the highest among all models.

Table 5.5 Statistical information regarding various regression models [89]

Performance Factor	Linear			2FI			Quadratic		
	R_a^2	R_p^2	AP	R_a^2	R_p^2	AP	R_a^2	R_p^2	AP
Cooling capacity (Q_c)	0.93	0.92	37.29	0.96	0.92	31.51	0.99	0.98	61.88
Exergetic Efficiency (η_{ex})	0.96	0.94	41.63	0.95	0.89	25.56	0.99	0.99	178.71

Based on the selected quadratic regression model, a pair of equations ((Eqs. 5.3) and (Eqs. 5.4)) are derived for both performance parameters.

$$Q_c = -170.499 + 0.129843 \times T_{HPT,in} + 0.248833 \times T_{LPT,in} - 1.26053 \times T_{cond} + 2.24539 \times T_{evp} - 0.000030 \times T_{HPT,in} \times T_{LPT,in} - 0.000713 \times T_{HPT,in} \times T_{cond} + 0.001073 \times T_{HPT,in} \times T_{evp} - 0.001067 \times T_{LPT,in} \times T_{cond} + 0.00075 \times T_{LPT,in} \times T_{evp} - 0.037244 \times T_{cond} \times T_{evp} - 0.000155 \times T_{HPT,in}^2 - 0.000092 \times T_{LPT,in}^2 + 0.018459 \times T_{cond}^2 + 0.016837 \times T_{evp}^2 \quad (5.3)$$

$$\eta_{ex} = 822.49780 + 0.802289 \times T_{HPT,in} - 0.138538 \times T_{LPT,in} - 10.54080 \times T_{cond} + 5.96932 \times T_{evp} - 0.000077 \times T_{HPT,in} \times T_{LPT,in} - 0.001053 \times T_{HPT,in} \times T_{cond} - 0.000627 \times T_{HPT,in} \times T_{evp} + 0.000317 \times T_{LPT,in} \times T_{cond} + 0.000267 \times T_{LPT,in} \times T_{evp} - 0.001333 \times T_{cond} \times T_{evp} - 0.000223 \times T_{HPT,in}^2 - 0.000015 \times T_{LPT,in}^2 + 0.016852 \times T_{cond}^2 - 0.010193 \times T_{evp}^2 \quad (5.4)$$

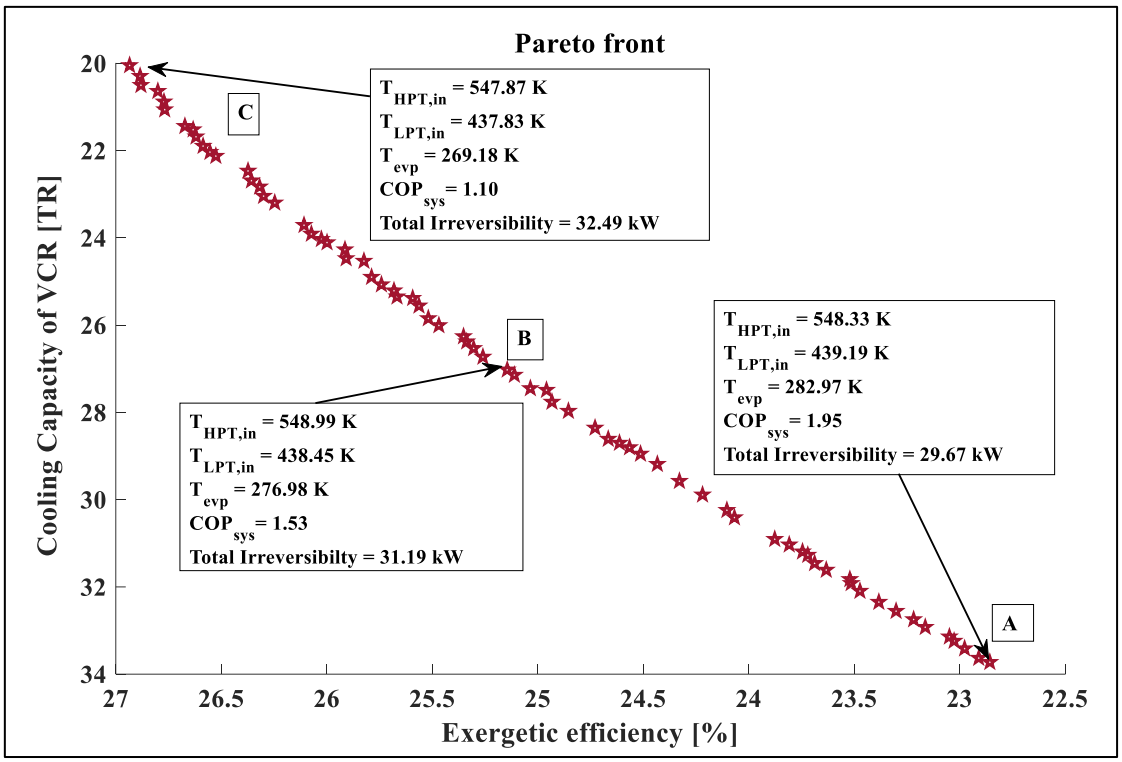

Fig. 5.23 Pareto front calculated using GA for cooling capacity and exergetic efficiency of ORC-VCR for Benzene-R601

These equations are subsequently implemented for optimization. Cooling capacity and exergetic efficiency comprise the objective function. The aforementioned concern is then resolved by employing multi-objective optimization by using a genetic algorithm (MOGA) [95]. MOGA is a metaheuristic technique that generates a large variety of solutions that seek to provide all possible trade-offs between two or more objective functions. Consequently, Pareto optimality has been achieved. During the execution of the genetic algorithm [84] the following parameters were selected: population size of 200, crossover probability of 0.8, and Pareto front population percentage of 0.35. In addition, the used selection function is 'tournament' with a size of 2 and 'intermediate' crossover functions.

The Pareto front depicted in Fig. 5.23 is a set of optimal solutions that illustrate the trade-off between cooling capacity and exergetic efficiency, given that the maximum values of exergetic efficiency correspond to minimum cooling capacity and vice versa. To illustrate the various parameters and their patterns, therefore, two extreme points ('A' and 'C') and one intermediate point ('B') were arbitrarily selected. It is evident that all

optimal solutions exhibited by these results are obtained close to the condenser temperature of 308 K (35°C).

The ORC-VCR system operating at point 'A' exhibits the highest cooling capacity (33.72 TR) as well as the COP (1.95). At this point, the exergetic efficiency and total irreversibility are obtained as 22.85% and 29.67 kW respectively. The condenser temperature which is 308.03 K (34.88°C), is suitable for ambient temperature of 25°C – 30°C. From the perspective of operating cost, point 'A' is most suitable providing the $T_{LPT,in}$ of 439.19 K. Though, the exergetic efficiency is low (accordingly highest irreversibility) at this point, the dominant performance parameter is COP which reflects the operating cost while utilizing the energy from the engine exhaust (as the $T_{HPT,in}$ at point 'A' is close to the maximum value provided i. e., 548.33 K).

On the contrary, Point 'C' exhibits the lowest COP along with the lowest cooling capacity. From the thermodynamic viewpoint, exergetic efficiency at this point is found to be the highest. The condenser temperature 308.06 K (34.91°C) is suitable for higher ambient temperature. It also requires a comparatively lower $T_{LPT,in}$ of 437.83 K to operate on the approximately same temperature of engine exhaust as similar to that at point 'A'.

Point 'B' (an intermediate point), on which the system performance on the intermediate values of performance parameters (exergetic efficiency i.e., 25.14% & COP i.e., 1.53). therefore, the ORC-VCR system can operate on any of these points according to the availability of solar heat and ambient temperatures. Based on these operating parameters suitable trade-offs between several operating parameters can be obtained.

CHAPTER 6
CONCLUSIONS AND SCOPE FOR FUTURE RESEARCH

6.1 Introduction

This chapter demonstrates the concluding remarks perceived from the several analyses conducted on the CHP system.

6.2 Ultra-Low-Grade Waste Heat Integrated ORC-VCR System

An energy and exergy-based parametric analysis was conducted on the CHP system and its individual components. Based on the findings of this study, the following key conclusions have been drawn:

- The R1233zd(E)-R1233zd(E) refrigerant pair in the VCR cycle delivers an evaporator heat of 16.02 kW with a high COP of VCR of 4.45 and a power loop efficiency of 7.00%, indicating effective thermal performance.
- The exergetic efficiency of the CHP system decreases with increasing source temperature, with R1233zd(E)-R1233zd(E) showing the highest efficiency and the least rate of decline due to its favorable thermophysical properties.
- The COP of the CHP system increases with rising source temperature, with R1233zd(E)-R1233zd(E) achieving the highest COP owing to its superior thermal properties and greater evaporator heat absorption capacity.
- The evaporator heat increases with rising source temperature due to the higher rate of change of enthalpy of vaporization allows the evaporator to absorb more heat at the same evaporator temperature, with R1233zd(E)-R1233zd(E) exhibiting the highest heat absorption due to its favorable thermal properties.
- The system's COP and exergetic efficiency decrease with increasing ambient temperature, with R1233zd(E)-R1233zd(E) maintaining the highest COP and exergetic efficiency due to differences in evaporator heat and thermal properties of the refrigerants.
- The evaporator heat decreases with rising ambient temperature due to a rise in ambient temperature elevates the condenser pressure, which reduces the enthalpy of vaporization in the VCR cycle, with R1233zd(E)-R1233zd(E) exhibiting the

highest values and R600a-R1234yf the lowest, influenced by the thermos-physical properties.

- The multi objective genetic algorithm (MOGA) process demonstrated that the system obtains the highest COP of system and evaporator heat at a source temperature of 353.88 K and a specific ambient temperature. The ORC-VCR system demonstrates the maximum exergetic efficiency at lower source temperatures, approximately 338.05 K. Nevertheless, the thermodynamic efficiency of the ORC-VCR system is significantly influenced by the increase in ambient temperature in comparison to any other input parameter.

6.3 Solar and diesel engine exhaust-driven ORC-VCR system

The ORC-VCR system and its components undergo an energy and exergy-based parametric investigation. The optimal value of selected parameters is then determined using multi-objective optimization of the simulated model employing a genetic algorithm. Several conclusions are outlined below based on this research:

- Among the selected working fluids, Benzene-R601 demonstrated the best COP, cooling capacity of the VCR, and overall system efficiency, while Cyclohexane-R1234yf showed poor results.
- Increasing the inlet temperature of High-Pressure Turbine enhances both the cooling capacity of the VCR and the system's COP, although it also increases overall system irreversibilities. Conversely, raising the inlet temperature of Low-Pressure Turbine boosts the cooling capacity of the VCR but decreases the system's COP, reducing overall irreversibilities.
- The presented ORC-VCR system can substitute conventional Heating, Ventilation, and Air-Conditioning (HVAC) systems for the same cooling load, offering a viable alternative.
- An increase in condenser temperature reduces the COP and cooling capacity of the ORC-VCR system, whereas raising the evaporator temperature increases both COP and cooling capacity.

- Optimization using GA revealed that at the highest inlet temperature of High-Pressure Turbine and specific the inlet temperature of Low-Pressure Turbine, the system achieves maximum cooling capacity under lower ambient conditions. At higher ambient temperatures (around 50°C), the ORC-VCR system shows reduced COP and cooling capacity but increased exergetic efficiency. In contrast, at lower ambient temperatures (35°C), the system achieves higher COP and cooling capacity, with the lowest exergetic efficiency.

6.4 Future scope of study

To overcome the limitation of conventional vapor compression refrigeration systems, the ORC–VCR system offers several advantages particularly in terms of energy utilization and environmental performance. Unlike traditional VCR systems, which rely on electricity supplied from the power grid, the ORC–VCR system can operate using low-grade thermal energy obtained from sources such as solar energy, industrial waste heat, or engine exhaust gases. By utilizing energy that would otherwise be wasted, the system decreases requirement of conventional electricity generation and subsidizes to lower greenhouse gas emissions. In addition, its functioning costs can be reduced due to the use of readily available waste heat resources.

The current study has primarily focused on evaluating the thermodynamic and exergetic behaviour of the ORC–VCR system. The system is used to produced cooling effect and power through waste heat. However, the selection of suitable working fluids should also consider economic and environmental aspects. Future investigations may incorporate parameters such as working fluid purchasing and operating cost, Life Cycle Impact Assessment (LCIA), and Total Equivalent Warming Impact (TEWI), indicators to provide a broader assessment of system performance and sustainability.

Further, a combined assessment of technical performance, environmental consequences, and cost would support more informed decision-making during system design and operation. This wider outlook could contribute to the development of ORC–VCR systems that are both environmentally sustainable and energy-efficient, thus enhancing their potential for practical applications involving low-grade heat recovery and cooling effect.

References

1. Jeffry, L., Greenhouse gases utilization: A review. Fuel, 2021. 301(10): 121017. https://doi.org/10.1016/j.fuel.2021.121017.
2. Suchocki, T., *Introduction to ORC–VCC Systems: A Review.* Energies, 2025. **18**(1): p. 171.
3. Wang, H., R. Peterson, and T. Herron, *Design study of configurations on system COP for a combined ORC (organic Rankine cycle) and VCC (vapor compression cycle).* Energy, 2011. **36**(8): p. 4809-4820.https://doi.org/10.1016/j.energy.2011.05.015.
4. Liu, M., Y. Shi, and F. Fang, *Combined cooling, heating and power systems: A survey.* Renewable and Sustainable Energy Reviews, 2014. **35**: p. 1-22.https://doi.org/10.1016/j.rser.2014.03.054.
5. Jiang, H., et al., *Performance assessment of an organic Rankine–Vapor compression cycle (ORC-VCR) for Low-Grade compression heat recovery.* Energy Conversion and Management, 2023. **275**: p. 116492.https://doi.org/10.1016/j.enconman.2022.116492.
6. Liang, Y., Z. Yu, and W. Li, *A Waste Heat-Driven Cooling System Based on Combined Organic Rankine and Vapour Compression Refrigeration Cycles.* Applied Sciences, 2019. **9**(20): p. 4242.
7. Liang, Y., et al., *Experimental study on a heat driven refrigeration system based on combined organic Rankine and vapour compression cycles.* Energy Conversion and Management, 2021. **234**: p. 113953.https://doi.org/10.1016/j.enconman.2021.113953.
8. Liang, Y., Z. Yu, and W. Li, *A Waste Heat-Driven Cooling System Based on Combined Organic Rankine and Vapour Compression Refrigeration Cycles.* Applied Sciences, 2019. **9**(20): p. 4242.
9. Liang, Y., et al., *Experimental study on a heat driven refrigeration system based on combined organic Rankine and vapour compression cycles.* Energy Conversion and Management, 2021. **234**: p. 113953.https://doi.org/10.1016/j.enconman.2021.113953.

10. Kaşka, Ö., et al., *The performance assessment of a combined organic Rankine-vapor compression refrigeration cycle aided hydrogen liquefaction.* International Journal of Hydrogen Energy, 2018. **43**(44): p. 20192-20202.https://doi.org/10.1016/j.ijhydene.2018.07.092.
11. Wang, X., et al., *Investigating the System Behaviors of a 10 kW Organic Rankine Cycle (ORC) Prototype Using Plunger Pump and Centrifugal Pump.* Energies, 2020. **13**(5): p. 1141.
12. Taban, D., et al., *Exergoeconomic Analysis of a Mechanical Compression Refrigeration Unit Run by an ORC.* Entropy, 2023. **25**(11): p. 1531.
13. Malwe, P.D., et al., *Dynamic simulation and exergy analysis of an Organic Rankine Cycle integrated with vapor compression refrigeration system.* Sustainable Energy Technologies and Assessments, 2022. **53**: p. 102684.https://doi.org/10.1016/j.seta.2022.102684.
14. Goyal, A. and A. Sherwani, *Analysis of organic Rankine cycle integrated multi evaporator vapor-compression refrigeration (ORC-mVCR) system.* International Journal of Refrigeration, 2022. **138**.10.1016/j.ijrefrig.2022.03.014.
15. Xia, X., et al., *Thermodynamic, economic and environmental assessment of a novel organic Rankine cycle-vapor compression refrigeration system using zeotropic mixture.* Energy and Buildings, 2023. **301**: p. 113736.https://doi.org/10.1016/j.enbuild.2023.113736.
16. Sohrabi, A., A. Behbahaninia, and S. Sayadi, *Thermodynamic optimization and comparative economic analysis of four organic Rankine cycle configurations with a zeotropic mixture.* Energy Conversion and Management, 2021. **250**: p. 114872.https://doi.org/10.1016/j.enconman.2021.114872.
17. Tiwari, D. and V. Soni, *Multi-response optimization in the ORC-VCR system using the EDAS Method.* Energy and Buildings, 2024. **313**: p. 114281.https://doi.org/10.1016/j.enbuild.2024.114281.
18. S. Adibhatla and S. Kaushik, "*Energy, exergy and economic (3E) analysis of integrated solar direct steam generation combined cycle power plant*," Sustainable energy technologies and assessments, vol. 20, pp. 88-97, 2017.

19. A. Bejan, *Advanced engineering thermodynamics*. John Wiley & Sons, 2016.
20. I. Dincer and M. A. Rosen, *Exergy: energy, environment and sustainable development*. Newnes, 2012.
21. A. Bejan, G. Tsatsaronis, and M. J. Moran, *Thermal design and optimization*. John Wiley & Sons, 1995.
22. Malwe, P., et al., *Performance Investigation on Organic Rankine Cycle from a Low-temperature Heat Source.* Case Studies in Thermal Engineering, 2025. **68**: p. 105841.10.1016/j.csite.2025.105841.
23. Goyal, A. and A. Sherwani, *Analysis of organic Rankine cycle integrated multi evaporator vapor-compression refrigeration (ORC-mVCR) system.* International Journal of Refrigeration, 2022. **138**.10.1016/j.ijrefrig.2022.03.014.
24. Sleiti, A.K., M. Al-Khawaja, and W.A. Al-Ammari, *A combined thermo-mechanical refrigeration system with isobaric expander-compressor unit powered by low grade heat – Design and analysis.* International Journal of Refrigeration, 2020. **120**: p. 39-49.https://doi.org/10.1016/j.ijrefrig.2020.08.017.
25. Sleiti, A.K., et al., *Experimental investigation on the performance of a novel thermo-mechanical refrigeration system driven by an expander-compressor unit.* Applied Thermal Engineering, 2022. **212**: p. 118635.https://doi.org/10.1016/j.applthermaleng.2022.118635.
26. González, J., et al., *Selection of a suitable working fluid for a combined organic Rankine cycle coupled with compression refrigeration using molecular approaches.* Fluid Phase Equilibria, 2023. **572**: p. 113847.https://doi.org/10.1016/j.fluid.2023.113847.
27. Bounefour, O., A. Ouadha, and Y. Addad, *An exergy analysis of various layouts of ORC-VCC systems for usage in waste heat recovery onboard ships.* Marine Systems & Ocean Technology, 2020. **15**(1): p. 26-44.10.1007/s40868-020-00072-6.

28. Ononogbo, C., et al., *Opportunities of waste heat recovery from various sources: Review of technologies and implementation.* Heliyon, 2023. **9**(2).10.1016/j.heliyon.2023.e13590.
29. Saleh, B., *Parametric and working fluid analysis of a combined organic Rankine-vapor compression refrigeration system activated by low-grade thermal energy.* Journal of Advanced Research, 2016. **7**(5): p. 651-660.https://doi.org/10.1016/j.jare.2016.06.006.
30. Bounefour, O., A. Ouadha, and Y. Addad, *An exergy analysis of various layouts of ORC-VCC systems for usage in waste heat recovery onboard ships.* Marine Systems & Ocean Technology, 2020. **15**.10.1007/s40868-020-00072-6.
31. Iyengar, A., et al., *Effect Of Climatic Conditions On Performance Of ORC Using Environment-Friendly Working Fluids – Special Reference To India.* Journal of Mines, Metals and Fuels, 2022. **70**: p. 153-157.10.18311/jmmf/2022/30686.
32. Forman, C., et al., *Estimating the global waste heat potential.* Renewable and Sustainable Energy Reviews, 2016. **57**: p. 1568-1579.https://doi.org/10.1016/j.rser.2015.12.192.
33. Hung, T.C., T.Y. Shai, and S.K. Wang, *A review of organic rankine cycles (ORCs) for the recovery of low-grade waste heat.* Energy, 1997. **22**(7): p. 661-667.https://doi.org/10.1016/S0360-5442(96)00165-X.
34. Gado, M.G., et al., *Hybrid sorption-vapor compression cooling systems: A comprehensive overview.* Renewable and Sustainable Energy Reviews, 2021. **143**: p. 110912.https://doi.org/10.1016/j.rser.2021.110912.
35. Tashtoush, B.M., M.d.A. Al-Nimr, and M.A. Khasawneh, *A comprehensive review of ejector design, performance, and applications.* Applied Energy, 2019. **240**: p. 138-172.https://doi.org/10.1016/j.apenergy.2019.01.185.
36. Zeyghami, M., D.Y. Goswami, and E. Stefanakos, *A review of solar thermo-mechanical refrigeration and cooling methods.* Renewable and Sustainable Energy Reviews, 2015. **51**: p. 1428-1445.https://doi.org/10.1016/j.rser.2015.07.011.

37. Gao, P., et al., *Simulation and experiments on an ORC system with different scroll expanders based on energy and exergy analysis.* Applied Thermal Engineering, 2015. **75**: p. 880-888.https://doi.org/10.1016/j.applthermaleng.2014.10.044.
38. Anastasovski, A., P. Rasković, and Z. Guzović, *A review of heat integration approaches for organic rankine cycle with waste heat in production processes.* Energy Conversion and Management, 2020. **221**: p. 113175.https://doi.org/10.1016/j.enconman.2020.113175.
39. Yu, G., et al., *Simulation and thermodynamic analysis of a bottoming Organic Rankine Cycle (ORC) of diesel engine (DE).* Energy, 2013. **51**: p. 281-290.https://doi.org/10.1016/j.energy.2012.10.054.
40. Ghorbani, T., M. Yari, and F. Mohammadkhani, *Thermodynamic analysis and feasibility study of internal combustion engine waste heat recovery to run its refrigeration system.* AUT Journal of Mechanical Engineering, 2018. **2**(2): p. 253-262.
41. Ngangué, M.N., et al., *Working fluid selection for a high efficiency integrated power/cooling system combining an organic Rankine cycle and vapor compression-absorption cycles.* Energy, 2023. **277**: p. 127709.
42. Xia, X., et al., *Multi-layer performance optimization based on operation parameter-working fluid-heat source for the ORC-VCR system.* Energy, 2023. **272**: p. 127103.https://doi.org/10.1016/j.energy.2023.127103.
43. Goyal, A. and A. Sherwani, *Analysis of organic Rankine cycle integrated multi evaporator vapor-compression refrigeration (ORC-mVCR) system.* International Journal of Refrigeration, 2022. **138**.10.1016/j.ijrefrig.2022.03.014.
44. Bolaji, B., et al., *Energy and Thermal Conductivity Assessment of Dimethyl-Ether and its Azeotropic Mixtures as Alternative Low Global Warming Potential Refrigerants in a Refrigeration System.* Environmental and Climate Technologies, 2021. **25**: p. 12-28.10.2478/rtuect-2021-0002.

45. Zheng, N., J. Wei, and L. Zhao, *Analysis of a solar Rankine cycle powered refrigerator with zeotropic mixtures.* Solar Energy, 2018. **162**: p. 57-66.https://doi.org/10.1016/j.solener.2018.01.011.
46. Bu, X.B., H.S. Li, and L.B. Wang, *Performance analysis and working fluids selection of solar powered organic Rankine-vapor compression ice maker.* Solar Energy, 2013. **95**: p. 271-278.https://doi.org/10.1016/j.solener.2013.06.024.
47. Zhang, S., et al., *Thermo-economic assessment and multi-objective optimization of organic Rankine cycle driven by solar energy and waste heat.* Energy, 2024. **290**: p. 130223.https://doi.org/10.1016/j.energy.2023.130223.
48. Aneke, M., et al., *Thermodynamic analysis of alternative refrigeration cycles driven from waste heat in a food processing application.* International Journal of Refrigeration, 2012. **35**(5): p. 1349-1358.https://doi.org/10.1016/j.ijrefrig.2012.04.008.
49. Ashwni, A.F. Sherwani, and D. Tiwari, *Thermodynamic analysis of simple and modified organic Rankine cycle and vapor compression refrigeration (ORC–VCR) systems.* Environmental Progress & Sustainable Energy, 2021. **40**(3): p. e13577.
50. Karellas, S. and K. Braimakis, *Energy–exergy analysis and economic investigation of a cogeneration and trigeneration ORC–VCC hybrid system utilizing biomass fuel and solar power.* Energy Conversion and Management, 2016. **107**: p. 103-113.https://doi.org/10.1016/j.enconman.2015.06.080.
51. Saleh, B., *Energy and exergy analysis of an integrated organic Rankine cycle-vapor compression refrigeration system.* Applied Thermal Engineering, 2018. **141**: p. 697-710.https://doi.org/10.1016/j.applthermaleng.2018.06.018.
52. Nasir, M.T. and K.C. Kim, *Working fluids selection and parametric optimization of an Organic Rankine Cycle coupled Vapor Compression Cycle (ORC-VCC) for air conditioning using low grade heat.* Energy and Buildings, 2016. **129**: p. 378-395.https://doi.org/10.1016/j.enbuild.2016.07.068.

53. Yılmaz, A., *Transcritical organic Rankine vapor compression refrigeration system for intercity bus air-conditioning using engine exhaust heat.* Energy, 2015. **82**: p. 1047-1056.https://doi.org/10.1016/j.energy.2015.02.004.
54. Ashwni and A.F. Sherwani, *Thermodynamic analysis of hybrid heat source driven organic Rankine cycle integrated flash tank vapor-compression refrigeration system.* International Journal of Refrigeration, 2021. **129**: p. 267-277.https://doi.org/10.1016/j.ijrefrig.2021.05.006.
55. Garland, S.D., J. Noall, and T.M. Bandhauer, *Experimentally validated modeling of a turbo-compression cooling system for power plant waste heat recovery.* Energy, 2018. **156**: p. 32-44.https://doi.org/10.1016/j.energy.2018.05.048.
56. Grauberger, A., D. Young, and T. Bandhauer, *Experimental validation of an organic rankine-vapor compression cooling cycle using low GWP refrigerant R1234ze(E).* Applied Energy, 2022. **307**: p. 118242.https://doi.org/10.1016/j.apenergy.2021.118242.
57. Wang, H., et al., *Performance of a combined organic Rankine cycle and vapor compression cycle for heat activated cooling.* Energy, 2011. **36**(1): p. 447-458.https://doi.org/10.1016/j.energy.2010.10.020.
58. Sleiti, A. K., Al-Ammari, W. A., and Musharavati, F., 2023, "*Theoretical and experimental study on the selection of pure and mixed refrigerants for a power-cooling system driven by ultra-low-grade heat*," Thermal Science and Engineering Progress, 43, p. 101962.https://doi.org/10.1016/j.tsep.2023.101962
59. P, V. and D. Deshmukh, *A comprehensive review of waste heat recovery from a diesel engine using organic rankine cycle.* Energy Reports, 2021. **7**: p. 3951-3970.https://doi.org/10.1016/j.egyr.2021.06.081.
60. Hemadri, V.B. and P.M.V. Subbarao, *Thermal integration of reheated organic Rankine cycle (RH-ORC) with gas turbine exhaust for maximum power recovery.* Thermal Science and Engineering Progress, 2021. **23**: p. 100876.https://doi.org/10.1016/j.tsep.2021.100876.

61. P. Nag, "Engineering thermodynamics," *New Delhi,* 2008.
62. T. J. Kotas, *The exergy method of thermal plant analysis*. Paragon Publishing, 2012.
63. Y. A. Cengel, M. A. Boles, and M. Kanoğlu, *Thermodynamics: an engineering approach*. McGraw-hill New York, 2011.
64. S. Kaushik, V. S. Reddy, and S. Tyagi, "Energy and exergy analyses of thermal power plants: A review," *Renewable and Sustainable energy reviews,* vol. 15, no. 4, pp. 1857-1872, 2011.
65. P. Ahmadi, I. Dincer, and M. A. Rosen, "Exergy, exergoeconomic and environmental analyses and evolutionary algorithm based multi-objective optimization of combined cycle power plants," *Energy,* vol. 36, no. 10, pp. 58865898, 2011/10/01/ 2011, doi: https://doi.org/10.1016/j.energy.2011.08.034.
66. M. Ameri, P. Ahmadi, and A. Hamidi, "Energy, exergy and exergoeconomic analysis of a steam power plant: A case study," *International Journal of energy research,* vol. 33, no. 5, pp. 499-512, 2009.
67. U. M. Diwekar, *Introduction to applied optimization*. Springer Nature, 2020.
68. A. A. Bazmi and G. Zahedi, "Sustainable energy systems: Role of optimization modeling techniques in power generation and supply—A review," *Renewable and sustainable energy reviews,* vol. 15, no. 8, pp. 3480-3500, 2011.
69. Z. N. Pintarič and Z. Kravanja, "Suitable Process Modelling for Proper MultiObjective Optimization of Process Flow Sheets," in *Computer Aided Chemical*

    Engineering, vol. 33, J. J. Klemeš, P. S. Varbanov, and P. Y. Liew Eds.: Elsevier, 2014, pp. 1387-1392.
70. W. Forst and D. Hoffmann, *Optimization—theory and practice*. Springer Science & Business Media, 2010.
71. J. Nocedal and S. J. Wright, *Numerical optimization*. Springer, 1999.

72. K. Deb, "Evolutionary algorithms for multi-criterion optimization in engineering design," *Evolutionary algorithms in engineering and computer science,* vol. 2, pp. 135-161, 1999.
73. A. Ghaffarizadeh, K. Ahmadi, and N. S. Flann, "Sorting unsigned permutations by reversals using multi-objective evolutionary algorithms with variable size individuals," in *2011 IEEE Congress of Evolutionary Computation (CEC)*, 2011: IEEE, pp. 292-295.
74. D. E. Goldberg, "Optimization, and machine learning," *Genetic algorithms in Search,* 1989.
75. K. Deb, K. Sindhya, and J. Hakanen, "Multi-objective optimization," in *Decision sciences*: CRC Press, 2016, pp. 161-200.
76. N. Srinivas and K. Deb, "Muiltiobjective optimization using nondominated sorting in genetic algorithms," *Evolutionary computation,* vol. 2, no. 3, pp. 221248, 1994.
77. Valencia, G., Fontalvo, A., Cárdenas, Y., Duarte, J., and Isaza, C., 2019, "Energy and Exergy Analysis of Different Exhaust Waste Heat Recovery Systems for Natural Gas Engine Based on ORC," Energies, 12(12), p. 2378. https://doi.org/10.3390/en12122378
78. Bejan, A., 2002, "Fundamentals of Exergy Analysis, Entropy Generation Minimization, and the Generation of Flow Architecture," International Journal of Energy Research, 26, pp. 0-43. https://doi.org/10.1002/er.804
79. Khera, R., Arora, A., and Arora, B. B., 2023, "Performance analysis and multi-objective optimization of a vortex tube integrated single-stage vapour compression refrigeration cycle," International Journal of Refrigeration, 154, pp. 335-348.https://doi.org/10.1016/j.ijrefrig.2023.07.014
80. Kotas, T. J., 2012, The Exergy Method of Thermal Plant Analysis, , Paragon, Northampton, UK.
81. Mishra, A., Arora, B. B., and Arora, A., 2023, "Multi-Objective Optimization of an Inlet Air-Cooled Combined Cycle Power Plant," ASME Journal of

Thermal Science and Engineering Applications, 15(7). https://doi.org/10.1115/1.4062210

82. Sun, L., Han, W., and Jin, H., 2015, "Energy and exergy investigation of a hybrid refrigeration system activated by mid/low-temperature heat source," Applied Thermal Engineering, 91, pp. 913-923.https://doi.org/10.1016/j.applthermaleng.2015.08.061
83. Holland, J. H., 1992, "Genetic Algorithms," Scientific American, 267(1), pp. 66-73
84. Konak, A., Coit, D. W., and Smith, A. E., 2006, "Multi-objective optimization using genetic algorithms: A tutorial," Reliability Engineering & System Safety, 91(9), pp. 992-1007.https://doi.org/10.1016/j.ress.2005.11.018
85. *Fundamentals of Exergy Analysis, Entropy Generation Minimization, and the Generation of Flow Architecture.* International Journal of Energy Research, 2002. **26**: p. 0-43.10.1002/er.804.
86. Khera, R., A. Arora, and B.B. Arora, *Performance analysis and multi-objective optimization of a vortex tube integrated single-stage vapour compression refrigeration cycle.* International Journal of Refrigeration, 2023. **154**: p. 335-348.https://doi.org/10.1016/j.ijrefrig.2023.07.014.
87. 20. Kotas, T.J., *The Exergy Method of Thermal Plant Analysis,* . 2012, Northampton, UK: Paragon.
88. Zendehboudi, A., et al., *Modeling and multi-objective optimization of an R450A vapor compression refrigeration system.* International Journal of Refrigeration, 2019. **100**: p. 141-155.https://doi.org/10.1016/j.ijrefrig.2019.01.008.
89. Mishra, A., B.B. Arora, and A. Arora, *Multi-Objective Optimization of an Inlet Air-Cooled Combined Cycle Power Plant.* Journal of Thermal Science and Engineering Applications, 2023. **15**(7).10.1115/1.4062210.
90. Konak, A., D.W. Coit, and A.E. Smith, *Multi-objective optimization using genetic algorithms: A tutorial.* Reliability Engineering & System Safety, 2006. **91**(9): p. 992-1007.https://doi.org/10.1016/j.ress.2005.11.018.

91. Bao, J., et al., *Comparative study of combined organic Rankine cycle and vapor compression cycle for refrigeration: Single fluid or dual fluid?* Sustainable Energy Technologies and Assessments, 2020. **37**: p. 100595.https://doi.org/10.1016/j.seta.2019.100595.
92. Zendehboudi, A., Mota-Babiloni, A., Makhnatch, P., Saidur, R., and Sait, S. M., 2019, "Modeling and multi-objective optimization of an R450A vapor compression refrigeration system," International Journal of Refrigeration, 100, pp. 141-155.https://doi.org/10.1016/j.ijrefrig.2019.01.008
93. Konak, A., Coit, D. W., and Smith, A. E., 2006, "Multi-objective optimization using genetic algorithms: A tutorial," Reliability Engineering & System Safety, 91(9), pp. 992-1007.https://doi.org/10.1016/j.ress.2005.11.018
94. Zendehboudi, A., Mota-Babiloni, A., Makhnatch, P., Saidur, R., and Sait, S. M., 2019, "Modeling and multi-objective optimization of an R450A vapor compression refrigeration system," International Journal of Refrigeration, 100, pp. 141-155.https://doi.org/10.1016/j.ijrefrig.2019.01.008
95. Sayyaadi, H. and M. Nejatolahi, *Multi-objective optimization of a cooling tower assisted vapor compression refrigeration system.* International Journal of Refrigeration, 2011. **34**(1): p. 243-256.https://doi.org/10.1016/j.ijrefrig.2010.07.026.

LIST OF PUBLICATIONS AND RECOGNITIONS

PUBLICATIONS

1. Kumar, S., Arora, B. B., & Arora, A. (2025). Thermodynamic assessment and optimization of a solar and diesel engine exhaust-driven ORC-VCR system. *International Journal of Refrigeration, 170*, 325–339. https://doi.org/10.1016/j.ijrefrig.2024.11.035 (SCIE Indexed, Impact factor: 3.8)

2. Kumar, S., Arora, A., & Arora, B. B. (2026). Thermodynamic and multi-objective performance optimization of an integrated ORC–VCR system powered by low-grade waste heat. *Journal of Thermal Science and Engineering Applications, 18*(3), 1–34. https://doi.org/10.1115/1.4070282. (SCIE Indexed, Impact factor: 1.4)

3. Kumar, S., Arora, A., & Arora, B. B. (2023). Analysis of a combined ORC-VCC System with A Geo-Thermal Heat Source, *International Conference on Mechanical Engineering: Researches and Evolutionary Challenges-2023, NIT Warangal, 23-25 June, 2023*

4. Kumar, S., Arora, A., & Arora, B. B. (2024). Energy Analysis of ORC coupled VCR system using Renewable Heat Source, *International Symposium on Fusion of Science and technology- 2024 (ISFT-2024), J C Bose University of Science & Technology, YMCA, Faridabad, 04-08 January, 2024*

RECOGNITION

1. Research Excellence Award 2026 at DTU, New Delhi